POLITECNICO DI MILANO

Facoltà di Ingegneria dei Processi Industriali

Laurea Magistrale in Ingegneria dei Materiali

Investigation of 9-12wt.% Cr steels with the use of dilatometer

Relatore: **Prof. Walter NICODEMI**

Co-relatori: **Prof. Donato FIRRAO**

Prof. Marcel SOMERS

Prof. Carlo MAPELLI

Candidato:
Matteo VILLA
Matr. 720869

Anno Accademico 2008-2009

PREFAZIONE

Il lavoro di tesi presentato è nato dalla decisione di arricchire la mia esperienza personale attraverso un periodo di studio all'estero. La Danimarca, e nella fattispecie Copenhagen (o København come scriverebbe uno studente locale), sono stati scelti e per la particolare capacità dell'università DTU di accogliere gli studenti stranieri e per la riconosciuta qualità dell'insegnamento, caratteristiche che ne fanno una delle eccellenze europee in ambito tecnico scientifico. In questo contesto mi è stato possibile inserirmi nella collaborazione che l'azienda "Centro Sviluppo Materiali" ha istaurato con il gruppo di lavoro del professor Somers e del dottor Hald.

Le decisioni riguardanti argomento da trattare, struttura del lavoro e obbiettivi, sono state prese considerando gli strumenti e le competenze specifiche a disposizione. Inoltre, il lavoro è stato sviluppato in modo da conciliare una forte attività di ricerca bibliografica iniziale, specialmente su testi avanzati e specifici, con una attività sperimentale che facesse uso di metodi consolidati. Ciò è stato fatto consapevolmente in modo da esprimere a pieno le capacità di analisi e, più in generale di lavoro, sviluppate in questi anni di studio, piuttosto che dedicarsi alla messa a punto, spesso empirica, di componentistica sperimentale.

Il lavoro risultante si è presentato solido ma allo stesso tempo innovativo. Nel riportarlo all'interno di questo testo si è deciso di distaccarsi dalla forma classica del testo scientifico: parte del metodo sperimentale è stata presentata all'interno della sezione relativa ai risultati sperimentali, in modo da favorire la lettura.

Infine, in modo da rendere agevole la valutazione dei risultati presentati, i dati sperimentali ottenuti con le prove di dilatometria sono stati per la maggior parte riportati in appendice in forma grafica.

Investigation of 9-12wt.% Cr steels with the use of dilatometer

RIASSUNTO

ABSTRACT

Gli acciai 9-12wt.% Cr sono materiali importanti per applicazioni ad alta temperatura. Questo elaborato è inserito nel contesto delle ricerche volte allo studio delle trasformazioni micro-strutturali che determinano il comportamento di questa classe di materiali. In particolare si focalizza sulla trasformazione α'→γ e sull'uso del dilatometro come strumento di caratterizzazione.

Lo studio analizza le potenzialità della dilatometria accoppiata a misure di durezza ed all'analisi metallografica, e mostra come questa sia in grado di superare i limiti delle singole tecniche e fornire un panorama pressoché completo di informazioni riguardanti la trasformazione analizzata.

1) INTRODUZIONE

L'uso della dilatometria per lo studio di acciai è riportato da importanti studiosi del settore quali il professor Mittemeijer a il professor Bhadeshia. Tuttavia, la tecnica si presenta ancora lontana dall'essere stata completamente sviluppata, e ulteriori studi possono essere proposti. Il progetto si basa dunque su queste considerazioni.

L'analisi è stata effettuata grazie alla disponibilità dell'azienda "Centro Sviluppo Materiali SPA" a fornire strumentazione e competenze per un numero non superiore a 10 prove di dilatometria, e al supporto tecnico e logistico forniti dalla DTU di Copenhagen tramite il Prof. Marcel Somers e il Dott. John Hald.

Lo studio è stato sviluppato facendo riferimento all'attuale stato dell'arte; due tipologie di analisi sono state proposte: la prima è innovativa e si basa sulla comparazione dei coefficienti di dilatazione termica lineare per valutare quantitativamente la quantità di fase trasformata in un trattamento intercritico; la seconda è un'analisi cinetica effettuata grazie a test isocroni.

Gli acciai 9-12%.Cr sono stati scelti poiché rappresentano una classe importante di materiali per applicazioni nel settore energia, e si troveranno inevitabilmente ad essere al centro di numerosi studi nei prossimi anni.

La trasformazione $\alpha \rightarrow \gamma$ è stata scelta come oggetto di studio sia per l'importanza che riveste nel determinare le temperature dei trattamenti termici a cui sottoporre l'acciaio, sia sulla base della strumentazione a disposizione.

2) GLI ACCIAI 9-12wt.% Cr

Gli acciai 9-12wt.% Cr sono materiali utilizzabili per applicazioni ad alta temperatura quali componenti di impianti per la produzione di energia. Tra loro il P91, P92 e l'X20CrMoV 12-1 sono quelli maggiormente usati. Questi acciai sono normalmente forniti bonificati e mostrano struttura completamente martensitica.

Gli elementi che li caratterizzano sono il Cr, aggiunta più importante dal punto di vista quantitativo, che ne determina la resistenza a corrosione, e elementi quali V e Nb, in grado di formare fini precipitati (carburi e nitruri) stabili ad alta temperatura, che ne determinano la resistenza a creep. Co, Mo e W sono talvolta aggiunti per migliorare ulteriormente le proprietà del materiale alle alte temperature.

Dal punto di vista microstrutturale, le due fasi di equilibrio che si ritrovano in acciai Fe-Cr, sono la ferrite (fase α) e l'austenite (fase γ); la prima mostra una struttura meno compatta e che presenta una minore capacità di contenere in soluzione elementi quali C e N: ne risulta un forte cambiamento di volume durante la trasformazione α ↔ γ e la possibile formazione di precipitati durante un eventuale mantenimento ad alta temperatura in fase ferritica. Tali fenomeni di precipitazione danno luogo alla formazione di fasi secondarie quali carburi o nitruri.

Tuttavia la ferrite non è quasi mai presente in questo tipo di acciai, se non per lunghi mantenimenti ad alta temperatura, a causa dell'alto contenuto di elementi di lega che ne determinano una facile temprabilità. La trasformazione γ→α, che si avrebbe durante un raffreddamento dell'acciaio in condizioni di equilibrio (a velocità ipoteticamente nulla) a seguito del processo di austenitizzazione, in realtà non avviene ed il raffreddamento dà luogo alla formazione di strutture di non equilibrio. La fase α' (martensite) è la struttura che è attesa da un normale raffreddamento in aria del materiale e ne caratterizza il comportamento.

La martensite così formata è tuttavia troppo fragile per un impiego diretto: il successivo trattamento di rinvenimento ne determina le caratteristiche meccaniche di alta resistenza accoppiata ad una discreta resilienza che rendono il materiale adatto ad applicazioni strutturali. Il trattamento termico di rinvenimento viene effettuato ad una temperatura superiore a quella di esercizio, ma inferiore alla temperatura critica A_1. La corretta determinazione di tale temperatura risulta quindi fondamentale per una corretta preparazione dell'acciaio.

Inoltre, è durante questo trattamento che si ha la formazione dei fini precipitati secondari in grado di conferire a questa classe di acciai una notevole resistenza al fenomeno dello

scorrimento viscoso (creep); tali precipitazioni possono essere studiate in modo approfondito con tecniche di dilatometria accoppiate alla microscopia elettronica e a misure di durezza.

Infine, austenite residua e δ ferrite sono anch'esse fasi che possono essere presenti nell'acciaio; la loro presenza vuole comunque essere evitata in quanto degradano le proprietà del materiale in cui si trovano riducendone in modo drastico la resistenza meccanica.

3) ANALISI DELLE TRASFORMAZIONI DI FASE: TECNICHE E POTENZIALITA'

L'analisi delle trasformazioni allo stato solido viene effettuata riportando la frazione trasformata espressa in funzione del tempo e della temperatura. Per far questo, una proprietà fisica, connessa con i diversi stati, deve essere registrata. Le tecniche di calorimetria e dilatometria sono le più utilizzate e sono in grado di fornire le informazioni richieste registrando rispettivamente entalpia e elongazione del materiale.

L'analisi può essere effettuata a temperatura costante (analisi isoterma) o a velocità di riscaldamento/raffreddamento costante (analisi isocrona); in entrambi i casi è possibile valutare l'energia di attivazione di una trasformazione, ottenendo informazioni rilevanti sulla natura del processo, senza far ricorso ad alcun modello cinetico. Inoltre è possibile accoppiare differenti tecniche: differenti tecniche sono infatti in grado di mostrare in modo più o meno pronunciato differenti processi, rendendo importante una valutazione preliminare delle informazioni rilevabili ma anche dando spesso la possibilità di ottenere dati tra loro complementari.

In particolare, la dilatometria garantisce una migliore capacità di mostrare la formazione di precipitati, mentre la calorimetria differenziale risulta più indicata per il rilevamento delle temperature critiche riducendo l'incertezza connessa alla loro determinazione.

In letteratura si possono trovare svariati esempi di analisi sia isoterme che isocrone: curve CCT, TTT, analisi dei differenti stadi del trattamento di rinvenimento, sono solo alcuni esempi delle normali applicazioni delle tecniche sopra citate.

Inoltre è importante sottolineare la superiore capacità delle analisi isocrone di distinguere picchi relativi a differenti processi laddove essi non siano distinguibili con una analisi isoterma.

L'analisi cinetica viene normalmente effettuata assumendo la validità dell'equazione JMAK. Tuttavia, l'equazione JMAK (Equation 3) è stata sviluppata per descrivere processi di trasformazione a temperatura costante. Per una sua applicazione a processi isocroni, è richiesta una sua riformulazione. L'approccio seguito in questo studio è quello riportato da Mittemeijer in (9). Infine, il significato dell'esponente di Avrami "n" è stato interpretato secondo quando indicato da Christian (38).

4) VALUTAZIONE DELLE INCLUSIONI NON METALLICHE

Le inclusioni non metalliche sono sempre presenti negli acciai, sia in forma di solfuri metallici che come prodotti di disossidazione. Questi ultimi possono essere il risultato di un cattivo processo di fabbricazione ma essere anche intenzionalmente formati con lo scopo di ridurre al minimo l'ossigeno contenuto in soluzione nell'acciaio. Ossigeno in soluzione che risulterà alquanto limitato per gli acciai oggetto di questo studio, sia a causa della presenza di elementi ad alta affinità per l'ossigeno quali Cr e V, sia grazie alla tecnica di produzione in vuoto utilizzata (VIM).

Una corretta valutazione delle inclusioni non metalliche ne analizza quantità ma anche dimensioni, forma e distribuzione: tutti questi elementi sono infatti in grado di influenzare la capacità delle inclusioni di ridurre le caratteristiche del materiale.

Le inclusioni possono essere studiate sia con metodi macroscopici, come le prove di rottura, che microscopi, attraverso tecniche metallografiche. L'analisi metallografica in particolare è in grado di fornire indicazioni relative a tutti i parametri sopra citati, ma allo stesso tempo può risultare limitata dal punto di vista statistico: per questo motivo, procedimenti automatici che siano in grado di analizzare velocemente grandi superfici, risulterebbero particolarmente adeguati per l'analisi.

5) METODO SPERIMENTALE

Le tecniche utilizzate in questo studio sono state: prove di durezza, tecniche di microscopia, analisi composizionale (EDS) e dilatometria.

Le prove di durezza sono state effettuate con test Vickers, su campioni appositamente preparati.

La microscopia ottica è stata utilizzata per effettuare l'analisi metallografica; etching con l'agente Villella è stato scelto come metodo di attacco preferenziale della superficie metallica. Tecniche di microscopia elettronica sono invece state utilizzate per l'analisi delle inclusioni presenti nel materiale ricevuto.

Infine, i test di dilatometria sono stati effettuati presso il CSM di Roma sia per valutare le temperature critiche del materiale ricevuto, sia per analizzare quantitativamente la frazione trasformata durante i trattamenti termici intercritici, sia per valutare l'energia di attivazione della trasformazione $\alpha' \rightarrow \gamma$ e i parametri cinetici dell'equazione JMAK.

Le temperature critiche sono state determinate graficamente, rappresentando il coefficiente di dilatazione termica del materiale in funzione della temperatura a partire dai dati ottenuti sull'elongazione.

La frazione trasformata durante i trattamenti intercritici, è stata invece valutata comparando i coefficienti di dilatazione termica mostrati dal materiale a seguito del trattamento, con i dati relativi alle sole fasi austenitica e martensitica. I coefficienti sono stati valutati nello stesso intervallo di temperatura per le differenti fasi e una corrispondenza lineare è stata assunta per determinare la fase trasformata.

Infine, l'analisi cinetica è stata effettuata eseguendo 3 test isocroni a differente velocità "Φ".

L'energia di attivazione è stata determinata con una analisi di tipo "Kissinger". La fase trasformata è stata valutata a partire dai dati relativi alla lunghezza del campione, comparati alla lunghezza ipotetica del materiale completamente martensitico e austenitico, e rappresentata in funzione della temperatura "T" per differenti velocità di trasformazione. In seguito, le temperature alle quali la stessa quantità di materiale è risultata presente in fase trasformata sono state determinate ogni 10%. L'energia di attivazione è stata quindi determinata rappresentando il $\ln(T^2/\theta)$ in funzione di 1/T e moltiplicando la pendenza della retta ottenuta per la costante universale dei gas R.

I parametri dell'equazione JMAK sono stati determinati in seguito assumendo una trasformazione isocinetica. Il parametro cinetico "k_0" è stato determinato tramite l'Equation 13. Un' energia di attivazione costante per il processo e pari a 481,5 kJ/mol è stata supposta. Il valore di "n" è stato invece determinato rappresentando il $ln\left[ln\left(\frac{1}{1-f}\right)\right]$ in funzione di $\left[2ln(T) - \frac{E}{RT}\right]$ per una determinata velocità di riscaldamento e, allo stesso modo, in funzione del $ln\left(\frac{1}{\emptyset}\right)$ per una temperatura fissata.

6) CARATTERIZZAZIONE DEL MATERIALE RICEVUTO

Gli acciai utilizzati per effettuare lo studio sono stati la lega commerciale X20 CrMoV 12-1 e tre leghe sperimentali a bassissimo tenore di C preparate dall'azienda "Centro Sviluppo Materiali SPA" sede di Roma con tecnica VIM. Le colate sono state da 80Kg; successivamente il materiale è stato laminato in lastre di 20mm di spessore.

La microstruttura del materiale ricevuto è risultata un misto di martensite e δ ferrite risultante dal processo di lavorazione meccanica.

L'analisi inclusionale ha poi messo in evidenza la presenza di ossidi derivanti dal processo di disossidazione quali particelle di SiO_2 globulare o di ossidi misti di Al e Si in forma di stringhe di 10-

20 µm. La presenza di solfuri di mangenese è stata invece evidenziata solo dalla microscopia elettronica, in quanto si tratta di particelle globulari di dimensioni non risolvibili otticamente. La quantità totale di ossigeno contenuta nell'acciaio è stata poi stimata in circa 80ppm.

Infine, le temperature critiche del materiale laminato sono state valutate attraverso analisi dilatometriche; il trattamento di normalizzazione del materiale in pezzi da 11X17X10mm con un mantenimento di 1,5h a 1050°C ha quindi preceduto l'analisi sperimentale successiva.

7) RISULTATI SPERIMENTALI E DISCUSSIONE

Il materiale utilizzato è stato per prima cosa normalizzato come precedentemente descritto risultando totalmente martensitico a seguito del trattamento. Successivamente, l'acciaio è stato rinvenuto a differenti temperature con un mantenimento di 2h. L'intervallo di temperatura considerato è stato tra i 700 e i 940°C.

La lega 2504 e la commerciale X20CrMoV 12-1 sono state analizzate per l'intero intervallo considerato.

La lega 2504 ha mostrato la formazione di una seconda fase chiaramente visibile attraverso l'analisi metallografica: inizialmente a bordo grano (740°C), quindi in posizione interlaminare per temperature di trattamento superiore ai 750°C; infine, la seconda fase è risultata completamente sviluppata a 880°. Le misure di durezza si sono mostrate coerenti con quanto osservato attraverso le tecniche di microscopia; infatti il materiale trattato mostra un incremento progressivo della sua durezza all'aumentare della temperatura di trattamento nell'intervallo sopra indicato: questo comportamento suggerisce la formazione di austenite, rilevata quindi in seguito come martensite non rinvenuta (fase che mostra elevata durezza) a temperatura ambiente. Infine il test dilatometrico ha confermato la formazione di austenite aggiungendo dettagli quantitativi all'analisi.

L'analisi metallografica del X20CrMoV 12-1 non ha invece consentito di distinguere la formazione di alcuna seconda fase, non fornendo dati sul superamento delle temperature critiche. Le prove di durezza inoltre non sono state in grado di determinare con precisione i limiti della trasformazione lasciando aperta la questione sul motivo principale di incremento di durezza per temperature superiori agli 860°C. La solubilizzazione dei carburi non è infatti distinguibile dalla formazione di martensite non rinvenuta attraverso prove di durezza. Tuttavia, il ruolo centrale del C nell'incremento di durezza osservato è stato dedotto da dati di letteratura e simulazioni numeriche.

L'analisi cinetica è stata quindi effettuata per la lega 2504.

La misura dell'energia di attivazione per la trasformazione si è dimostrata fortemente influenzata dalla temperatura rilevata: a seguito di incoerenze ritrovate nei dati, le curve sono

state spostate prendendo come riferimento la temperatura di martensite start. L'energia di attivazione è stata quindi misurata ostante e pari a circa 480 kJ/mol.

Il dato ottenuto è troppo grande per indicare una trasformazione controllata unicamente da processi diffusivi e indica la presenza di processi di nucleazione durante l'intero svolgimento della trasformazione.

La coesistenza di processi diffusivi e di nucleazione è confermata anche dall'analisi JMAK attraverso il valore di "n" che, negli stati iniziali della trasformazione, è compreso tra 1,5 e 2,5. Il successivo decremento di "n" è stato spiegato principalmente attraverso fenomeni di impingement.

8) CONCLUSIONI

Lo studio ha mostrato le potenzialità dell'accoppiamento di metallografia, prove di durezza e dilatometria per analizzare la trasformazione α'→γ in acciai 9-12wt.% Cr. In particolare la metallografia si è dimostrata in grado di determinare con precisione il superamento delle temperature critiche per gli acciai a bassissimo tenore di carbonio, mentre si è dimostrata inefficace laddove quest'ultima condizione non è soddisfatta. Le prove di durezza al contrario mostrano dati solo relativamente affidabili: i fenomeni di precipitazione/solubilizzazione non vengono distinti dalla formazione di austenite e, anche in assenza di fenomeni secondari, le temperature critiche appaiono spostate rispetto alla loro posizione reale.

La dilatometria consente di aggiungere dati quantitativi e di analizzare la cinetica del processo, completando così il quadro di informazioni necessarie ad uno studio completo del fenomeno analizzato.

9) PROSEGUIMENTO DEL LAVORO

A seguito del successo dimostrato nel valutare la trasformazione per le leghe sperimentali, l'analisi metallografica è stata estesa ad altri due materiali dimostrando anche in questo caso le sue potenzialità nel riconoscere la formazione di martensite non rinvenuta in acciai a basso tenore di carbonio.

TABLE OF CONTENTS

TABLE OF FIGURES

ABSTRACT

The aim of this project is to study the potentials of dilatometry for the investigation of 9-12wt.% Cr steels. In particular, the project focuses on the α'→γ transformation in normalized extra low carbon steels. The analyzed alloys had been set up by CSM in order to study the behavior of 9-12wt.% Cr steels during long term high temperature exposure. Commercial X20CrMoV 12-1 have been analyzed too.

In order to investigate the potentials of the technique, dilatometry has been coupled with optical microscopy and hardness measurements.

This study shows how optical microscopy and hardness measurements give useful information about the critical temperatures A_1 and A_3, why these techniques are limited, and how dilatometry has the possibility to overcome these limits.

Furthermore, the potential of isochronal dilatometry to investigate the kinetic of transformations is shown.

1. INTRODUCTION

The use of dilatometer for investigation of steels is reported by important scientist like professor E.J. Mittemeijer and professor H.K.D.H. Bhadeshia; professor Mittemeijer, in particular, used the technique to study steels, presenting kinetic analyses and pushing its limits further. However, the potential of dilatometry is far from being fully developed. This project was based upon this concept, using it as foundation for further experiments.

In order to developed the analysis, CSM gave the opportunity for 10 dilatometric tests. These were coupled with standard metallographic techniques and hardness measurements performed at DTU.

The analysis had been based on a review of the reported state of the art. Two analysis had been proposed: the first is a new proposal, and is based on comparison of linear expansion coefficients for quantitative analysis of the fraction of austenite formed during an intercritical treatment; the second is a kinetic analysis performed with isochronal tests.

9-12wt.% Cr steels were chosen since they represent one of the most important materials for energy, and will be a key point in research activity in the next years.

2. 9-12wt.% Cr STEELS

2.1. BACKGROUND

Martensitic steels containing 9-12wt.% Cr are materials suitable for high temperature applications as they combine good strength, high temperature stability, high oxidation resistance and good possibility to be processed (1).

In particular, 9-12wt.% Cr steels are widely used in power plants since they fulfill all the necessary requirements at moderately low prices. Among them P91 (X10CrMoVNb 9-1), P92 (X10CrWMoVNb 9-2), X12CrMo9-1 and X20CrMoV 12-1 are the most commonly used. In this field, the opportunity for higher temperature and pressure exposure is a central point to gain efficiency and the driving force for research activities.

Other important applications are in gas and hydraulic turbines, aircraft and missile parts, oil and nuclear industries, high pressure applications, tools, dies and molds (1).

Regarding their structure, *"these steels are generally furnished after normalizing and tempering heat treatments, with final microstructure consisting in fully tempered martensite"* (2). Tempered martensite that consist *"of ferrite subgrains with carbides or nitrides precipitated on prior austenite grain boundaries, ferrite subgrain boundaries and on dislocation between the subgrains*" (3).

This class of steels is often characterized by the addition of strong carbide and nitride formers like V and Nb; this addition is necessary to improve creep resistance causing precipitation of fine carbo-nitrides during tempering. Moreover W and Mo could be suitable for further additions.

9-12wt.% Cr steels suffer from poor weldability. Weld joints are very brittle and problematic post weld treatments have to be performed (4); these can cause failure if incorrectly done.

2.2. ALLOYING ELEMENTS

Chromium is the most relevant alloying element in terms of quantity and gives the name to the class of steel. "*The lower and upper Cr contents are defined in order to maintain sufficient oxidation resistance and complete hardenability respectively*" (5).

Carbon is useful to form carbide and its content has been limited (normally < 0.2wt.%) for weldability reasons. Further developments are nowadays in the direction of extra low carbon steels.

Nitrogen and Boron are also used to form fine precipitates. The formation of fine precipitates is important for the stability of the material at high temperature.

Vanadium and Niobium are the carbide, nitride and boride formers; when added their content is about 0.06% for Nb, and 0.2% for V. Tantalum can also be added.

Molybdenum and Tungsten are also added but their content is not well defined; increasing their content is one of the possible developments in the chemistry of these steels. Their strengthening mechanism is both solution strengthening and precipitation hardening due to precipitation of intermetallic $Fe_2(Mo,W)$ Laves phases during creep exposure.

V, Nb, Cr, Mo, W are all ferrite forming elements. Austenite formers like Ni and Co are added in order to prevent the formation of ferrite. Co is preferred, since Nickel decreases the critical A_1 temperature, but is rather expensive.

2.3. STRUCTURAL FEATURES

2.3.1. Phase diagram

Fe, Cr and C are the most important elements in defining the structure of Cr steels. The possible equilibrium phases are austenite, ferrite and carbides. In order to illustrate the stability region of the different structures and consequently the obtainable ones in equilibrium condition, the phase diagrams Fe-C for a fixed Cr content (12%) and Fe-Cr for a fixed C content (0.1%) are presented in Figure 1 and Figure 2 respectively.

2.3.2. Ferrite

Ferrite, phase α in Figure 1 and Figure 2, has a body centered cubic structure. It is the most stable phase in a large range of composition and temperatures, but it is obtained only in few conditions, like after long time exposure at high temperature or during hot working operations. Normally its presence is avoided because of its low mechanical strength.

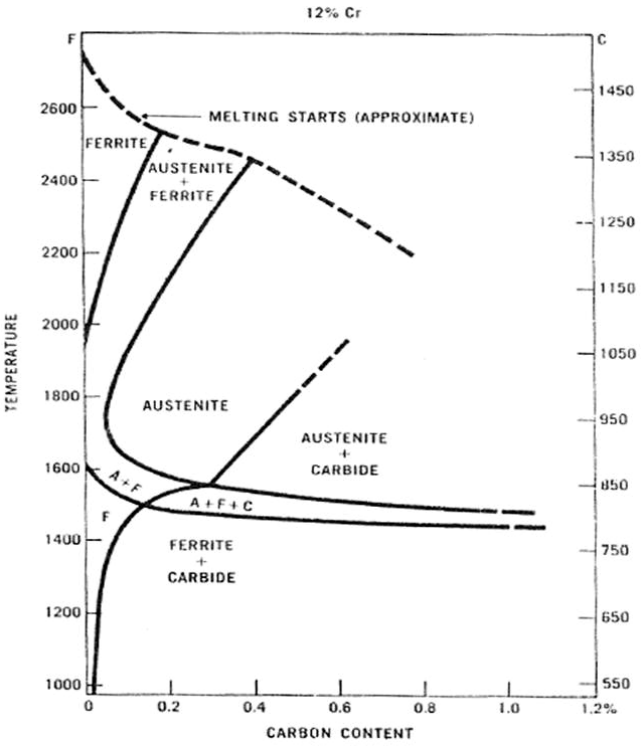

Figure 1. Phase diagram Fe-C for 12%Cr content (1).

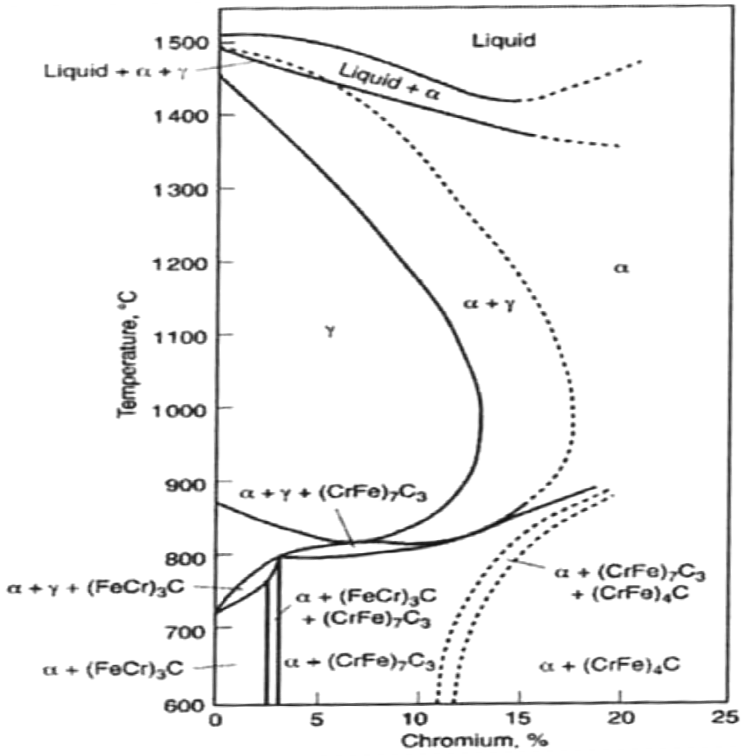

Figure 2. Phase diagram Fe-Cr for 0.1%C content (6).

2.3.3. Austenite

Austenite, phase γ in Figure 1 and Figure 2, has a face-centered cubic structure. This structure is more closely-packed than a body centre cubic, but has larger interstitial spaces. As a result, solubility of interstitial element like C and N is larger but, on the other hand, "*diffusion of both substitutional and interstitial solute occurs much more rapidly in ferrite than in austenite*" due to lower free space for atoms to move (7).[1]

Larger solubility implies that carbide and nitride are less stable in the austenitic matrix than in ferrite and they can be dissolved. This process is generally intentionally done in order to homogenize the structure and to obtain complete hardenability and it is called austenitization; it is performed maintaining the material at high temperature. If the following cooling is performed in air the process is called normalization and is used to recover the material to an original reference state.

The different packaging of α and γ phases is visible in a dilatometric experiment: the α→γ transformation can be easily visualized due to a strong contraction of the sample.

The α→γ transformation occurs between A_1 and A_3: the temperature of appearance of austenite is defined A_1, while A_3 defines the temperature where the material is fully austenitic; A_1 and A_3 are called critical temperature for the steel.

The α→γ transformation is a pretty fast transformation compared to phenomena like precipitations or dissolutions (Figure 3).

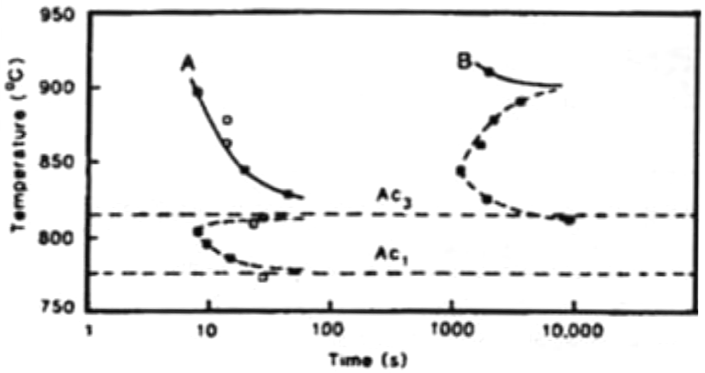

Figure 3. Reaustenitization, TTT curves determined by isothermal dilatometry in a Fe-10%Cr-0.2%C steel; curve A: complete austenitization; curve B: end of carbide dissolution (8).

[1]To be precise, free space is not an appropriate definition. It is the opportunity for atoms to jump from a position to another to be lower; so it is the "size of the passage" from an interstitial space to another site to be smaller.

Moreover, transformation temperature and velocity are a function of composition, temperature of maintenance, and heating rate. Dilatometric measurements can be used to study the influence of these different parameters and for the determination of the activation energy for the transformation, giving useful indications on the nature of the process (9), (10), (11), (12). As a matter of fact, the way in which austenite forms is not always the same and it is dependent on different aspects: for example the microstructure present before the heating process has a very large influence. "*In microstructure consisting of ferrite and spheroidized cementite particles, austenite forms first at the interface between carbide and ferrite… austenite formation depends on carbon diffusion through the austenite as the carbide dissolves*" (13). In martensitic microstructures two processes can take place: equiaxed morphologies can arise when austenite forms at the prior grain boundaries or the morphology could be acicular (or lath-like) when the austenite forms by nucleation between laths of martensite. In the latter case a shear mechanism takes place. This process is characteristic of Fe-Ni C free alloys (13) and of microduplex 9-12wt.% Cr steel (Figure 4) (5),(14).

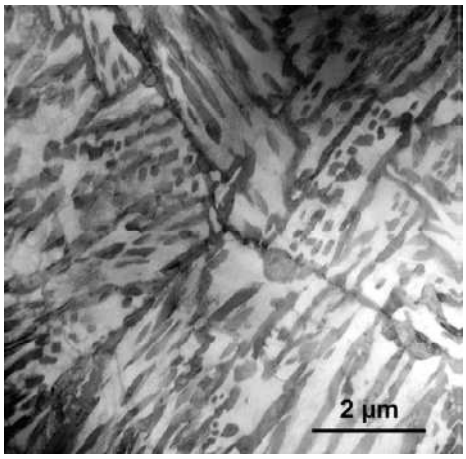

Figure 4. TEM investigation of a 10%Cr, 6%Co, 4%Ni, %Mn, Mo, V, Nb, N steel: microduplex structure after normalization at 1175°C for 1h followed by 4h tempering at 600°C (5).

Austenite's microstructure depends on the austenitization process: both time and temperature of the heat treatment are relevant. Higher temperature or longer time both contributed to an enlargement of the austenite grain; fine stable precipitates like NbC, on the other hand, can contribute to avoid this phenomenon.

The dimension of the austenitic grain can be studied at room temperature analyzing the resulting martensite. In martensitic steels, by the use of optical microscopy, "*the austenite grains are revealed rather clearly by etching differences associated with varians orientations of martensite in the different austenite grains*" (13). Afterwards, grain size determination from image analysis can be assessed.[2] Figure 5 shows different grains as revealed by optical microscopy.

[2] Different methods can be used. Methods are for example reported in (15) and (13).

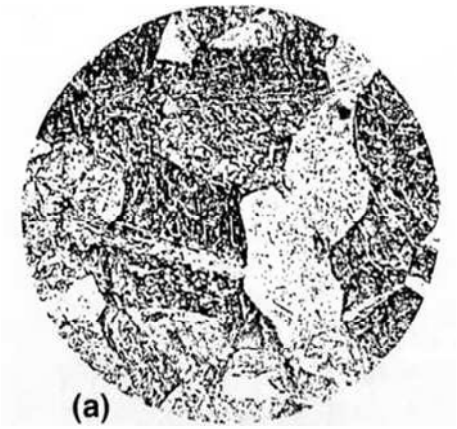

Figure 5. Martensitic microstructure: different grains are visible due to etching inhomogeneities (13).

2.3.4. Martensite

Equilibrium phases are not the only ones that can be observed in steels. As a matter of fact, during cooling, the austenitic γ phase can transform into ferrite α or into metastable martensite α', depending on the cooling rate.

As already mentioned, ferrite is almost never present in this family of steels: high content of alloying elements results in an easy quenching behavior. Ferrite could only appear if very slow cooling rates are performed; in the class of steels under analysis, an air cooling process is fast enough to grant the formation of a fully martensitic structure in rather big components (self-quenching behavior): "*slow cooling could only produce these effects* (ferrite in X20CrMoV 12-1) *when air cooling section sizes 500mm in diameter and greater*" (16). This concept is quantitatively illustrated by the use of CCT diagram. Two examples of CCT curves for the X20CrMoV 12-1 steel are shown in Figure 6.

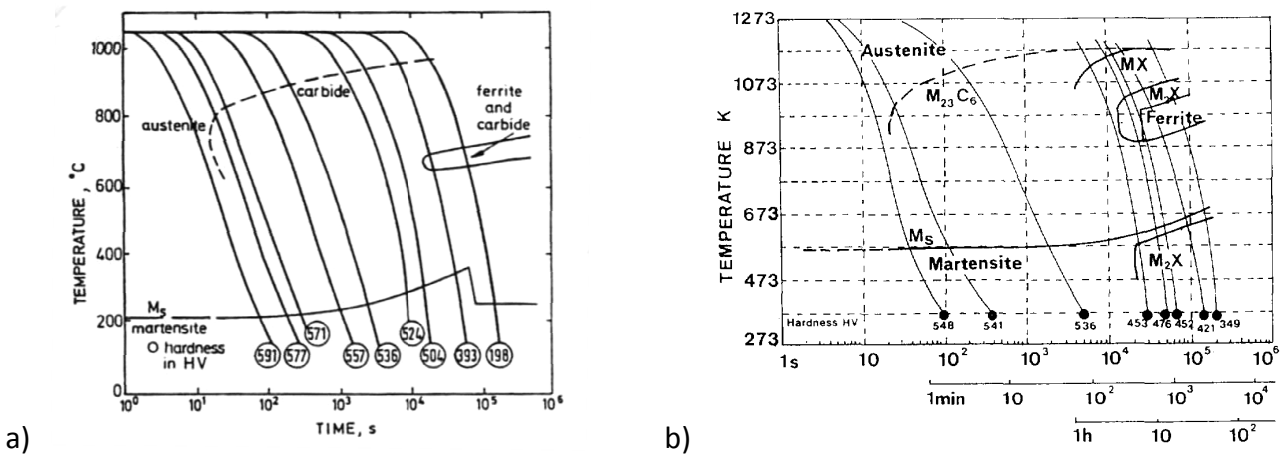

Figure 6. CCC diagram for X20CrMoV 12-1 a)→ (16); b)→(17).

Figure 6 also shows that hardness measurements could be performed to detect the formation of ferrite. Moreover it is visible that, even for fully martensitic steel, the obtained hardness is a function of the cooling rate. This is confirmed even by Briggs and colleagues: "*air-cooled steels tend to show slightly lower hardness values than quenched specimens*" (1). This means that for a correct comparison between hardness measurements the cooling rate has to be kept almost constant between the different tests.

The γ→α' transformation is a diffusionless phenomenon: martensite is developed by a coordinate movement of atoms in a shear process. Due to the nature of the transformation, the transformation rate depends on temperature but is independent of time; the transformation occurs between constant temperatures that are opportunely called martensite start M_s and finish M_f.

M_s is strongly influenced by the alloying elements, and can be predicted using an empiric equation, which for 8-14wt.% Cr steels is shown in Equation 1:

$$M_s = 635 - 474(C + 0{,}86N) - (17Cr + 33Mn + 17Ni + 39V)$$

Equation 1. Empirical equation to determinate Ms in 8-14%wt. Cr steels; the equation is valid if the elements contents are expressed in wt.% (14).

The obtained microstructure is different dealing with different carbon contents: high carbon contents favor "plate" like martensite (higher than 0.8% for a fully plate like) while "lath" martensite is formed in low carbon alloys (lower than 0.6% for a fully lath like). For 9-12wt.% Cr steels, due to their low carbon content, only "lath" martensite can be expected. "*These laths consist of parallel arrays or packets of basic units which are 0.1 to 0.5 micrometer thick"*(18). By the use of optical microscopy the structure could be detected: *"the individual lath cannot generally be resolved by optical microscopy, and it is the packets of laths that are visible"*. About its growing process, "*the packet grows either by formation of nonadjacent but parallel variants or by successive nucleation and growth of parallel laths adjacent to one another. The transforming grain of austenite may also be portioned by the formation of non parallel variants in different regions of the grain"* (19).

An example of microstructure resulting from a fully martensitic transformation in a martensitic steel, as it appears by the use of optical microscopy, is shown in Figure 7.

However the etching process is very important in determining what kind of structure can be visualized. For example, in C-steels, Picral is very slow in attacking un-tempered martensite while Nital or Villella´s are able to clearly develop its basic structure. On the other hand "*undissolved particles of cementite in tempered steel that are visible after etching in Picral cannot be discerned among the background structure so strongly developed by Villella's reagent*" (19).

This means that the visible aspects are not universal aspects: they are dependent on the etching process and different etchings have to be performed in order to revealed different features. Moreover, attention has to be paid during comparison in order to avoid meaningless analysis.

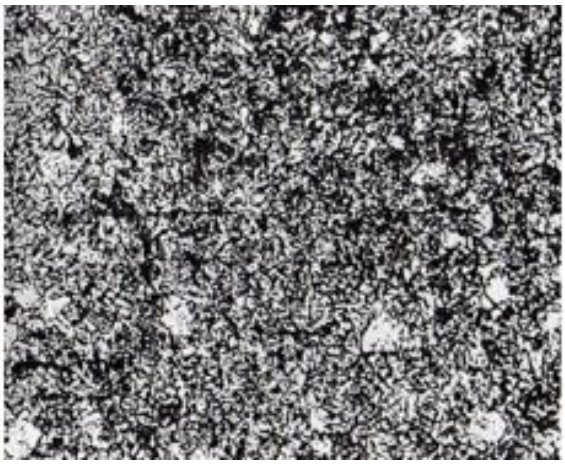

Figure 7. Martensitic stainless steel AISI 410 stripped in the hardened condition after annealing at 802°C, holding for 30 min at 954°C, and air cooling. The structure is ferrite-free martensite; electrolytic etching in HCl-methanol; 500X (20).

From the crystallographic point of view, martensite shows a tetragonal b.c.t. structure; this structure is strongly connected to ferrite. Martensite comes from a distortion of the b.c.c lattice due to the impossibility for C to dissolve in the interstices of the lattice. The tetragonality of the structure is connected with the carbon content as shown in Figure 8.

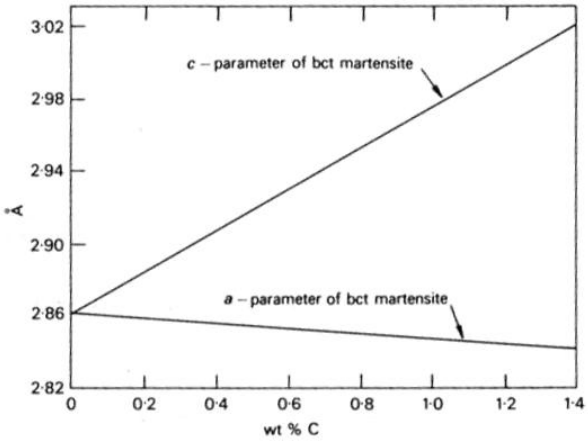

Figure 8. Effect of the carbon content on the lattice parameters of martensite [Å] (7).

2.3.5. Tempered martensite

Tempering is a heat treatment consisting of heating and maintaining the steel at a temperature higher than the one planned for service but lower than A_1. "*Tempering is performed in order to recover ductility from the hard and brittle martensite*" (21). For this family of steel "*the temperature range for tempering is usually in the 680-780°C depending on the properties required*" (21): high strength steels are obtained with lower treatment temperature while higher ductility is obtained increasing the temperature. As already mentioned, the upper temperature limit is A_1: if this temperature is overcome, and austenite forms during tempering, brittle fresh martensite is obtained during cooling making the treatment meaningless.

During tempering, important precipitation phenomena occur; these precipitations are called secondary, to distinguish them from the ones that can occur during the austenitization process called primary, and are mainly carbides and nitrides.

Precipitation can be subdivided in three stages. First of all nucleation of particles occurs; nucleation is mainly controlled by the thermodynamic driving force and the interfacial energy. Growth of the formed particles follows; during this stage both volume fraction and precipitate size increase, but any new particle is formed; diffusion is assumed to play a central role in controlling the process. In the end coarsening occurs; coarsening is controlled by the decreasing of the total interfacial energy: the largest particles grow while the smaller ones are dissolved and disappear; the volume fraction remains constant during this last process.

Carbides and nitrides precipitate as fine particles along inhomogeneities like prior austenite grain boundaries, martensitic lath boundaries and dislocations (21). Carbides are not visible by optical microscopy for low temperature treatments while they become visible increasing tempering temperature due to faster growth and coarsening (19). Figure 9, for example, shows dispersed carbides in a carbon steel after tempering at 700°C for 2 h. Nitrides are too small to be detected by optical microscopy.[3]

Precipitation phenomena and their features can be studied coupling different techniques, like microscopy and hardness measurements (23), with a dilatometer (24), (25), (26). Differential scanning calorimetry (DSC) or both (dilatometry and DSC) can be used as well: "*the combination of these two experimental techniques is very powerful and allows the identification of all the stages occurring during tempering*" (27).

[3] Their typical dimensions are by far lower than the detecting capabilities of optical microscopy; dimensions of nitrides are reported for example in (2), (21) and (22).

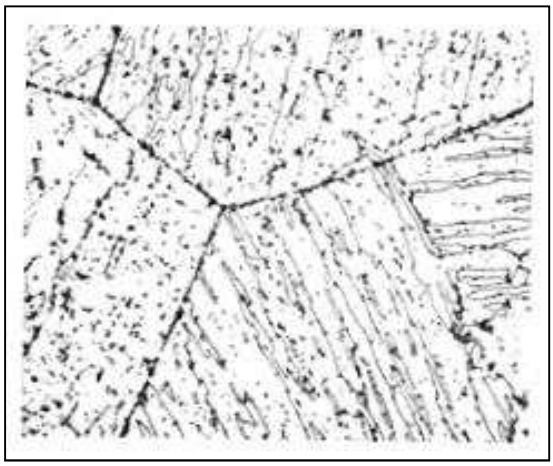

Figure 9. Microstructure of lath martensite in a Fe-02%C alloy after tempering at 700°C for 2h. Light micrograph; Nital etching; 500X (13).

About hardness measurements, hardness of martensite is very much influenced by C and N. First of all it is a function of C content and strongly increases with it (19). The same is true for nitrogen and its influence is evident even in tempered martensite (28).

Moreover, performing hardness measurement, precipitation hardening due to secondary precipitation is visible (Figure 10). The resulting structure can be studied by microscopy techniques; electronic microscopy clearly shows the presence of precipitates (a SEM picture revealing the presence of carbides in tempered steel is shown in Figure 11).

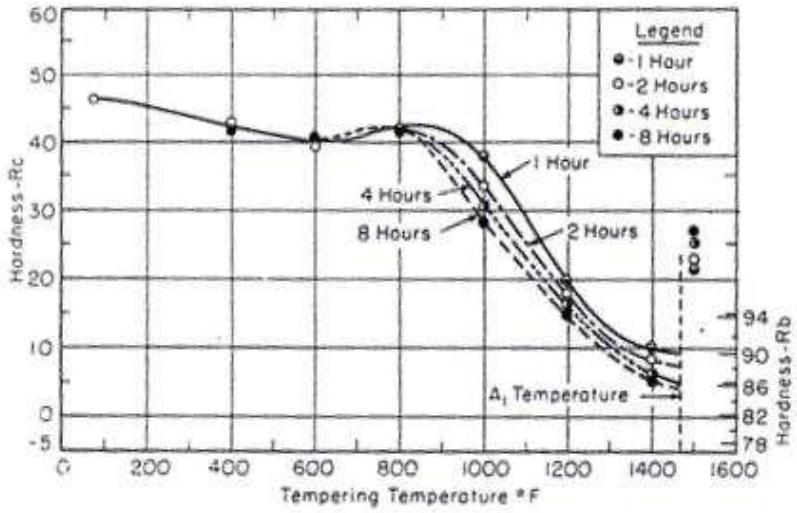

Figure 10. Effect of tempering temperature and time on hardness of a quenched and tempered 12% Cr steel (29).

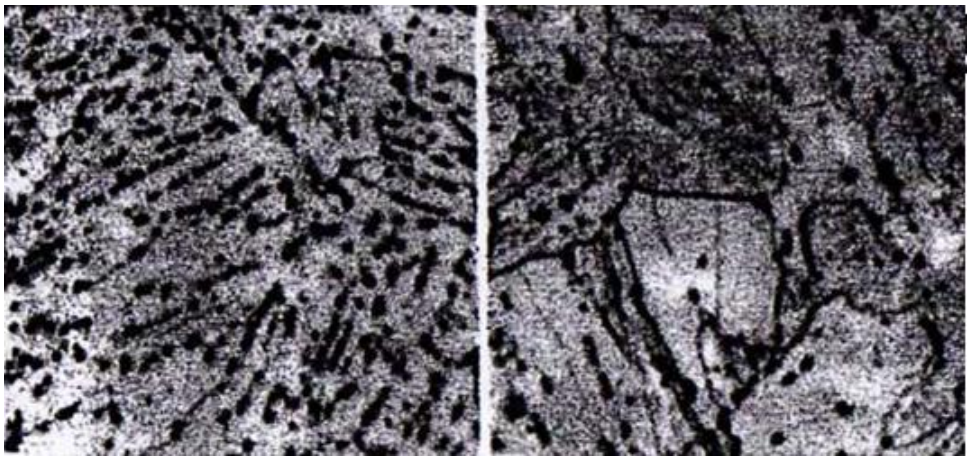

Figure 11. 12% Cr steel: microstructure of a sample quenched and tempered 2h; Picric-HCl etching; 2500X; a)-->760°C, b)-->815°C (29).

Normally, solution hardening of the matrix due to interstitials is stronger than precipitation hardening; consequently steels are much harder when C or N are dissolved into the matrix.

From the point of view of optical microscopy, Cr steels microstructure is easily revealed by etching in Villella. The typical aspect of tempered martensite in Cr steels, as revealed by optical microscopy after Villella's etching, is shown in Figure 12. This is not very different from the one obtainable for fresh martensite. As a matter of fact, when tempered martensite is present with untempered one, they are normally not distinguishable (30). An opportunity to distinguish them is sometimes represented by a weak etching reagent; for example, in carbon steel using Picral or Sodium bisulfate tempered martensite could be revealed as it is more reactive to etching reagent than that formed after quenching (19).

Figure 12. AISI 410 forging, hardened by holding 1h at 982°C and air quenched; finally tempered 2h at 566°C and air cooled. The resulting structure is tempered martensite and carbide; Villella's reagent; 100X (20).

However, other methods have to be performed in order to clearly show the presence of the two different phases. Many of them are unable to indicate the amount of fresh martensite (or as well, the amount of austenite formed during the maintenance at high temperature), its growing aspect, as well as the real A_1, but have other interesting features.

Hardness measurements, for example, can be assessed: this is a very common method. Hardness is expected to increase when A_1 is overcome due to formation of fresh martensite during the subsequent cooling; however "*a conflict takes place between the softening which results from tempering the initial martensite and the hardening due to the formation of new martensite area*" (30). As a result, the increasing in hardness is shifted to treatment temperatures that result higher than A_1.

A dilatometer can be used to study the phenomenon as well: a contraction due to austenite formation is visible. Moreover, the fraction transformed can be measured precisely by comparison of the linear expansion coefficient (30).

In the end, it has to be mentioned that the opportunity to visualize quench cracks in tempered steels by optical microscopy is given. Quench cracks are easily distinguished as they are covered by oxide during tempering in air (Figure 13).

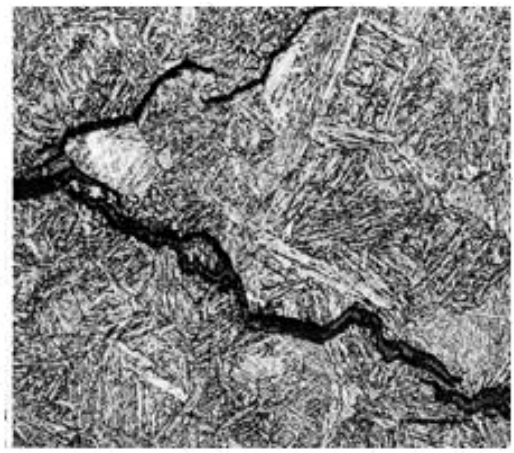

Figure 13. Martensitic stainless steel AISI 410 forged, hardened, tempered and finally etched in Villella's reagent; 100X (20).

2.3.6. δ-Ferrite

Ferrite and austenite can also be observed as δ ferrite and retained austenite. However, in order to achieve optimum strength, it is important to have a fully martensitic structure at room temperature: δ-ferrite and retained austenite have to be avoided.

δ ferrite is also called residual ferrite to distinguish it from α ferrite formed during tempering even if they show the same structure.[4]

As shown in Figure 1 and Figure 2 the amount of austenite that can be obtained is a function of temperature and composition. Only steels that are treated to become fully austenitic at high temperature show afterwards a fully martensitic structure after cooling. The fraction of untransformed phase during the maintenance at very high temperature is afterwards revealed as δ ferrite at room temperature.

This means that both composition and austenitization temperature have to be balanced to avoid the unwanted structure. Temperatures that are too low to fully develop austenite are not suitable. Moreover "*the austenitizing temperature is selected to give complete solution of carbide without excessive grain growth or formation of delta ferrite*" (1). The highest suitable temperature becomes relevant when a hot forming treatment is performed; if this temperature is exceeded, δ-ferrite appears (Figure 1 and Figure 2) and, if a fast cooling follows, it results in the maintenance of the unwanted structure. The resulting structure is shown in Figure 14 on "as forged" material: "*this hot worked structure consists of larger, more elongated banded delta ferrite than in a martensite matrix*" (20).

Hardness measurement can be performed to identify the presence of δ ferrite as the resulting structure is much softer.

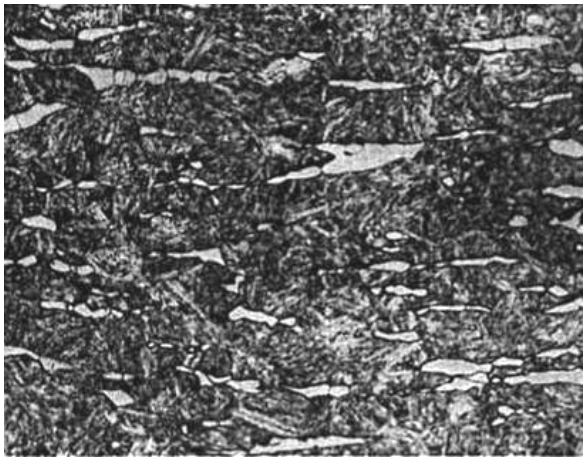

Figure 14. AISI 410 as forged; Villella's reagent; 100X (20).

[4] Actually, residual ferrite is a better definition since ferrite shows as an open field in the state diagram for this class of steel; however in this report we are going to use the terminology "δ-ferrite" in conformity to the specific scientific literature.

2.3.7. Retained Austenite

Retained austenite can be found in steels if M_f is not overcome during cooling. This happens, in normal conditions, when M_f is below room temperature. Alloying elements all contribute (with the exception of Co) to decrease M_f but C is by far the strongest one. Normally a carbon content higher than 0.3-0.4% is necessary to decrease M_f below room temperature (Figure 15). This is not the case for the class of steels analyzed. However, M_f could be just below room temperature for an X20CrMoV 12-1 steel and a very small amount of retained austenite could be present in the steel (31), (1). Nevertheless "*small volumes of retained austenite, are not easily detected by optical microscopy*" (19): this means that nothing clearly observable with this technique could be identified as retained austenite in our case.

In the end it has to be mentioned that all the retained austenite in these kinds of alloys decomposes during tempering: no retained austenite is expected to be found in tempered steels.

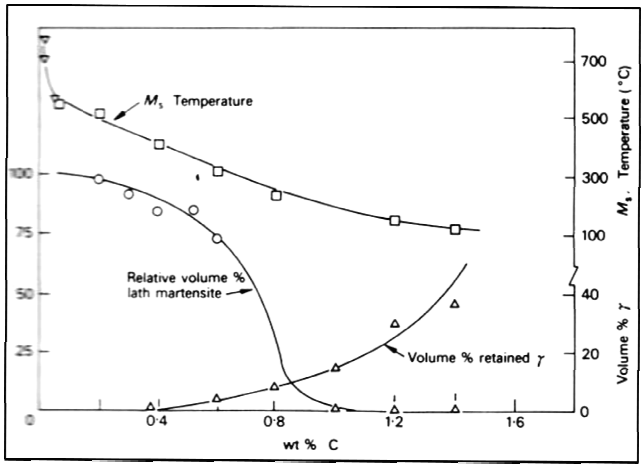

Figure 15. Ms, fraction of lath martensite and fraction of retained austenite as a function of T for martensitic steels (7).

2.3.8. Secondary phases

Secondary phases that form in 9-12wt.% Cr steels are principally carbides, nitrides and Laves phases. Carbide and nitride nucleate, grow and can start coarsening during tempering while Laves phase first develops after a long time of high temperature exposure (3). Borides, silicides, chi and sigma phases can also form.

Moreover many studies have been carried out on Z-phase; this phase forms after very long exposure at high service temperatures since it is considered to be the cause of failure due to dissolution of MX particles leading to a reduced creep resistance (2), (21).

Figure 16 illustrates the most common precipitates in a 9-12wt.% Cr steel after exposure to high temperature for a long period of time.

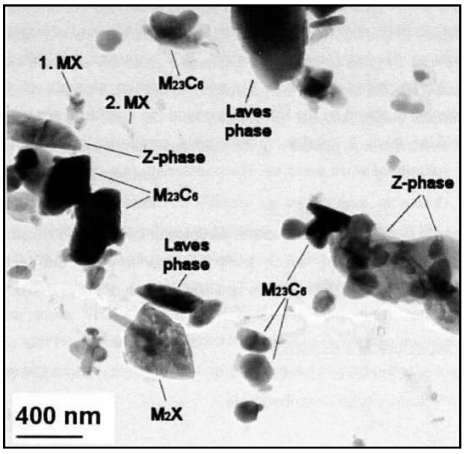

Figure 16. Common precipitates in 9-12wt.% Cr steels after long time exposure at high temperature. The matrix is ferrite. SEM picture (21).

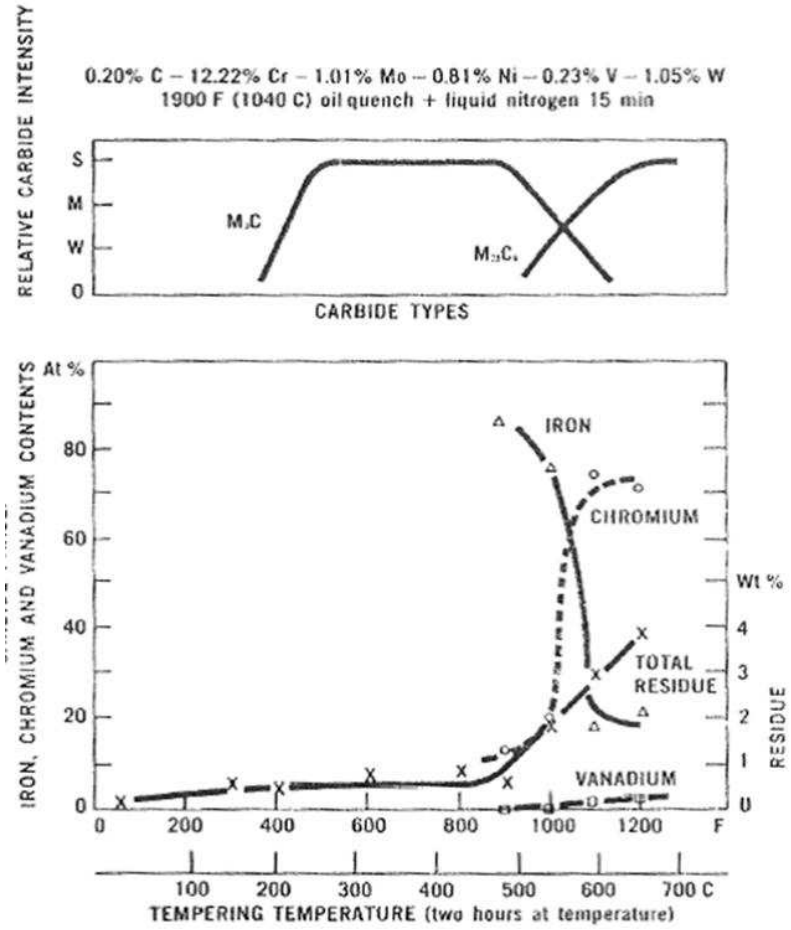

Figure 17. Carbide phases as a function of tempering temperature after 2h exposure (1).

Carbides can be formed by many elements as Fe, Cr, V and Nb; they have been object of many studies and a lot of data are available on their forms and stability in different alloys. Figure 17 shows the fraction of different carbides formed during tempering in an X20CrMoWNiV 12-1 steel. As shown, $M_{23}C_6$ is the most stable carbide (also Figure 16) and dissolves all the other carbides (except NbC) during tempering, "*it has a cubic crystal structure and consist mainly of Cr and C*" (21).

During tempering other compounds develop: they can be grouped in M_2X and MX. The firsts have a hexagonal structure and are almost completely Cr_2N; they are stable in high nitrogen content alloys and normally precipitate on grain boundaries and dislocations. The second group is formed by f.c.c. V and Nb carbo-nitrides and precipitated as primary MX at high temperature on austenite grain boundaries or as secondary (during tempering) particles on imperfections within the grains (21).

Gavrilijuk and Berns presented a complete review about precipitates in 9-12wt.% Cr steels: "*Hexagonal M_2X precipitates were found after tempering at temperatures above 400°C along fine cubic (NbV)X particles precipitated beyond 700°C. Cubic (FeCrV)(CN) and (NbV)(CN) precipitates were identified after ageing at temperatures up to 500°C, while beyond 600°C, $M_{23}C_6$ and Cr_2N are formed on the grain and interlath boundaries. With increasing nitrogen content $M_{23}C_6$ precipitates in the structure of tempered martensite is replaced by Cr_2(CN) particles*" (24).

As already mentioned in 2.3.5, precipitation phenomena and their features can be studied by the use of a dilatometer. Different behavior is observed for martensitic steel if C or N or both are added to the steel. In general three different phenomena are visible by dilatometry (24):

- Low temperature carbide or nitride precipitation (100-200°C);
- Residual austenite disappearance (550-600°C for C added; higher temperature or even not always visible for N steels);
- Precipitation of stable carbide and nitride (250-300°C for carbide; higher temperature for nitride).

Coupling the technique with electronic microscopy the nature of precipitates can be analyzed (25).

Moreover, the stability of precipitates in the austenite matrix is very important since these particles could be found after austenitization. This has to be avoided, as already specified, as the austenitization process is performed in order to fully dissolve them. The solubility of many compounds is shown in Figure 18. It can be seen that some compounds are difficult to dissolve. For example, TiC and NbC are the most difficult carbides to be dissolve and could easily stay un-dissolved even at the highest possible treatment temperature (7).

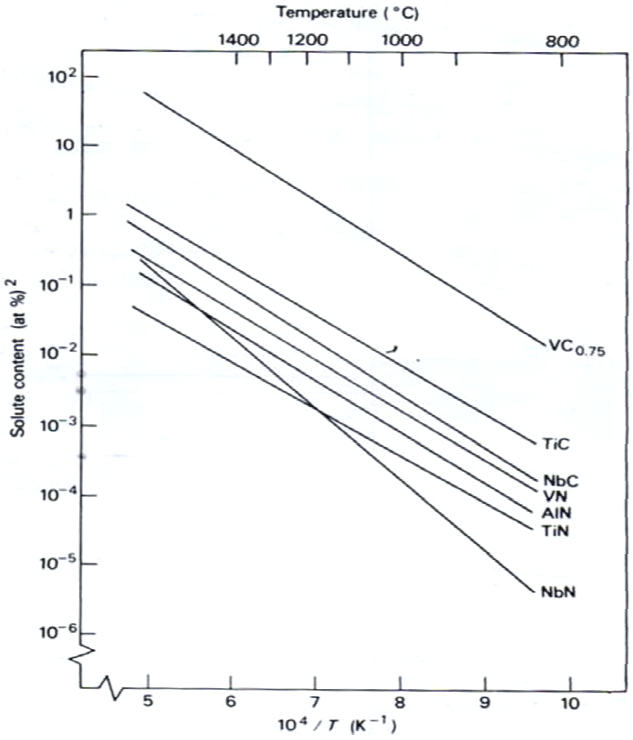

Figure 18. Solubility products of carbides and nitrides in austenite as a function of temperature (7).

3. PHASE TRANSFORMATION ANALYSIS: TECHNIQUES AND POTENTIAL

3.1. INTRODUCTION

3.1.1. Introduction to solid state transformations

Transformations can be divided in two main groups: diffusive transformations and diffusionless transformations. Diffusionless transformations involve a cooperative movement of atoms in a shear process: martensitic transformations are an example of diffusionless processes. On the other hand, diffusion dependent processes can be further classified in transformations with no changes in number of phases and composition, like allotropic transformations, or transformations involving changes in composition and number of phases, like decompositions (32).

The transformed phase can form through a nucleation and growth process or involve a nucleation free process. If the first is the case, the transformation rate will not increase monotonically with time; the maximal transformation rate will be reached after a certain period of time from the beginning of the process.

During the transformation process, heat can be released. Transformations involving heat development are referred to as first order. If that is the case the transformation will happen with a delay: when a thermal cycle is performed, a hysteresis process between the direct and the inverse transformation will appear. As a matter of fact, transformation temperatures will not be equal to the equilibrium temperatures and phenomena of supercooling and superheating will happen.

The α-γ transformation is a first order transformation. As a result, transformation temperatures will be different during an heating cycle and a cooling cycle: if A_1 and A_3 represent the critical temperature for the steel in equilibrium conditions, it is common practice to refer to Ac_1 and Ac_3 for the effective critical temperatures during a heating cycle; Ar_1 and Ar_3, on the other hand, indicate the critical temperatures for the steel in a cooling process.

Delaying processes are particularly important for transformations governed by a nucleation and growth process; as a matter of fact, the controlling process for the transformation can change due to a change in treatment conditions. Nucleation is promoted by supercooling/superheating phenomena, and strongly increases with supercooling/superheating; growth phenomena are instead controlled by atomic diffusion and proceed faster at higher temperature: diffusion

processes are normally considered thermally activated processes.[5] Diffusionless transformation are a-thermal.

3.1.2. Analysis principles for solid state transformations

In order to analyze a solid-state transformation, the degree of transformation (or the fraction transformed), has to be recorded as a function of time and temperature. This means that a physical property, connected with the different states, has to be monitored. Some examples are hardness, specific length, electrical resistivity, enthalpy, magnetization,…

In particular, when a physical property of a substance is measured as a function of temperature, while the substance is subjected to a controlled temperature program, a thermal analysis is being performed. The most common thermal analyses are DTA, DSC and dilatometry.

Decision about the technique used to monitor the transformation has to be performed accurately since different phenomena and sensitivity can be explored using different techniques. This means that the best technique has to be chosen for the singular purpose. On the other hand, test coupling can result in more information so that various complementary techniques can be combined.

Dilatometry and differential scanning calorimetry (DSC) are common techniques able to record a signal, elongation and enthalpy respectively, which is somehow related to the degree of transformation. The change in the property as a function of temperature T is not directly proportional to the fraction transformed. Nevertheless, a linear correspondence (Equation 2) can normally be assumed as a good approximation:

$$X_\beta = \frac{\lambda - \lambda_\alpha}{\lambda_\beta - \lambda_\alpha}$$

Equation 2. Fraction of phase β as a function of the physical properties λ.

Performing the analysis, attention has to be paid in order to avoid meaningless correspondence between recorded property and fraction transformed. For example, significant errors may occur performing the analysis, if a very small fraction is transformed or if the transformation is almost complete. Moreover, if the analysis is performed in non isothermal condition, the connection between recorded property and fraction transformed is related to the coefficient of linear expansion or the specific heat coefficient of the steel: during the analysis assumptions about their values have to be set.

[5] A thermal activated process shows an Arrhenius type dependence on T.

In a direct comparison DSC is considered to be better for detecting transformation temperatures A_1 and A_3 as it grants higher precision: Tokunaga and colleagues reported a scattering of 30°C for temperatures A_1 and A_3 by dilatometry versus less than 1.3°C reported for DSC (12); an accurate analysis about uncertainties in determination of transformation temperature by dilatometric experiments, was performed by Bhadeshia and colleagues in (33) referring to M_s: a standard deviation of 12°C is considered as achievable.

The decomposition of retained austenite is more readily investigated by DSC measurement than by dilatometry; moreover DSC is able to detect transformation that do not produce a change in length, like magnetic ones.

On the other hand, dilatometry is preferred for individuate carbide precipitation that are not clearly revealed by DSC (27).

Dilatometry and its potentiality will be a central topic of this work and the techniques will be analyzed further in 5.4; an example of a dilatometric curve obtained on an X20CrMoV12-1 is shown in Figure 19.

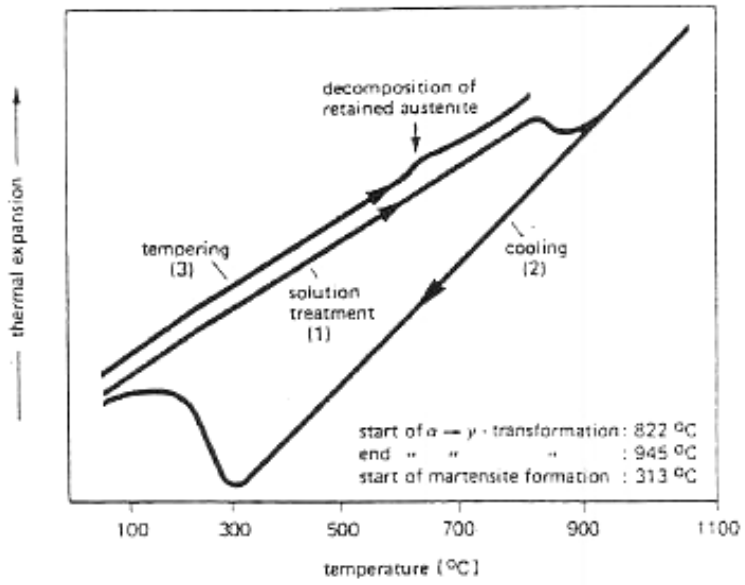

Figure 19. Dilatometric curve for a X20CrMoV steel; the typical phenomena occurring during the test are also presented in the picture (31).

3.2. ISOTHERMAL ANALYSIS

In isothermal analyses the sample is heated or cooled to the temperature of analysis. The physical property of interest is then recorded as a function of time (Figure 20). Afterwards, the fraction transformed can be inferred from the recorded physical property. Very important in

performing the analysis is to remember that significant errors may occur in the value calculated for the fraction transformed "f", if it is very small or very large: value between 0,2 and 0,8 are normally preferred.

The activation energy "E" for the transformation can be assessed without any assumption about a kinetic model. Measuring the activation energy "E" is important since this information can be used to determine the mechanism controlling the transformation. Mittemeijer illustrates the procedure to assets "E": "*the activation energy can be determined from the slope of the straight line obtained by plotting ln(Δt) versus 1/T*" (9). The graphical procedure is shown in Figure 21.

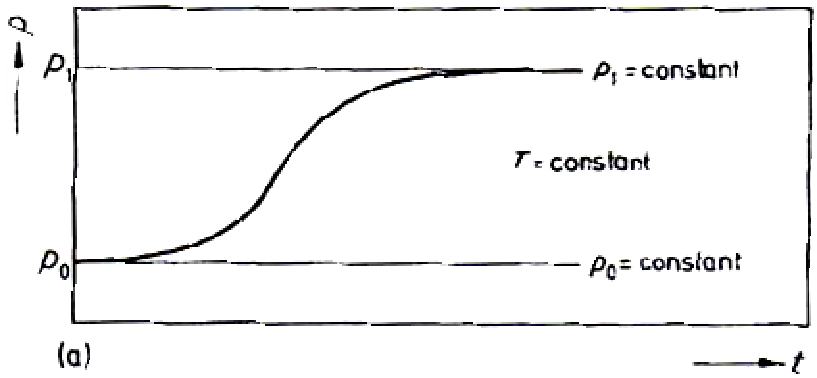

Figure 20. Behavior of the physical property, p, sensitive to the stage of transformation during isothermal analysis (9).

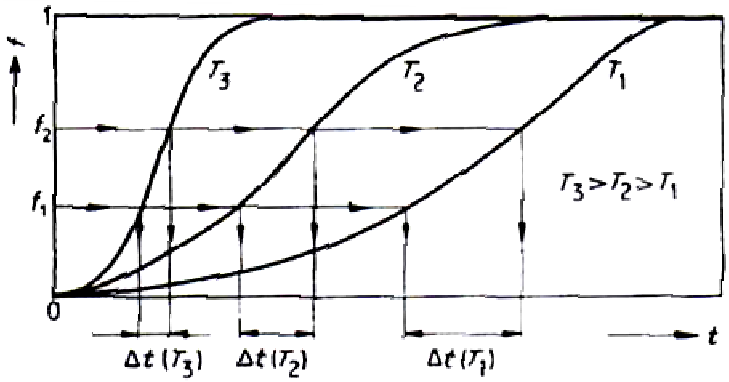

Figure 21. Procedure for calculate the activation energy for a transformation with an isothermal analysis (9).

Moreover, different processes can act, or be dominant, at different stages of the transformation; if this is the case, the analysis performed taking into account different stages of transformation results in different values of activation energy; this analysis is performed dividing the range of transformed fraction "f" in different parts (ex. 0.2→0.5; 0.5→0.8) (9). The considered reaction is not isokinetic as it doesn't shows a constant value of "E".

In the end, considerations about the first and second derivates of the fraction transformed "f" versus time are important.

Firstly, df/dt represents the transformation rate. In a homogeneous reaction, where "*the probability for the transformation to occur is the same for all locations in the virginal system, … the transformation rate decreases monotonically*"(9). On the other hand, "*heterogeneous reactions, as transformation where nucleation and growth play a role, in general exhibit a maximal transformation rate at some t>0*"(9).

Secondly, the maximal transformation rate is identified mathematically by imposing $d^2f/dt^2 = 0$. It can be demonstrated that during isothermal analysis this happens exactly at the same value of fraction transformed "f", independently from the temperature of maintenance (9). This information can be useful in performing the analysis where equal values of "f" have to be considered.

3.3. NON-ISOTHERMAL ANALYSIS

In a non-isothermal analysis the physical property is recorded as a function of temperature as shown in Figure 22. Between non-isothermal analyses, isochronal ones are of major interest as a kinetic analysis can be performed fairly straightforwardly.

Again, the activation energy "E" for the transformation can be measured without any assumption about a kinetic model. The procedure is explained by Mittemeijer assuming a thermally activated transformation: "*the activation energy can be determined from the slope of the straight line obtained by plotting* $\ln({T_f}^2/\emptyset)$ *versus* $1/T_f$" (9). The graphical procedure is shown in Figure 23.[6]

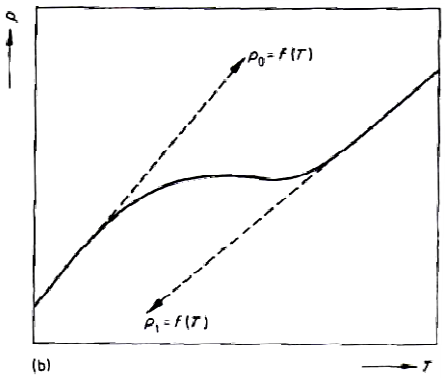

Figure 22. Behavior of the physical property, p, sensitive to the stage of transformation during non-isothermal analysis (9).

[6] The method is more generally a "Kissinger-like analysis" since it is based on the equation $\ln\left(\frac{{T_f}^2}{\emptyset}\right) = \frac{E}{RT_f} + constant$.

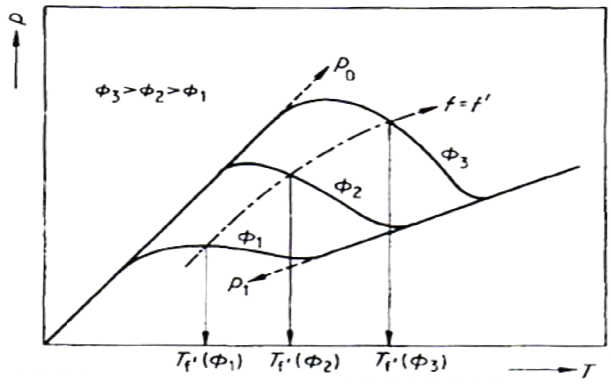

Figure 23. Procedure for calculate the activation energy for a transformation with a non-isothermal analysis (9).

In non isothermal transformations, isokinetic reactions required nucleation and growth rates to have the same temperature dependence. This condition is not satisfied in most of the cases; however, if a kinetic analysis is performed, isokinetic behavior is normally superimposed in order to simplify the analysis.

Moreover, all the considerations about the fraction transformed "f" presented in 3.2 are valid for non-isothermal analysis too.

The only difference regards $d^2f/dt^2 = 0$: as a matter of fact this condition is satisfied at the same value of "f" only in an approximate way.[7]

3.4. DILATOMETRY AND DIFFERENTIAL SCANNING CALORIMETRY (DSC): EXAMPLES OF APPLICATION

3.4.1. Introduction

In order to study the opportunities given by those two techniques, a literature review has been performed; our focus has been in particular on dilatometry.[8]

[7] The mathematical analysis of the approximation introduced is presented by Mittemeijer (9) and will not be reported here.

[8] A small collection of works, not directly mentioned here, regarding the use of dilatometry to analyze transformation occurring in steels is presented by Bhadeshia and colleagues at:
http://www.msm.cam.ac.uk/phasetrans/teaching.html

3.4.2. Isothermal analysis

Isothermal analysis is first of all used to construct transformation-time-temperature (TTT) curves. These are representing the evolution of transformation during time at different temperatures.

Normally TTT curves are used to determine the obtainable structure in steels, during a cooling process, starting from fully austenitic steels. This test is a very common one.

Isothermal transformation is often used to study the tempering stages of steels. However, isochronal analyses are normally preferred. As a matter of fact, an isothermal maintenance, in many occasions, is not able to distinguish between different processes, since different peaks can overlap, and the analysis can't be performed (9). Figure 24 shows the considered problem.

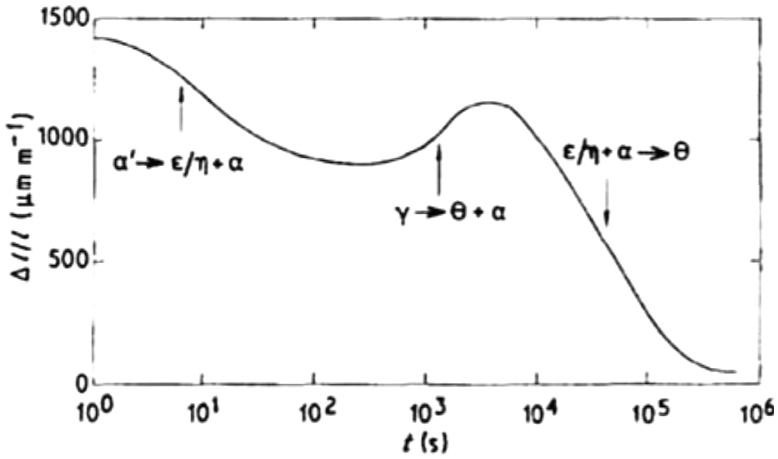

Figure 24. Impingement of different processes during tempering of a C steel in an isothermal test (9).

Transformation and dissolution times during an austenitization process can be analyzed as well (8). However, some problems can be considered in performing this kind of test and only few studies and data are available in literature. An example of debating problem is the way to obtain fast heating: austenitization time could be too fast for furnace heating and, on the other hand, it seems to be accelerated by faster magnetic induced heating (8).

Moreover, an example of isothermal kinetics analysis involving the γ→α transformation in steels can also be found in literature (34).

Furthermore, isothermal dilatometric curves, followed by a heating / cooling cycle, have been used to determine the austenite content in alloyed steel treated at different temperatures (30).

3.4.3. Isochronal analysis

Many examples of isochronal analysis of steel, with the use of dilatometry or DSC, can be found in literature. Both phenomena occurring during heating and cooling can be studied. The most common study regards the different stages of tempering and the determination of continuous cooling transformation (CCT) curves.

CCT curves are used to predict the obtainable structure of steels at different cooling rate and are of practical use in everyday metallurgy. In analogy to TTT curves they are constructed during cooling, starting from a fully austenitic steel. An example of CCT has already been shown in Figure 6.

Isochronal analysis to study tempering stages have been done on different alloys as well; some example have been considered for a review: analysis has been done by Gavriljuk and Berns on martensitic stainless steels (24), by Servat and Cizeron (23) on a low alloyed steel, and on Fe-Cr-N steels by Wiedermann and colleagues (25).

In all reported studies, analyses are based on dilatometric curves; all the analyses have been performed with a normalization process followed by a heating process to the tempering temperature. The heating rate had been chosen between 50°C/h and 1200°C/h depending on the steel features. Afterwards, data have been plotted as elongation $\Delta L/L_0$ versus temperature T or, to increase the detecting capability, in a differential form, as linear expansion coefficient "α" as a function of temperature T.

Coupling dilatometry with calorimetry further information have been added: Figure 25 shows an example of the different features visible coupling the two techniques. In the end, coupling the analysis with hardness measurements, optical and electronic microscopy, XRD, etc... the different peaks observed have been recollected to different phenomena occurring in the steel.

Mittemeijer and others performed the same kind of tests, on different alloys, but taking into consideration a series of test performed setting different heating rates: from slow 300°C/h to very fast 180000°C/h heating rates had been used.[9] In this way, they were able to study the kinetics of the processes involved and the type of transformation occurring (27),(9),(26).

The same kind of kinetics analysis was used to determine the processes involved in the γ→α transformation in low nitrogen steels and carbon steels (10),(11). In these studies the controlling process resulted to be different due to differences in the behavior of the alloy. As a matter of fact, when the transformation mainly occurs in dual phase γ+α regions, a diffusion controlled mechanism is often dominant. On the other hand, interface controlled mechanisms normally governs the transformation rate when the transformation occurs in the single phase α zone.

[9] Normally, heating rates below 1200°C/h are chosen.

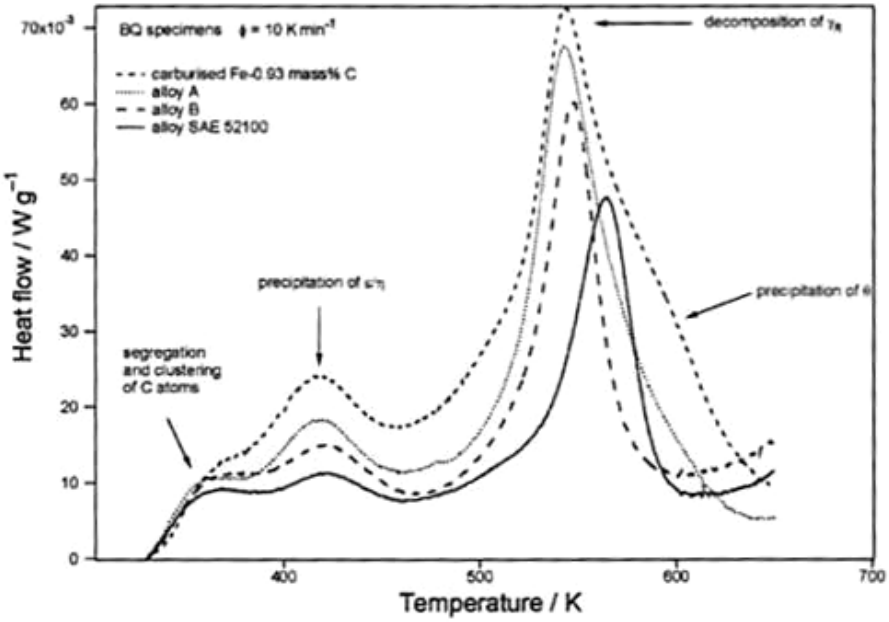

DSC curves of four martensitic specimens on isochronal annealing

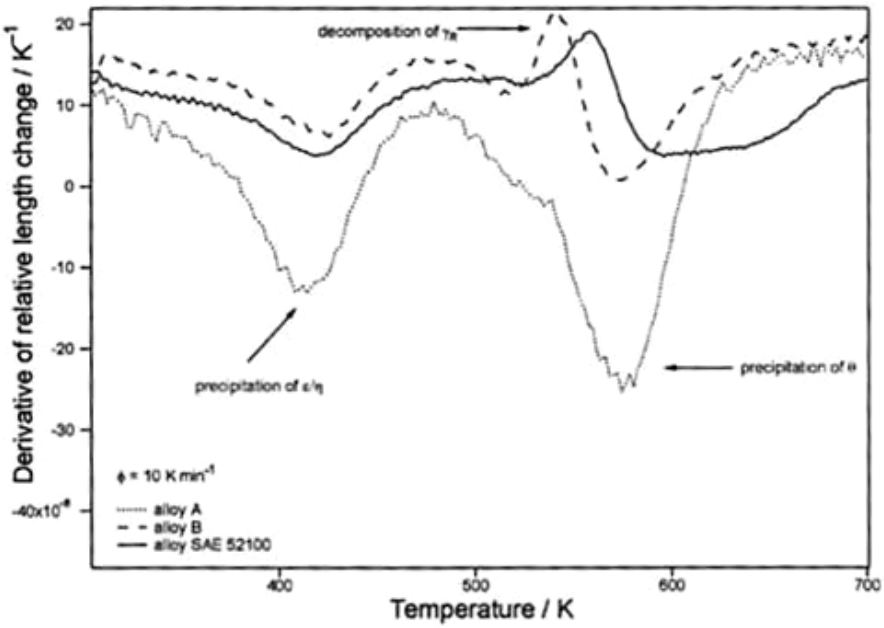

Derivative of relative length change on isochronal annealing of three martensitic specimens

Figure 25. Isochronal curves for a C steel during tempering by the use of DSC and dilatometry. Precipitation of carbides is more visible by dilatometry; on the other hand, the decomposition of retained austenite is clearer with DSC (27). Examples are reported in (9) too.

The α→γ transformation can be studied as well. It is possible to construct continuous heating transformation (CHT) curves: an example is shown in Figure 26. Kinetics analysis of the transformation can be performed. Examples are presented on carbon steels by Oliveira and colleagues (35) and by Capdevilla and colleagues (36). Heating rate between 360°C/h and 3600°C/h had been used.

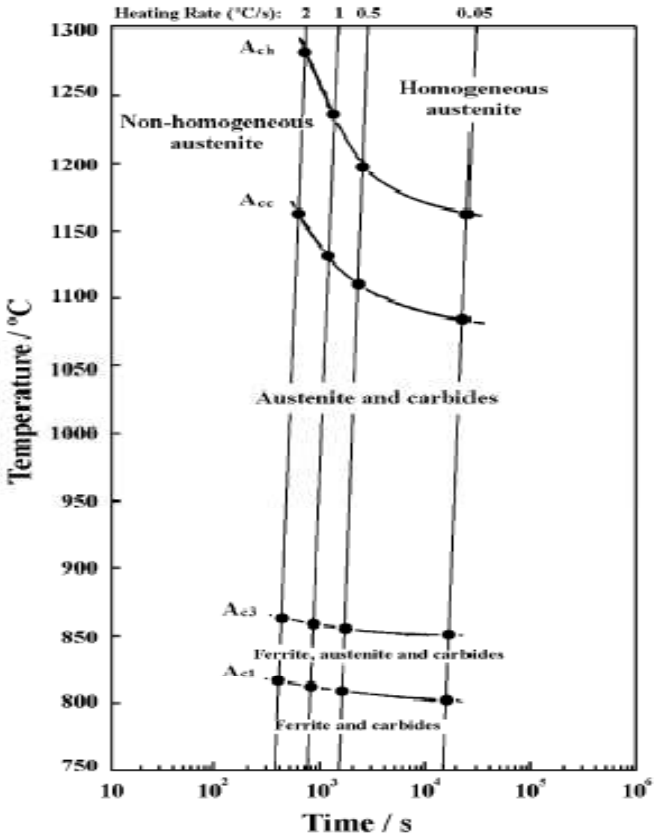

Figure 26. CHT curve for an X45Cr13 steel (37).

3.5. KINETIC ANALYSIS

3.5.1. The Johnson-Mehl-Avrami-Kolmogorov (JMAK) equation.

Modelling of transformation kinetics is normally done assuming a general behavior described by the JMAK equation:

$$f = 1 - \exp\left(-k_{(T)}t^{n}\right)$$

Equation 3. The JMAK equation. "k" represent the rate constant for the nucleation and is a function of temperature; time is expressed by the parameter "t"; "n" represent the Avrami coefficient and is related to the transformation process.

The JMAK equation is a general expression describing transformation processes involving a nucleation and growth process in isothermal conditions. The expression can be theoretically derived considering the process of nucleation and growing of a new phase. Assuming constant nucleation rate and growing rate, and considering a spherical shape for the fraction transformed, the following expression can be derived:

$$f = 1 - \exp\left(-\frac{\pi}{3}\dot{N}G^3t^4\right) = 1 - \exp\left(-k_{(T)}t^4\right)$$

Equation 4. The JMAK equation for constant nucleation and growing rates for isothermal condition (32).

"$\dot{N}$" denotes the nucleation rate, while "G" represent the expression for the growing rate of the new phase.

The value of "n" is then connected to nucleation and growing rates in the transformation. A general rule to interpret its meaning can be expresses as follows (32): nucleation contribution is 1 if nucleation is constant, between 0 and 1 if nucleation is decreasing, above 1 for increasing nucleation rate; growing rate contribution is related to the growing shape and assume a value 1, 2 and 3 for 1, 2 and 3 dimensional growing respectively.

Christian (38) is reporting a deeper analysis adding information: the value of "n" is related to the process controlling the transformation; the above reported rule for "n" is valid only for interface controlled linear growths. When long range diffusion is controlling the transformation, the quadratic dependence of growing on time give rise to a decreasing in the value of "n" in relation to the growing part by a factor 2.

Table 1 is given by Christian.

Moreover "n" can vary during the transformation; a variation in the value of "n" can be appointed to a variation of the nucleation rate or to impingement phenomena.

When nucleation sites are not randomly distributed in the volume, but result concentrated in specific positions (normally near other nucleation sites), the overall nucleation rate decreases more rapidly than does the untransformed volume. As a result, nucleation sites will be available only at the earlier stages of transformation; moreover, different kind of nucleation sites can be available: if that is the case, saturation will occur first for the ones that nucleate faster or those with lower "dimensionality" (edge before surfaces); when a nucleation site is saturated, the others will still take part in the nucleation process and contribute to the formation of new transformed particles (38).

As mentioned, impingement phenomena can be considered too. Two types of impingement are possible: hard impingement indicates a mutual spatial interference of growing region (this impingement naturally occur in a transformation involving the whole volume); on the other hand, it is possible to refers to soft impingement when the interference arises due to competition for the availability excess of solute in diffusion processes (38).

Finally, when diffusion controlled processes are considered, the JMAK equation can be used only to analyze the early stages of transformations: "*The exponential growth law summarized in Avrami's equation is valid for linear growth under most condition, and approximately valid for early stages of diffusion controlled growth*"(38).

Table 1. Meaning of the Avrami exponent "n" in the JMAK as reported by Christian (38).[10]

Polimorphic changes, discontinuous precipitation, eutectoid reactions, interfaced controlled growth, etc.
- $n > 4$ → *Increasing nucleation rate* - $n = 4$ → *Constant nucleation rate;* - $3<n<4$ → *Decresing nucleation rate;* - $n = 3$ → *Zero nucleation rate (saturation of point sites);* - $n = 2$ → *Grain edge nucleation after saturation;* - $n = 1$ → *Grain boudaries nucleation after saturation*
Diffusion controlled transformations.
- $n > 2\frac{1}{2}$ → *All shapes growing from small dimension, increasing nucleation rate;* - $n = 2\frac{1}{2}$ → *All shapes growing from small dimension, constant nucleation rate;* - $1\frac{1}{2} < n < 2\frac{1}{2}$ → *All shapes growing from small dimension, decreasing nucleation rate;* - $n = 1\frac{1}{2}$ → *All shapes growing from small dimensions, zero nucleation rate;* - $n = 1 - 1\frac{1}{2}$ → *Growth of particles of appreciable initial volume;* - $n = 1$ → *Needles and plates of finite dimensions small in comparison with their separation or thickening of long cylinders (after complete edge impingen* - $n = \frac{1}{2}$ → *Thickening of very large plates (after complete edge impingements);* - $n = \frac{2}{3}$ → *Precipitation on dislocations*

3.5.2. The JMAK equation for non-isothermal transformations.

In order to study non-isothermal transformations, the Avrami equation has to be adapted; this can be done with different approaches: further on the approach indicated by Mittemeijer in (9) will be considered.[11]

Let's consider the fraction transformed as a function of a hypothetical state variable β (determined by the T-t path followed). The JMAK equation can be expressed as follows:

$$f = 1 - exp(-\beta^n)$$

Equation 5. General form of JMAK as a function of the state variable β.

[10] Other authors are doubtful about the real potential of the results presented by Christian for interpreting the transformation processes, but its utility for check the overall behavior of a model based on the independent prediction of nucleation and growing rates is accepted. Look for exemplum R.W. Cahn and P. Haansen, "Physical metallurgy", published by "North Holland physics publishing" on 1983.

[11] A different approach is presented in Appendix A.

Moreover, let's set β as $\beta = k_{(T)}t$ and consequently, for non-isothermal conditions, $\beta = \int k_{(T)}dt$.

Assuming an Arrhenius type relation for the constant $k = k_0 e^{-(E/RT)}$,[12] the integral for β can be approximated to $\beta = \frac{T^2}{\emptyset}\frac{R}{E}k_{(T)}$. Finally, inserting the expression for β in Equation 5, the JMAK equation becomes:

$$f = 1 - \exp\left[-\left(\int k_{(T)}dt\right)^{\mathrm{n}}\right] = 1 - \exp\left[-\left(\frac{T^2}{\emptyset}\frac{R}{E}k_{(T)}\right)^{\mathrm{n}}\right]$$

Equation 6. The JMAK equation for non-isothermal conditions. "k" represents the rate constant for the nucleation and is a function of temperature; time is expressed by the parameter "t"; "n" represents the Avrami coefficient and is related to the transformation process; "Φ" is the heating rate and "E" the activation energy for the transformation.

The analysis is normally performed assuming "n" and "E" not to be functions of temperature. This means that isokinetic reaction are supposed and that, in diffusion controlled processes, a constant composition for equilibrium phases is assumed during the whole transformation process.

[12] As reported by Mittemeijer in (9) that supposition is universally accepted but has no theoretical justification.

4. NON METALLIC INCLUSION RATING

4.1. STEEL CLEANING

4.1.1. Introduction

Non metallic inclusions are always present in steels. Inclusions can be classified in different types: sulfides and products of desoxidation (alumina, silica and globular oxides).

Inclusions can be present in metals as a result of unwanted process during production, but can also be the result of voluntary element additions performed in order to control the oxygen content in the steel.

As a matter of fact oxygen is the most unwanted element in steels and the addition of oxidants, such as aluminum, ferrosilicon or carbon, is a common practice to reduce the oxygen content in melted steel. As a result, the oxygen is removed from solution, both as gas (CO) or forming precipitates called inclusions.

These inclusions are also unwanted but their content can be reduced by other techniques like degassing, bubbling or lime injection. The result is that the majority of the products of desoxidation rise in the melt and can be collected as a suspension which can be removed. The ones that remain in the liquid result in inclusions after the solidification process.

The quality of the resulting steel depends on the ability to control the desoxidation process, so the O content, as well as the content of other dangerous elements like S, P, and H. Moreover, inclusions are also important: not only has their total volume to be considered, but even their dimensions, distribution and shape. All these factors depend on the ability of the producer and the opportunities given by the techniques used during production.

Two common primary practices to produce super-alloyed steel are "*Argon* Oxygen *Decarburization*" (AOD) and "Vacuum Induction Melting" (VIM).

As the extra low carbon alloys that had been analyzed in the experimental part of this project are produced with VIM technique this will be described in more details.

4.1.2. Vacuum induction melting (VIM)

VIM is a refining process used especially to produce extra low carbon, high chromium content steels. "*VIM furnace consists of a ceramic-lined crucible built up around water-cooled*

induction coils. The crucible is mounted in a vacuum chamber" (39) . The charge is separated into three components: virgin material, reactive elements that are strong oxide formers like Al, Ti, Ca, Mg and Zr and previously vacuum-melted alloy of the wanted composition (revert). The furnace is brought under vacuum and power is applied to the induction coils. The coils generate a magnetic field, inducing a current in the charge material, which consequently is heated and, as it becomes liquid, stirred. When the charge is melted, bath agitation can be enhanced by auxiliary induction or bubbling of Argon. During this period, degassing of the steel takes place due to vacuum condition: hydrogen content below 1ppm is achieved while nitrogen content below 20ppm is possible only in absence of strong nitride formers like Cr, V and Al. Moreover desoxidation of the melt and decarburization takes place as CO develops. O content below 10ppm can be reached. In order to reduce the sulfur content, Ca is normally added.

The advantage of a VIM process, compared to AOD is that it produces the lowest possible oxygen content in the alloy. Moreover, a VIM process grants better control of the composition, but unfortunately only low production rates are possible (39). VIM is the process to be chosen if a small amount of material has to be produced, thus being a good technique for research purposes.

4.2. CHARACTERIZATION

4.2.1. General principles

Non metallic inclusions can be studied using macroscopic and microscopic methods. Macroscopic methods include macro-etching and fracture test while microscopic methods are assessed essentially with microscopy techniques. Macro etch indicate inclusion content and distribution, while microscopic examination is used to determine size distribution, number and types of inclusions.

Tests are prepared by cutting and machining a section and eventually etching with a suitable reagent. Inclusions are then revealed and their appearance can be compared with standard micrographs in order to recollect inclusions under different types and class. Their nature can be recognized thanks to their different hardness (their appearance differs after machining) or through selective etching.

Preparation is extremely important. Poor polishing results in unsatisfactory rating as it will result in polishing defects. "*These defects, such as pits, dragged out inclusions, etc., will appear at low magnification as dark areas which could be mistaken for inclusions*" (40).

When steel is hot worked, the inclusions are oriented in the direction or rolling or forging. Different inclusions have different behavior in these conditions: "*the hard and brittle inclusions break up, and the particles of inclusion are strung out while the plastic ones are elongated to some extent with the steel*" (40). Aluminum-silicate inclusions, for example, are present in hot rolled

steels as strings of particles in the direction of rolling, while sulfides are more easily deformed by the forming processes. Other structures, like calcium-alumate, remain refractory at high temperature and retain completely their shape during rolling.

In the end, it has to be considered that ingots are heterogeneous, therefore the exact distribution of inclusions ingot to ingot, and top to bottom, will vary. These inhomogeneities make it difficult to generalize the results.

Concerning oxides it has to be considered that only a small part of them can be observed with optical microscopy. As a matter of fact, the current technology in steel making has eliminated most of the observable part represented by large size oxide, while the main part is too small to be observable.

The general aspect of the most common inclusions in the direction of rolling as revealed by optical microscopy is shown in Figure 27.

a)

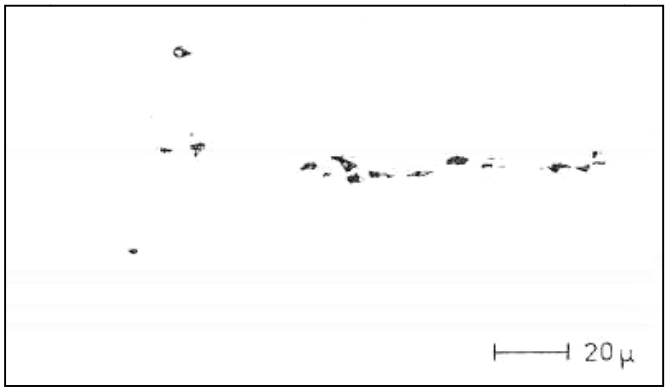

b)

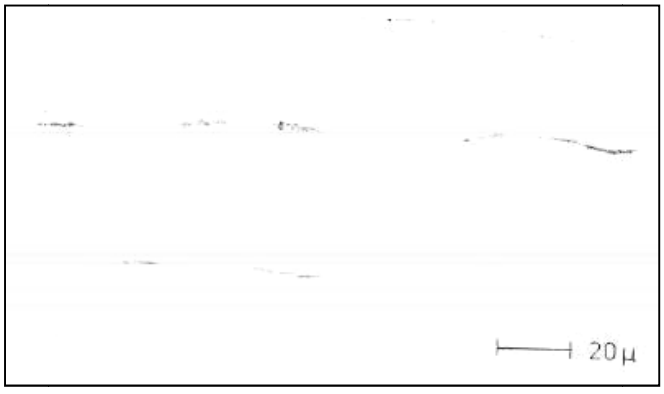

Figure 27. General types of alumina/oxides a), and sulfide b) (40).

4.2.2. Oxygen content

"*The amount of oxide inclusions is proportional to the oxygen content in steel*" (40). Even with the limitations introduced by inhomogeneities, experimental techniques and data assessment, an estimation of the degree of the total amount of oxygen remaining in the steel can theoretically be performed by optical microscopy techniques, using image analysis.

Figure 28 shows experimental results by ASM for the determination of the O content[13] in steel with SiO_2 and Al_2O_3 fraction area analysis, based on theoretical results by Bergh and Lindberg (41).

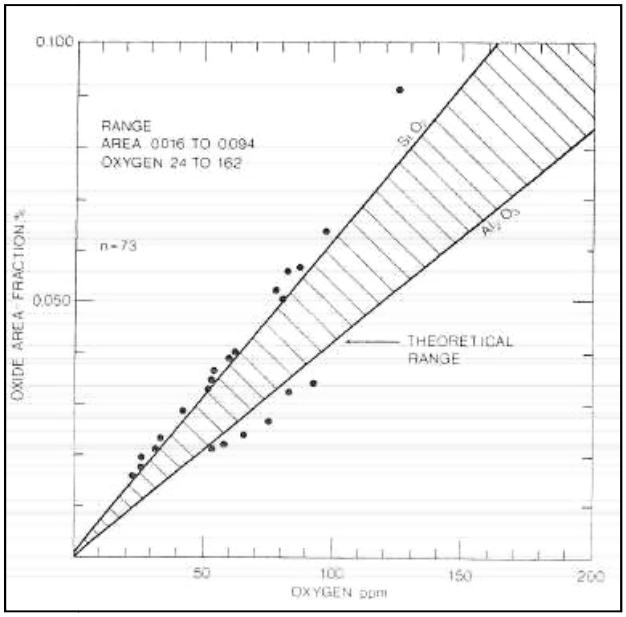

Figure 28. Relationship between oxygen, parts per million, and oxide area fraction, percent (40).

Automatic methods for inclusion assessment have been proposed in the past by setting up machines able to identify and classify inclusions on large surface area by image analysis (40).

[13] To be underlined that the total oxygen content is considered; both bound oxygen and oxygen in solution are included. The last is only a small part of the total content and cannot be inferred by this method.

5. EXPERIMENTAL METHODS: INSTRUMENTS AND PREPARATION

5.1. HARDNESS MEASUREMENTS

5.1.1. Introduction

Hardness can be defined as the property of a material to resist plastic deformation. For a long time, hardness has been assessed by resistance to scratching or cutting. Relative hardness of minerals can be assessed by reference to the Mohs scale that ranks the ability of materials to resist scratching by another material. However, relative hardness tests are limited since they do not provide any quantitative value.

Nowadays, the usual method to achieve a hardness value is to measure the depth or area of an indentation left by an indenter of a specific shape, with a specific force applied for a specific time. There are three principal standard test methods for expressing the relationship between hardness and the size of the impression: Brinell, Vickers, and Rockwell. Measurements of hardness Vickers have been performed for our investigation and will be described in more detail.

5.1.2. Hardness Vickers

In a Vickers test, the surface is subjected to a pressure for a determined time by means of a pyramid-shaped diamond.

The indenter employed is a square-based pyramid whose opposite sides meet at the apex at an angle of 136º. The diamond is pressed by a load into the surface of the material, and the diagonals of the resulting indentation are measured with the aid of a calibrated microscope (Figure 29).

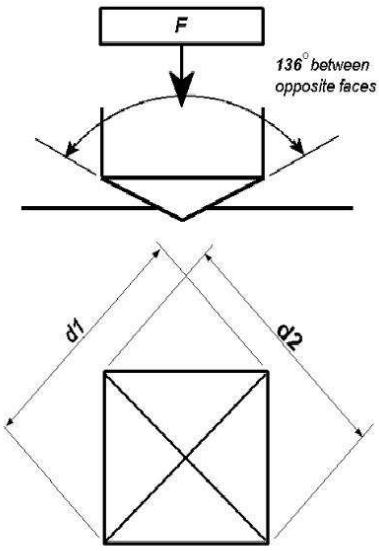

Figure 29. Hardness measurements: methodology

5.1.3. Instrument and preparation

Hardness measurements were performed on polished samples with a DIA TESTOR $2R_C$, fabricated on 08/06/1961 by OTTO WOLPERT-WERKE, GmbH LUDWIGSHAFEN a. Rh.; Vickers hardness H_{V_10Kg} performed with a pyramidal indenter under a force of 100N for 10s had been chosen for measuring.

The preparation of the samples was as follows:

- Cleaning in ethanol;
- Mold in a mixture of Diallylphatalate hot molding resin (ISO FAST by STRUERS) and phenolic hot molding resin (MULTIFAST BROWN by STRUERS). A PEDOPRESS machine by STRUERS has been used. Temperature of 180°C for 8 minutes has been maintained followed by 5 minute cooling in water;
- Polished with the use of an ABRAMIN by STRUERS with water at 150rpm. In sequence 80-220-600-1200 Piano with 30N on 6 samples for 2 minutes followed by 1000 SiO_2 for 4 minutes.

5.2. OPTICAL MICROSCOPY

5.2.1. Principles

5.2.1.1. Introduction

"*The basic function of a microscope is to reveal details too minute to be visible with naked eye*" (42). Therefore, the essential characteristics of the optical system are resolution and magnification.

The magnifying system, for an optical microscope, is made of the objective, the oculars and the eye / camera. The objectives produce a real, magnified image in the plane of the diaphragm of the ocular that further magnifies it in a virtual image seen by the eye. Finally, the lens of the eye, converts the virtual image to a real image on the retina. The same function of the eye is absolved by the lens of the camera and the photographic film or the screen in micro-photography (42).

The resolution is the ability of a lens system to reproduce fine detail. Resolution is always limited and limitation arises due to aberrations in the lenses, that can be reduced, and diffraction effects, that are unavoidable. Diffraction limits image resolution, since a single point is revealed on the image plane as a series of light and dark alternated rings surrounding a bright central disc.

Defining two objects as distinguishable if their diffraction discs overlap less than one half, the theoretical limit of resolving two discrete points MRD (minimum resolved distance) becomes:

$$MRD = \frac{0{,}61\lambda}{NA}$$

Equation 7. Minimum resolved distance for a microscope; λ is the wavelength of the light and NA the numerical aperture of the system (43).

"NA" is the numerical aperture of the lenses and can be roughly defined as a measure of the diameter of a lens compared to its focal length or, alternatively as "*the ability of the lenses to collect diffracted light*" (44). NA is affecting resolution and brightness and can be enhanced using a media with higher diffraction index (oil instead of water/air).

Moreover, distortions of the image can occur due to aberration of the system. Monochromatic light and small NA help reducing aberrations.

Finally contrast is very important since it defines the ratio of intensities between dark and light area and so the possibility to distinguish different features of a sample.

Optical (or light) microscopy involves visible light transmitted through, or reflected from, the sample. The resulting image can be detected directly by the eye, imaged on a photographic plate or captured digitally (42).

Further on, transmitted light microscopy will not be treated and only reflected light microscopy will be covered.

5.2.1.2. Bright field microscopy

Bright field microscopy is the simplest microscopical technique. Light is generated by a source, collected and focused onto the specimen. Here light is partially absorbed, partly refracted and partial reflected from the sample. Reflected light is collected and used to make the image.

An ideally polished surface is flat and then is able to uniformly reflect the light. This means that the sample after polishing ideally appears completely bright. The system is able to detect only the structures that break this uniformity. Polishing defects like scratches or pores are visible. Dust particles and inclusions are visible too.

To be able to distinguish the different microstructures of steels, an etching process has to be performed. During etching some structures are preferentially attacked and the discontinuity created on the surface can be detected by the system.

5.2.1.3. Darkground or darkfield microscopy

Darkfield illumination is a technique that greatly improves the contrast of many specimens. This technique is able to show the presence or absence of particles even too small to be resolved by collecting light in an indirect way. Darkground technique is the "*technique of choice to show dust or other inclusions*" (42). However, measurement may be made of the number of particles, "*but a description of their size or shape is not so certain*" (42). Low magnifications are considered better for darkfield microscopy (44).

A good description of the method is given by Rost and Oldfield: "*The specimen is illuminated by a hollow cone of oblique rays of light that do not enter the objective directly, but may be reflected, refracted or diffracted into the objective by the specimen. Since no direct light enters the objective, an empty field appears black, and a specimen appears brightly illuminated against a dark background*" (42).

The method requires a stop in the condenser blocking out the central rays of light while allowing the lateral rays to illuminate the sample.

The resulting image is a function of many parameters (light exposure, time of exposure, NA, …) making it difficult to setting up an experimental method suitable for image analysis.

5.2.1.4. Polarized light microscopy

"*Some of the most valuable observations possible with light microscope are those made with polarized light*" (43). However, a deep study of polarized light microscopy is beyond the scope of this project and only its principal features and potentialities will be analyzed.

Polarized light differs from ordinary light since it has a single vibration direction perpendicular to the direction of propagation. Ordinary light can easily be polarized with a filter (Figure 30).

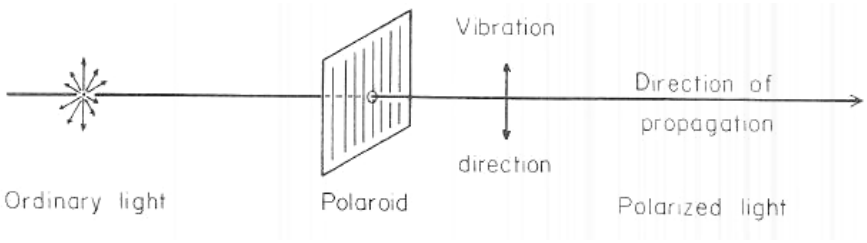

Figure 30. Polarization of light (43).

Polarized light microscopy gives information about anisotropic crystals that cannot be revealed by ordinary microscopy as these anisotropies are visible due to polarization.

As a matter of fact, polarized light microscopy is able to distinguish the differences in the optical properties of a material in different directions. Glasses and crystals in the cubic system show isotropic optical properties; all the other crystals show different optical properties associated with their crystallographic orientation.

In theory, polarized light microscopy can be used to observe crystalline inclusions and dust particles in martensitic extra low carbon steel since they generally don't have a cubic structure while the iron-chromium matrix is almost ideally body centered cubic.

5.2.2. Etching

Etching is performed in order to preferentially attack structures and be able to distinguish steel features during observation under the microscope.

Table 2. List of the most common used chemical etchants (46).

Etchant	Composition	Conc.	Conditions	Comments
Kalling's No. 1	Distilled water CuCl2 Hydrochloric acid Ethanol	33 ml 1.5 grams 33 ml 33 ml	Immersion etching at 20 degrees Celcius	For etching martensitic stainless steels. Martensite will be dark and the ferrite will be colored.
Kalling's No. 2	CuCl2 Hydrochloric acid Ethanol	5 grams 100 ml 100 ml	Immersion etching at 20 degrees Celcius	For etching duplex stainless steels and Ni-Cu alloys and superalloys.
Kellers Etch	Distilled water Nitric acid Hydrochloric acid Hydrofluoric acid	190 ml 5 ml 3 ml 2 ml	10-30 second immersion. Use only fresh etchant	Excellent for aluminum and alloys - immersion for 10-20 seconds ; titanium alloys immersion for 10-20 seconds.
Kroll's Reagent	Distilled water Nitric acid Hydrofluoric acid	92 ml 6 ml 2 ml	15 seconds	Excellent for titanium and alloys. Swab specimen up to 20 seconds.
Nital	Ethanol Nitric acid	100 ml 1-10 ml	Seconds to minutes	Most common etchant for Fe, carbon and alloys steels and cast iron - Immerse sample up from seconds to minutes; Mn-Fe, MnNi, Mn-Cu, Mn-Co alloys - immersion up to a few minutes.
Marble's Reagent	CuSO4 Hydrochloric acid Water	10 grams 50 ml 50 ml	Immerse or swab for 5-60 seconds.	For etching Ni, Ni-Cu and Ni-Fe alloys and superalloys. Add a few drops of H2SO4 to increase activity.
Murakami's	K3Fe(CN)6 KOH Water	10 grams 10 grams 100 ml	Pre-mix KOH and water before adding K3Fe(CN)6	Cr and alloys (use fresh and immerse); iron and steels reveals carbides; Mo and alloys uses fresh and immerse; Ni-Cu alloys for alpha phases use at 75 Celcius; W and alloys use fresh and immerse; WC-Co and complex sintered carbides.
Picral	Ethanol Picric acid	100 ml 2-4 grams	Seconds to minutes Do not let etchant crystallize or dry –explosive	Recommended for microstructures containing ferrite and carbide.
Vilella's Reagent	Glycerol Nitric acid Hydrochloric acid	45 ml 15 ml 30 ml	Seconds to minutes	Good for ferrite-carbide structures (tempered martensite) in iron and steel

Different etching techniques can be used: electrolytic etching, chemical etching and physical etching (thermal); Petzow has given a very complete review about all the different methods and their characteristics (45).[14] In particular, chemical etching is by far the most common technique and is able to detect the majority of steel features, thanks to dissolution rate differences in a specific chemical agent. Table 2 shows different kind of chemicals used in metallography and their principal features.

Electrolytic etching, on the other hand, generates the visible pattern on the surface thanks to a RED-OX reaction.

5.2.3. Instruments and preparation

The samples were polished as described in 5.1.3, and the following treatment was added:

- 4000 SiO_2 for 3 minutes with water;
- 3 µm diamond in a DP-SUSPENSION with multidoser by STRUERS on a MD MOL, ϕ305mm with water as a lubricant, with 50N for 3 minutes;
- 1 µm diamond in a DP-SUSPENSION with multidoser by STRUERS on a MD NAP, ϕ305mm with ethanol as a lubricant, with 50N for 3 minutes.

Finally, different etching methods were used:

- Vilella´s solution makes of 1% 2-4-6-TRINITROPHENOL and 5% HCl in ethanol for 10s;
- Kalling II reagent for 10s;
- Mechanical etching with a cotton swab in diluted Aqua regia (3 parts of Hydrochloric acid, 1 of Nitric acid, 4 of water) for 40s;
- Electrolytic etching in NaOH for 40s at 20V.

An optical microscope OLYMPUS GX 41 was used for bright field microscopy. Inclusion analysis was performed with a NEOPHOT 30 instrument.

5.3. ELECTRON MICROSCOPY

5.3.1. Principles

In scanning electron microscopy (SEM), an electron beam scans the sample's surface. The interaction between the beam and the sample generates different signals; the detection of

[14] Other review of etching methods can be found in literature; For example “Acciai comuni e speciali” by G. Guzzoni edited in Milano on 1943, or “Introduzione agli acciai inossidabili” by Walter Nicodemi, edited in Paderno Dugnano (MI) by AIM on 2008 (II edition).

specific signals produces the wanted information. Three signals provide the greatest amount of information in SEM: secondary electrons, backscattered electrons, and X-rays.

Secondary electrons are emitted from the atoms occupying the top surface, few nanometers in depth, and produce a readily interpretable image. The contrast in the image is determined by the number of emitted secondary electrons and thus by the sample morphology while resolution is determined by the dimension of the primary electron beam. A resolution of few nanometers can be achieved.

Backscattered electrons are primary electrons which are scattered elastically from the nuclei of the atoms in the solid. The contrast in the image is determined by the atomic number of the elements in the sample, since elastic scattering is promoted by high atomic number elements. The image will therefore show the distribution of different chemical phases in the sample: only phases that present differences in composition can be distinguished. These electrons are emitted from a deeper area in the sample and consequently the resolution in the image is not as good as for secondary electrons.

Finally, interaction of the primary beam with atoms in the sample causes electronic transitions which result in the emission of X-rays. The emitted X-ray have an energy determined by the electronic configuration which is characteristic for an element. Detection and measurement of the energy permits elemental analysis (Energy Dispersive X-ray Spectroscopy or EDS). EDS can provide rapid qualitative, or with adequate standards, quantitative analysis of elemental composition. The signal comes from few micrometers in depth, depending on the absorption capacity of the sample (its atomic weight). X-ray detection may be used to form maps or line profiles, showing the elemental distribution in a sample surface. Moreover EDS can be used to identify the composition of different phases with a point identification technique.

5.3.2. Instrument and preparation

A JEOL JSM-5900 Scanning Electron Microscope was used. The instrument has a LaB_6 filament.

Samples were prepared as for optical microscopy; afterwards they were covered with a thin layer of physically vapor deposited carbon in order to promote conductivity.

5.4. DILATOMETRY

5.4.1. Principles

"*Dilatometry is a very sensitive experimental tool to analyze the length (volume) changes and the kinetics of solid state phase transformations*" (47). In particular, it "*is one of the most powerful techniques for the study of transformation in steels, because it permits real-time monitoring of the extent of reaction in terms of dimensional changes due to transformation*" (48).

The dilatometer measures the dimension of a sample versus time and temperature, recording both transformation strain and thermal strain. The length of the sample can be measured directly or in differential dilatometry. In the second case the difference in length between the specimen to be investigated and a reference sample is measured.

Conventional dilatometers utilize a furnace in order to heat and cool the sample; in this method the high thermal inertia on the system is limiting the maximal velocity of analysis. On the other hand, in high speed dilatometry, the specimen is positioned along the axis of a cylindrical heating coil, which is connected to a RF power generator. The magnetic field around the coil induces currents in the specimen, which is consequently heated up. As a result, the response of the system depends on the thermal characteristics of the specimen rather than those of the furnace.

The temperature of the sample is recorded using a thermocouple that is spot welded to the sample, and referenced by means of a constant temperature bath. The specimen can be enclosed in vacuum, or in inert atmosphere; if the second is the case a smaller degree of decarburization can result.

Fast quenching rates can be achieved by the use of high pressure jets of gas directed through the chamber. Both nitrogen and helium are used. Helium is used as quenching gas in high cooling rate experiments, because its thermal conductivity is higher than that of nitrogen.

Thermal gradients can develop in the specimen during fast thermal cycles; this may cause difficulties in the interpretation of the observed changes in specimen dimensions and is considered the main source of experimental error.

The dimensions of the specimen are somewhat arbitrary, but they have to be designed such that they are sufficiently thick to prevent free surface effects from altering transformation kinetics, but, at the same time, dimensions must be small enough to allow rapid changes in temperature (47), (49).

5.4.2. Instrument and preparation

Dilatometry were performed by CSM in Rome.

An ADAMEL LHOMARGY was used. The instrument is granted for a maximal temperature T_{max} of 1600°C and works in vacuum at 10^{-2}Torr.

Samples were cylinder of 5mm in diameter and 25mm long, obtained through machining (turning of the body and grinding of the parallel faces) of the as-rolled material.

6. EXPERIMENTAL RESULTS

6.1. MATERIAL AS RECEIVED: DESCRIPTION AND CHARACTERIZATION

6.1.1. Composition and preparation

Commercial alloy X20CrMoV 12-1 and extra low carbon experimental alloys (2422, 2504, 2536) prepared by "Centro Sviluppo Materiali" (CMS) in Rome were studied. Alloys composition is shown in Table 3.

The experimental alloys provided by CSM were prepared as 80Kg ingot model alloys produced by Vacuum Induction Melting (VIM). The ingot was afterwards rolled to a 20 mm thick plate.

Table 3. Alloying elements: average chemical composition of the obtained specimen as given by CSM.

Steel	Fe	Ni	Co	Cr	W	Mo	Nb	Cu	V	Al	Ti	C	B	N	Si	Mn	P	S
X20	Bal	0.66		11.5		0.91			0.33			0.19		0.03	0.23	0.49		
2422	Bal	1.29	0.02	11.9	<0.005	<0.005	0.08	<0.005	0.19		<0.005	0.005		0.06	0.40	0.32	<0.005	
2536	Bal	1.24	0.01	8.7	0.01	0.03	0.08	0.01	0.20		0.01	0.004		0.06	0.39	0.32	0.01	0.005
2504	Bal	1.27	0.02	11.6	<0.005	<0.005	<0.005	<0.005	0.23	0.003	<0.005	0.002	<0.005	0.09	0.40	0.31	<0.005	0.003

6.1.2. Microstructure

The structure for the materials as received, shown in Figure 31, is a mixture of fresh martensite and untransformed δ-ferrite (white phase) resulting from the hot working process; the presence of δ-ferrite is clearly revealed by electrolytic etching in NaOH as shown in Figure 32.

Hardness measurements confirmed that the structure was not fully martensitic ($H_{V\_10Kg} \approx$ 250 which is very low for fresh martensite).

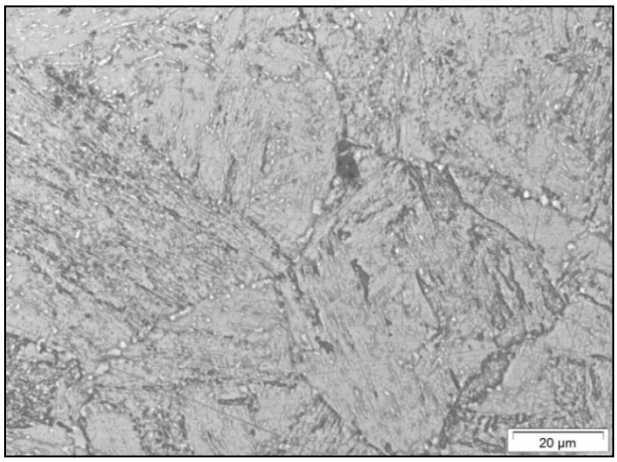

Figure 31. Alloy 2504 as rolled. Optical microscope; Villella's etching 10s. δ-ferrite in this picture doesn't show any preferential direction as the surface shown is perpendicular to the rolling direction.

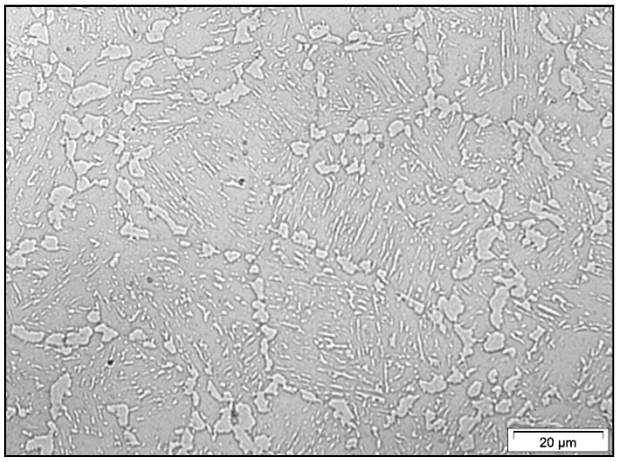

Figure 32. Alloy 2422 as rolled. Optical microscope; electrolytic etching, 20V, 40s, in a solution of NaOH 20%.

6.1.3. Inclusion analysis

6.1.3.1. Introduction and experimental method

The total oxygen content was not indicated by CSM. As the steel contains element that are important in defining its behavior and have high affinity for oxygen, like Cr, V and Nb, the structure was investigated without etching to look for non metallic inclusions.

Samples were analyzed in the rolling direction in order to obtain all the possible information. Polishing was performed as described in 5.2.3.. The last passage was modified to increase preparation quality. Lubrification with ethanol was increased; polishing time was set to 5 minutes, while the force was decrease to 30N. No etching was performed.

Electron microscopy was applied to recognize type and typical aspect of the inclusions. The surface was analyzed comparing the image resulting from secondary electrons (SE) and backscatter electrons (BE) in order to distinguish between surface effects and particles. Then, the nature of inclusion was studied with Energy Dispersive Spectroscopy (EDS).

Finally, a characteristic oxide particle was used as a reference in order to calibrate image analysis on a larger scale by the use of optical microscopy.

Optical bright field microscopy was used to perform image analysis: 10 pictures for a total surface area of 3.7mm^2. The magnification was 100X. Contrast and brightness were adjusted on the base of the calibration.[15] The fraction of surface area occupied by oxides was evaluated quantitatively.

6.1.3.2. Experimental results

In optical microscopy a large amount of particles is visible. Their principal shapes are 10-20µm long strings and globular particles with mean radius of a few micrometers (Figure 33). Through electron microscopy the nature of these particles was recognized: strings are Al/Si oxide, while globular particles are mainly SiO_2 or oxide-sulfide hybrids (Figure 34). Also Ti, V and Nb are present in small quantities in the inclusions. On the other hand, MnS based inclusions are present as small particles that cannot be revealed by optical microscopy (Figure 34, Figure 35).

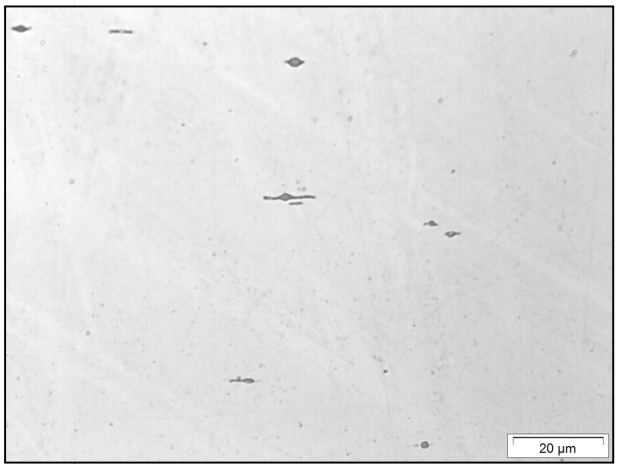

Figure 33. Alloy 2536 as rolled. Optical microscope; no etching. Surface parallel to the rolling direction.

[15] The surface area of the considered particle was measured to be 17.9 square micrometers by SEM image analysis. For OM image analysis, the brightness of the image was kept constant during the acquisition process and then digitally adjusted in order to obtain the same surface area value for the considered particle. Moreover contrast was enhanced to its maximum value in order to clearly distinguish matrix (white) and inclusions (black).

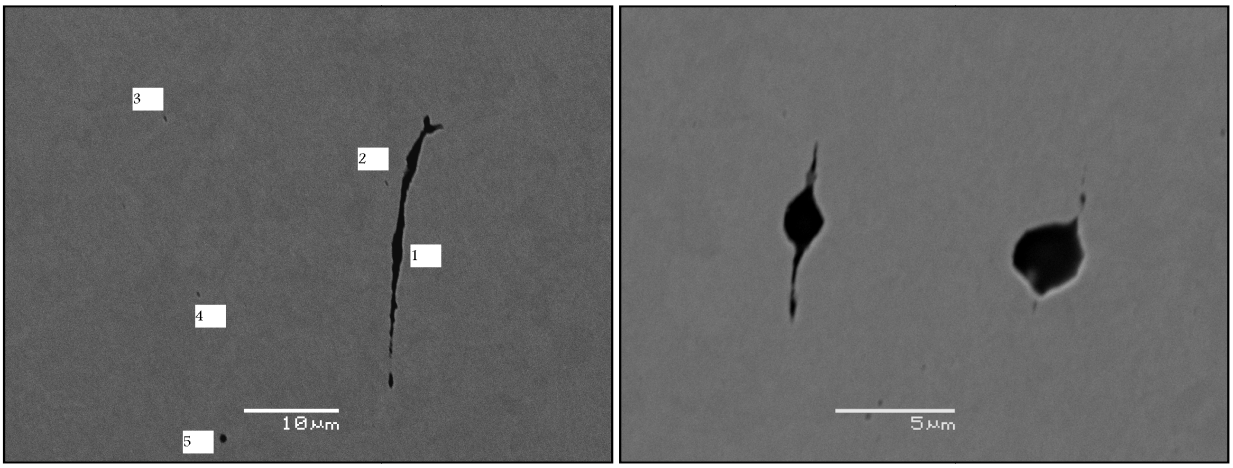

Figure 34. Alloy 2536 as rolled. Electron microscopy, 15kV; no etching. BE images. On the left: 1) String oxide [at. composition by EDS: 33,94%O, 17,3%Al, 37,84%Si, 5,72%Ti, 3,09%V, 2,11%Nb]; 2-3-4) MnS inclusions appear very small; 5) Hybrid particle [at. composition by EDS: 9,5%O, 46,72%Si, 7,55%Ti, 13,73%V, 7,89%Nb, 6,86%S, 7,75%Mn]; on the right: SiO_2 globular oxides.

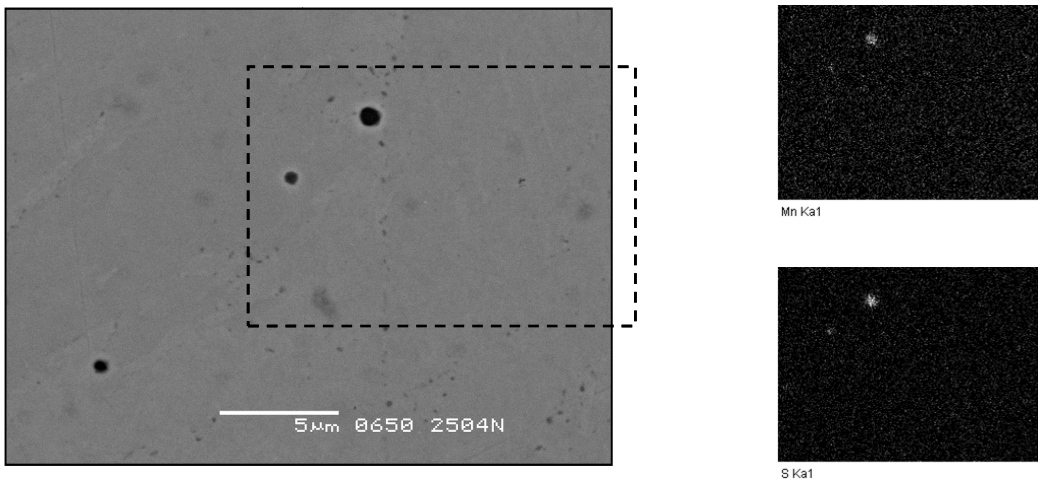

Figure 35. Alloy 2504 as rolled. MnS based inclusions as appear on a plane perpendicular to the rolling direction. Electron microscopy 15kV; no etching. BE image (left). Map analysis of the enlighten windows by EDS (right).

The oxygen content in the steel was estimated basing the analysis on the results presented by ASM (40). Image analysis was used to determine the fraction of area occupied by oxides. SEM image was used as calibration.[16] Figure 36 shows the result of the image elaboration process.

[16] The surface area occupied by particle 1 in Figure 36 (determined by SEM) had to be equal to the surface area occupied by the same particle in OM after the elaboration.

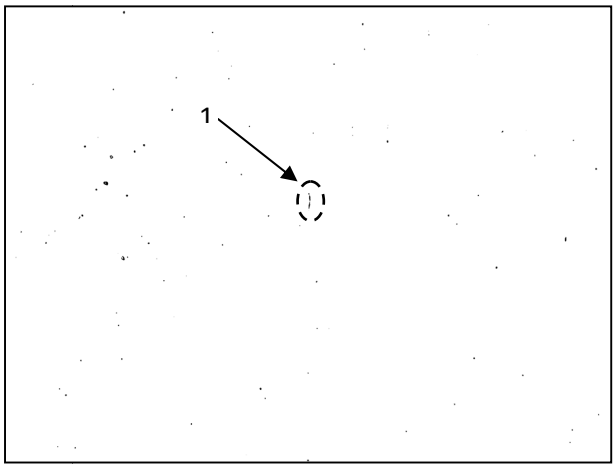

Figure 36. Alloy 2536 as rolled. Optical microscopy 100X; no etching. Image analysis result, calibration picture; 0,37mm^2. The fraction of "black area" is equal to 0,0497%.

The average fraction occupied by oxides was found to be 0,0496% ±0,0001%. Assuming all visible structures are oxides and SiO_2 as the only kind of oxide present, an oxygen content of $\approx 80ppm$ can be estimated in the steel.

This result is pretty high but still consistent with extra low carbon steels. Moreover, the method is expected to overestimate the content as polishing defects cannot be eliminated, and its general accuracy was expected to be low due to statistical limitation (a larger surface area and more than one ingot have to be considered if a complete analysis is wanted).

6.1.4. Critical temperatures determination

6.1.4.1. Experimental method

The critical temperatures of the materials as rolled have been determined by dilatometry. The samples were heated to 1050°C and subsequently air cooled to room temperature. In order to determine the critical temperatures, very low heating rates are necessary. A heating rate of 3°C/min was applied. Figure 37 shows an example of the obtained dilatometric curves.

As the analysis had to be performed graphically, the detecting capability was enhanced plotting the results in a differential form. This step was done applying a smoothening effect, taking into consideration 21 data point, as shown in Figure 38. In this way an artifact is introduced and the critical temperatures result shifted of few degrees to lower temperature.

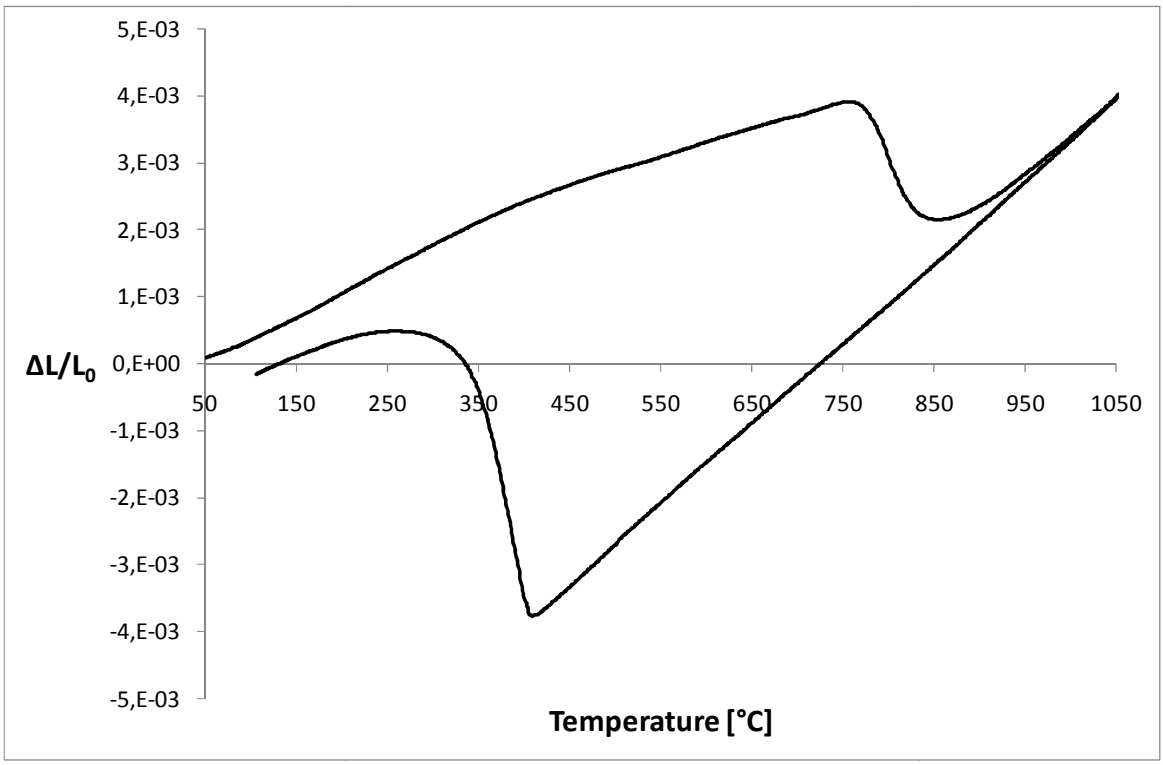

Figure 37. Alloy 2504; dilatometric curve, sample "b".

=(C31-C11)/(B31-B11)

	B	C	D	O	P	Q
10	T	ΔL/L0	α			
11	20	2,00E-06				
12	20	2,00E-06				
13	20	2,00E-06				
14	20	2,00E-06				
15	21	2,00E-06				
16	21	4,00E-06				
17	21	4,00E-06				
18	21	4,00E-06				
19	22	4,00E-06				
20	22	6,00E-06				
21	22	6,00E-06	=(C31-C11)			
22	23	6,00E-06	2,40E-06			
23	23	6,00E-06	2,00E-06			
24	24	8,00E-06	2,33E-06			
25	24	8,00E-06	2,67E-06			
26	24	8,00E-06	2,33E-06			
27	24	1,00E-05	2,29E-06			
28	25	1,00E-05	2,57E-06			
29	25	1,20E-05	3,33E-06			
30	25	1,20E-05	2,86E-06			
31	25	1,40E-05	2,86E-06			

Figure 38. Smoothening effect applied on the data.

Finally, the methodology applied for the final graphical analysis is shown in Figure 39.

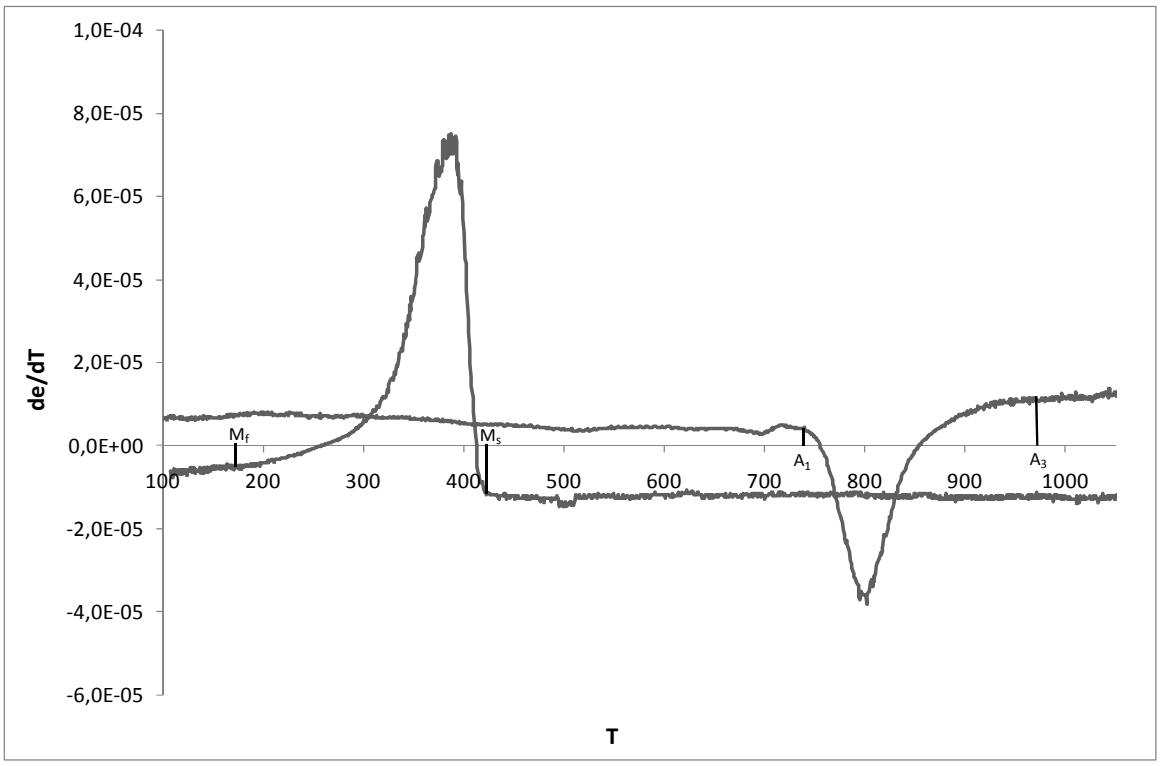

Figure 39. Alloy 2504 as rolled; dilatometric curve, sample "b"; the data are plotted as linear expansion coefficient alpha as a function of temperature.

In order to determine the critical temperatures of the material as rolled, three different samples denominated “a”, “b”, and “c” were used. The values considered was the average values.

6.1.4.2. Experimental results

Table 4 shows the result of the analysis performed.

Table 4. Critical temperature [°C] estimated by dilatometric curve for the experimental alloys as rolled. The value is the average resulting from the 3 different tests performed, approximated to the nearest decade.

Alloy	A_c1	A_c3	M_s	M_f
2422	740	1000	450	130
2504	730	960	430	140
2536	730	880	490	150

6.1.5. Samples preparation for further analyses

The material was cut into pieces of 11X17X10mm and normalized with an austenitization process at 1050°C for 1.5h.

The transformations occurring during heat treatment were studied using different methods: hardness measurements and microstructure investigation with light optical microscopy.

Moreover, dilatometric measurements were performed in order to study the kinetic of the α'→γ transformation and to make a quantitative analysis of the fraction of austenite formed for different treatment temperatures.

6.2. HARDNESS MEASURMENTS

Hardness measurements were performed on samples of alloys 2422, 2504, 2536, normalized at 1050°C for 1.5h and tempered between 700°C and 800°C within intervals of 10°C. The holding time was 2h. Then after the samples were cooled in air.

The results are shown in Figure 40.

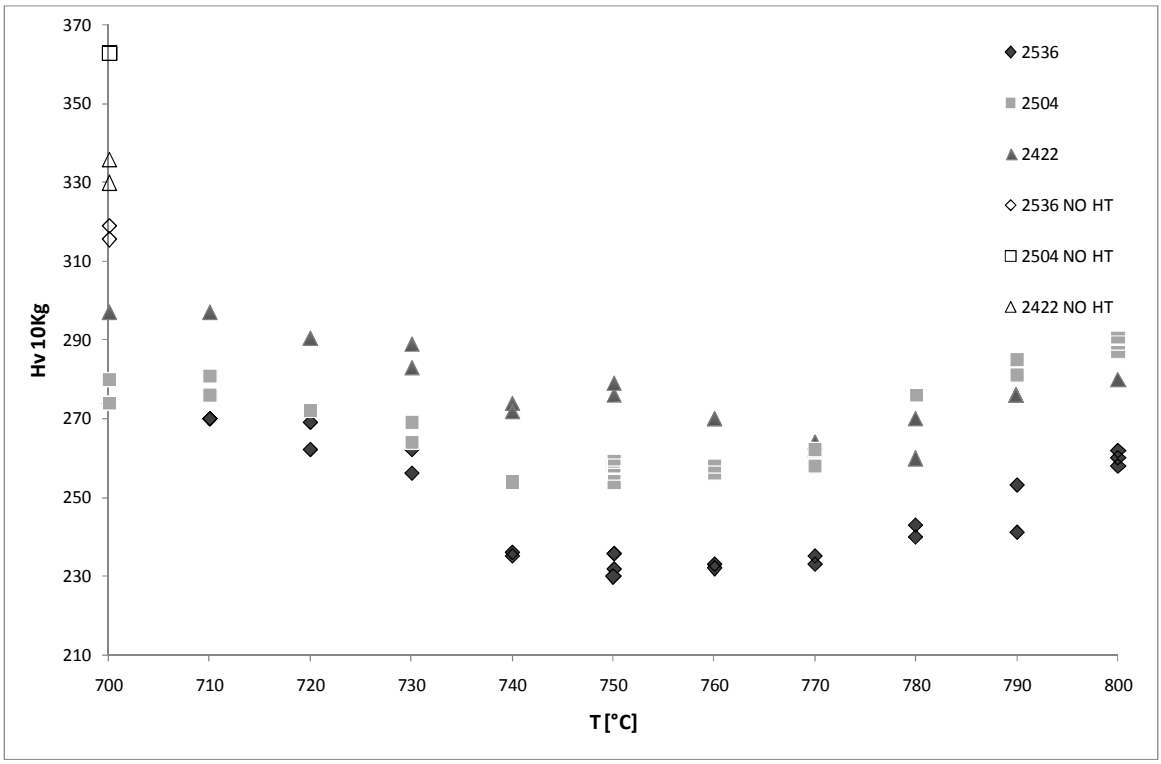

Figure 40. Hardness resulting from the tempering process as a function of the tempering temperature. NO HT means as normalized material.

The measurement process was performed at higher annealing temperature for alloy 2504 in order to look at the continuation of the austenitization process: the analysis was done between 800°C and 920°C with 20°C intervals.

Moreover a series of measurements was performed on X20CrMoV 12-1 between 720°C and 940°C at 20°C intervals. This was done in order to study the role of carbon in the transformation and identify the different structures obtained. The results are shown in Figure 41.

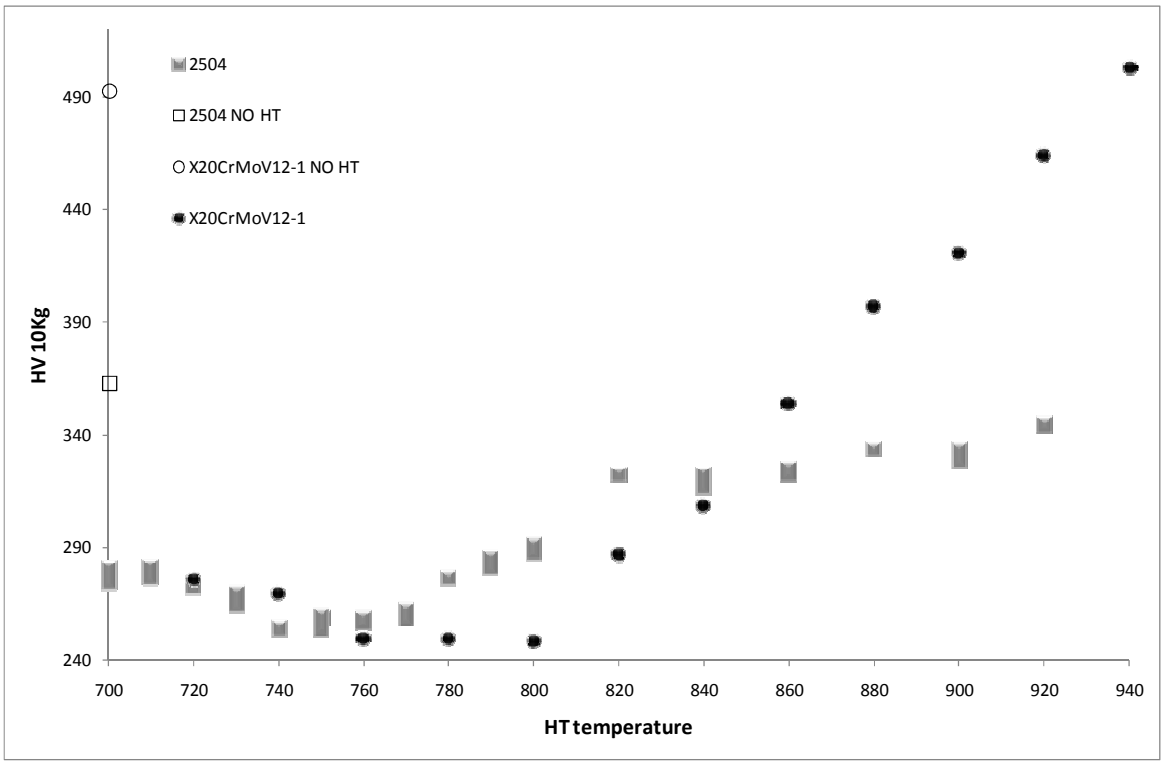

Figure 41. Hardness resulting from the tempering process as a function of the tempering temperature. NO HT means as normalized.

6.3. OPTICAL MICROSCOPY

Analyzing alloys 2422, 2536 and 2504 with the use of optical microscope, it is possible to follow the development of the microstructure at different temperatures. First of all the samples were normalized. The resulting structure for all the samples is fully martensitic and its typical aspect after Villella's etching is shown in Figure 42; alloy 2504 was chosen as an example.

All the samples were afterwards tempered at different temperatures. The structure resulting from the tempering process is a function of temperature and time (7). The time was kept constant at 2 hours. The expected microstructure of the alloy at room temperature is fully tempered martensite, for lower heat treatment temperatures where ferrite is the only thermodynamically stable phase; then, a combination of tempered and fresh martensite is

expected for the intermediate temperatures of maintenance; finally, fully fresh martensite, for sample treated in the γ region, is expected.

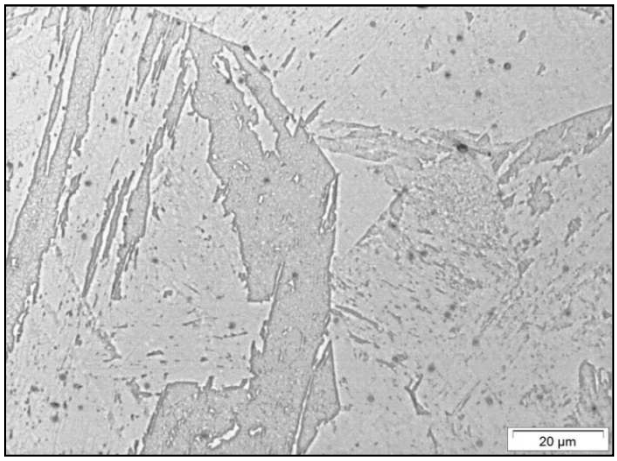

Figure 42. Alloy 2504 normalized at 1050°C. Optical microscope; Villella's etching 10s.

All the alloys were observed for treatment temperatures of 700°C, 750°C and 800°C. One phase could be seen in samples that were treated at 700°C while two different phases are visible for higher temperature.

The second phase, initially appears at grain boundaries: it is clearly visible in all treated samples at 750°C. At higher temperatures, intra-granular nucleation starts to occur. At 800°C the new phase develops almost exclusively at interlath locations.

Alloy 2504 was further analyzed, in order to study the evolution of the process, considering all the temperatures.

Between 740°C and 760°C the grain boundary position for the second phase is confirmed while, at higher temperatures, the new phase develops inside the grains, as already observed. The evolution goes on up to 860°C but, for treatment temperature of 880°C, the new phase appears to be completely developed. Finally, the resulting structure is a finer one correspondent to the observed phase after normalization at 1050°C.

Figure 43 shows the aspect of the samples observed after Villella's etching.[17]

The same kind of picture had been taken for steel X20CrMoV 12-1. The resulting microstructure is shown in Figure 44.

The most visible feature is the presence of carbide. As a result, the martensitic structure of the tempered martensite is well defined almost everywhere, giving a huge difference with an extra low C alloy.

[17] Images taken on alloys 2422 and 2536 are reported in Appendix B.

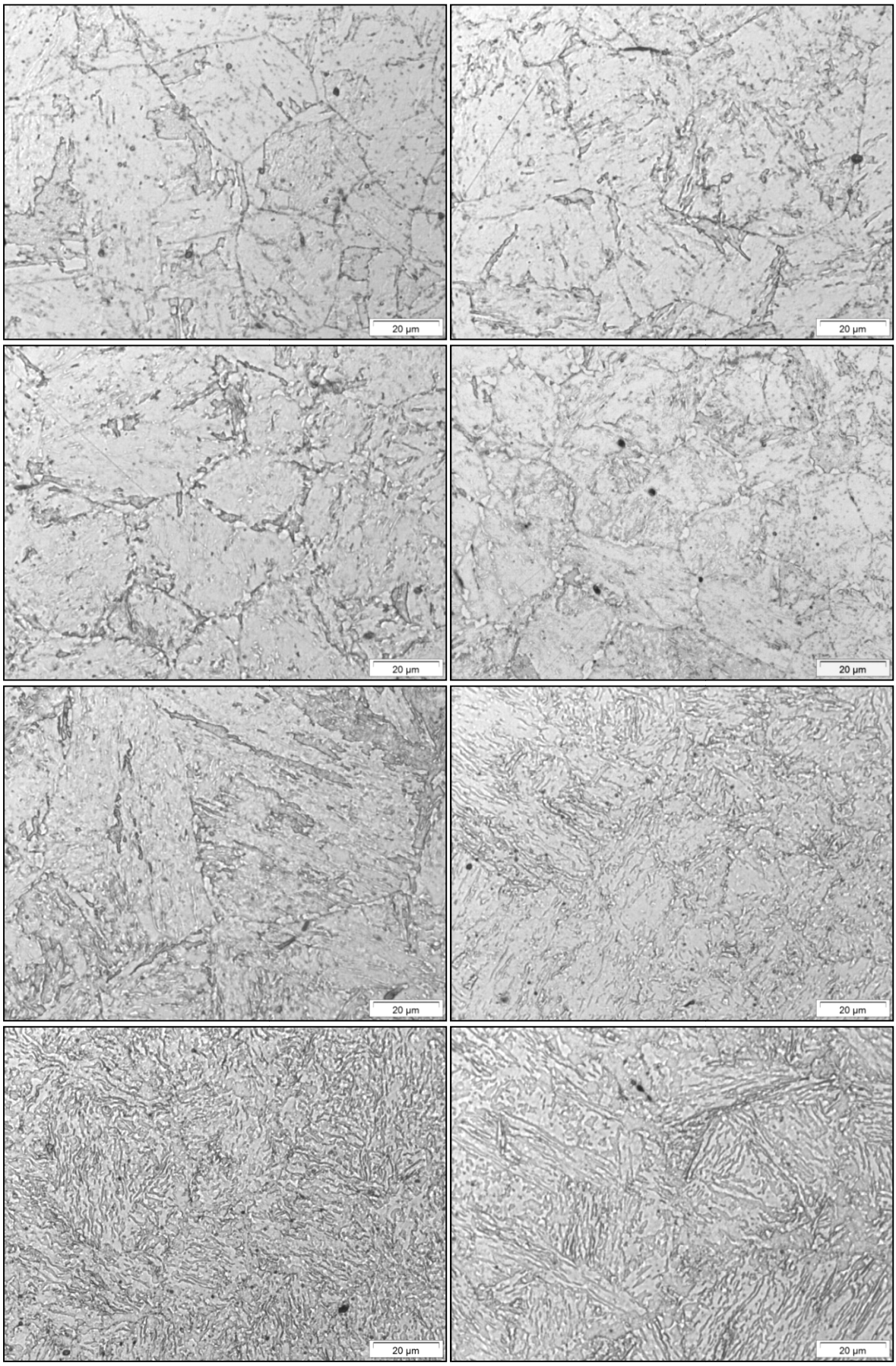

Figure 43. Alloy 2504 tempered for 2h after normalization; optical microscope; Villella's etching 10s; from the top: samples treated at 700°C (left), 730°C (right), 740°C, 750°C, 760°C, 770°C, 780°C, 790°C;…

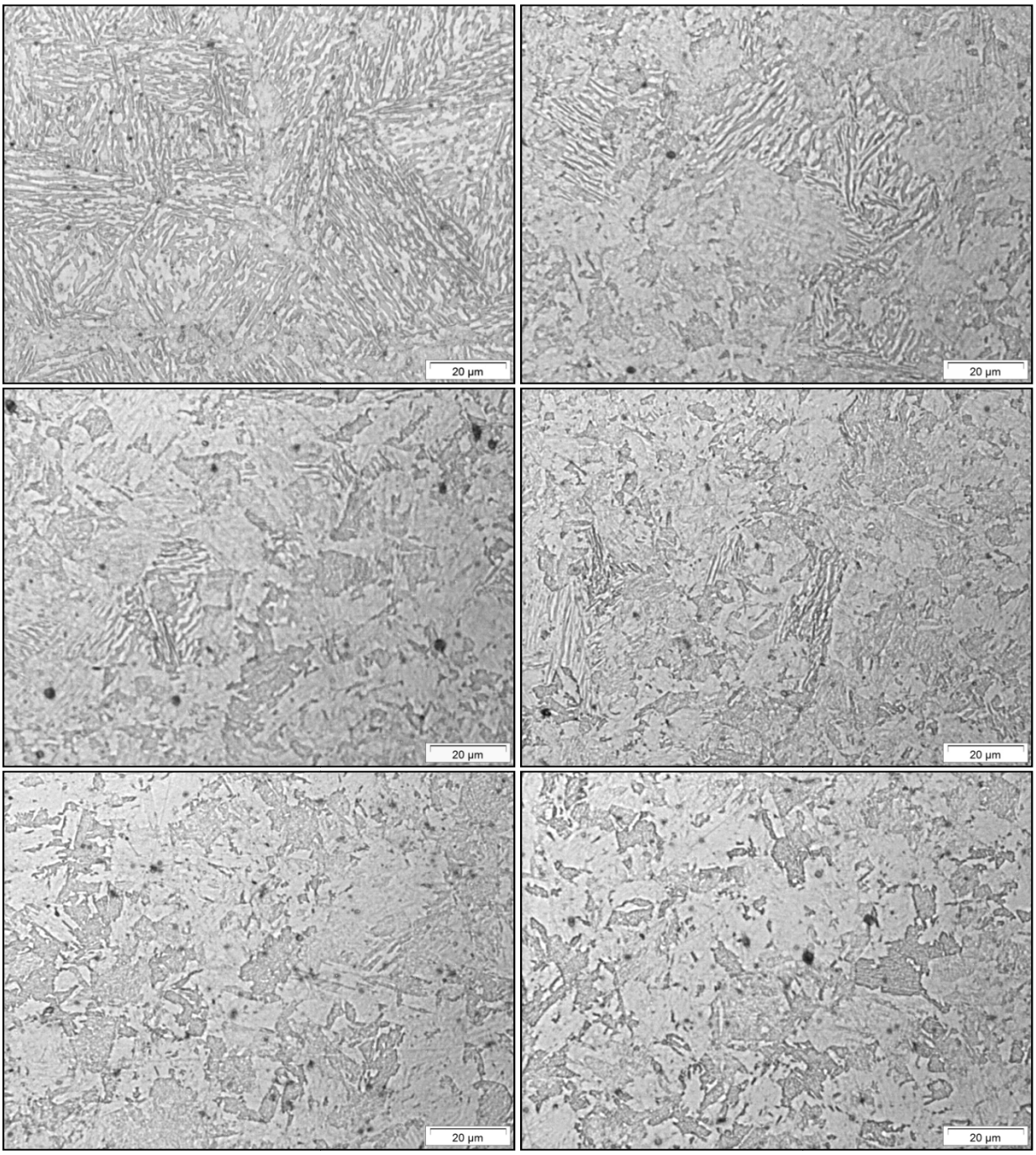

…continue: alloy 2504 tempered for 2h after normalization; optical microscope; Villella's etching 10s; from the top: samples treated at 800°C (left), 820°C (right), 840°C, 860°C, 880°C, 900°C.

On the other hand, it is not possible to distinguish the formation of a second phase; moreover, attention has to be paid to distinguish the differences due to different orientations of the martensitic variants inside the different austenitic grains, or etching dishomogeneities, from an eventual development of a second phase.

Figure 45 shows the aspect of the alloy due to different variant orientations as revealed by optical microscopy after Villella's etching. The same is visible in Figure 44 for treatment temperatures of 800, 820°C.

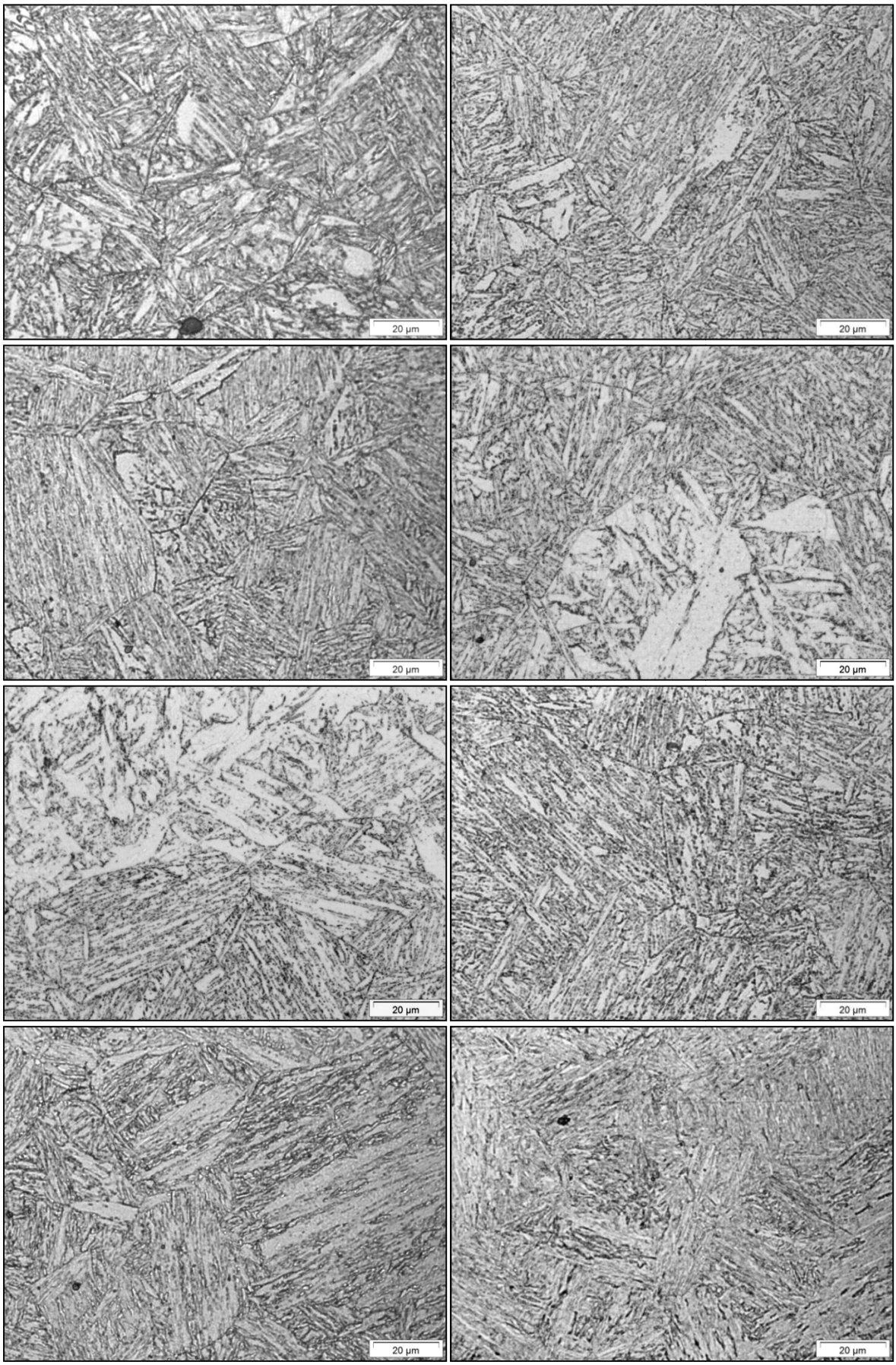

Figure 44. X20CrMoV 12-1 tempered 2h after normalization; optical microscope; Villella's etching 10s; from the top: samples treated at 740°C; 760°C; 780°C; 800°C; 820°C; 840°C; 860°C; 880°C;...

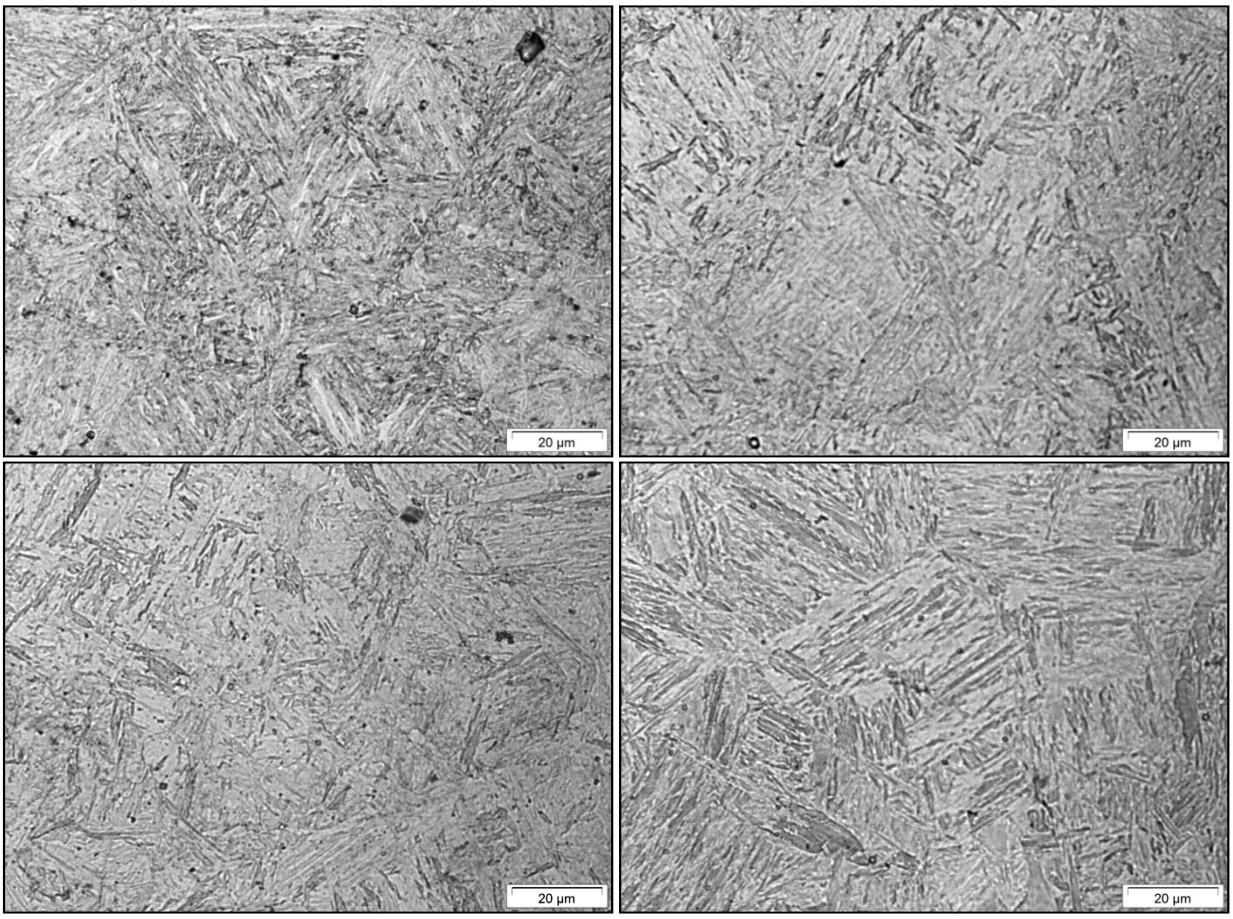

…continue: X20CrMoV 12-1 tempered 2h after normalization; optical microscope; Villella's etching 10s; from the top: samples treated at 900°C; 920°C; 940°C, as normalized.

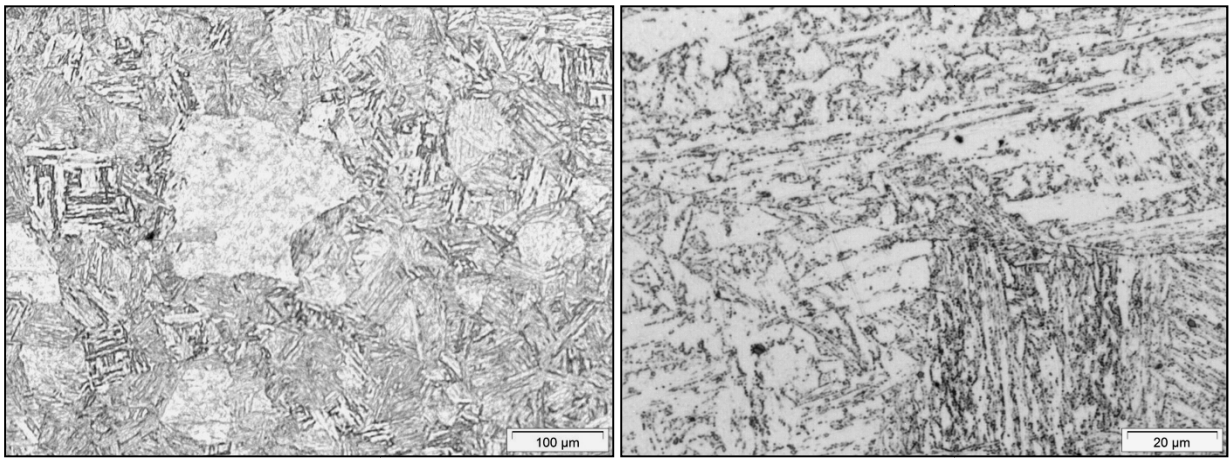

Figure 45. Alloy X20CrMoV 12-1 tempered 2h at 860°C after normalization; optical microscope, Villella's etching 10s.

In order to distinguish between the two different phases, Aqua regia and Kalling II reagent were used too, but no further information on this point is given.

With regard to carbides, an additional observation can be done. They appears to become spherical during tempering and this process is more evident increasing treatment temperature. On grain boundaries up to 840°C speroidized carbide are visible; at 860°C carbides cannot be revealed by the etching: this is visible on grain boundaries where they are no more observable (Figure 44). Finally, for treatment temperature of 880°C they are not clearly revealed any more by Vilella's etching.[18]

Kalling II reagent is not giving further information, while Aqua regia appeared to be a better reagent to reveal carbides. Carbide appears light blue and are easily distinguished.[19] They appears spherical but not distributed in dimension; that indicates a dimension smaller than the resolution power of the microscope meaning that their real shape actually cannot be revealed. In Figure 49, the presence of carbides in the steel is shown and their progressive dissolution increasing the treatment temperature is visible.[20]

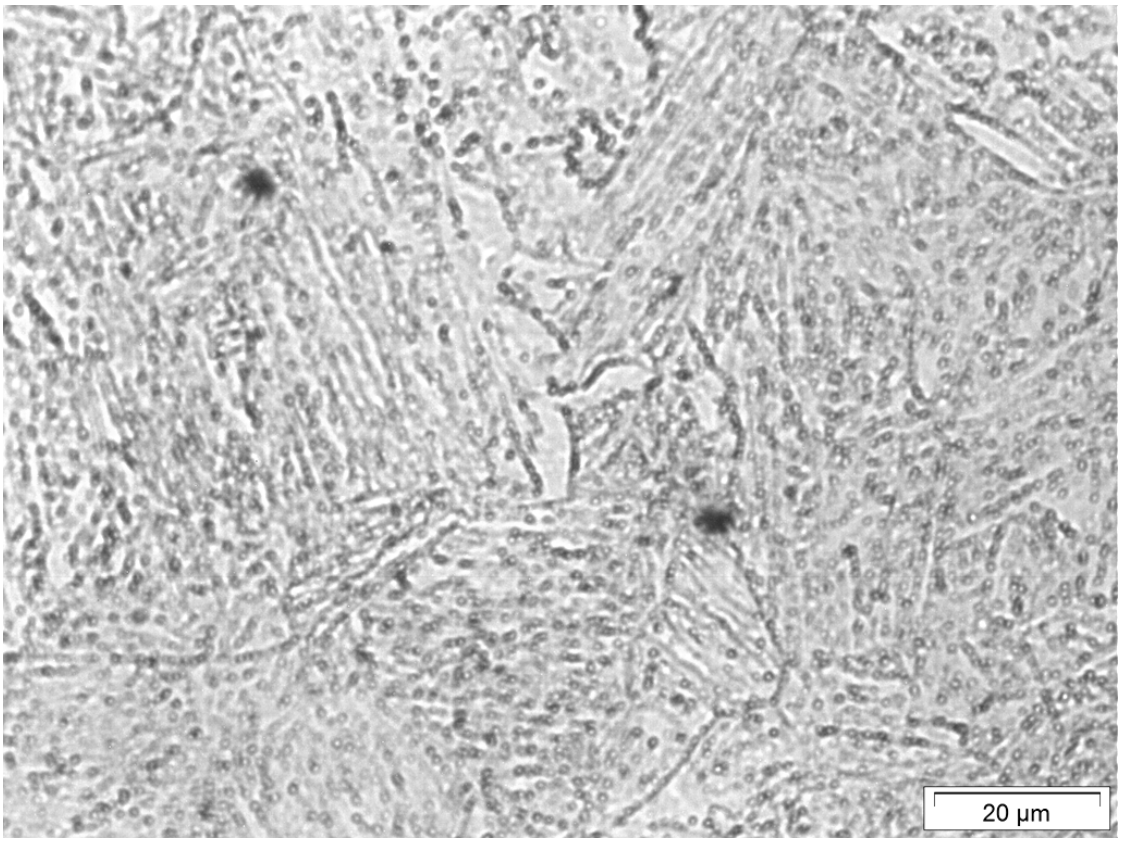

Figure 46. X20CrMoV 12-1 tempered 2h after normalization; optical microscope; Aqua regia etching 40s; sample treated at 760°C;…

[18] Details of the images taken on samples treated at 840°C and 880°C are shown in Appendix B.

[19] Exempla of colored images are reported in Appendix B.

[20] Oil can be used as media in order to increase the resolution of the microscope. Results are reported in Appendix B.

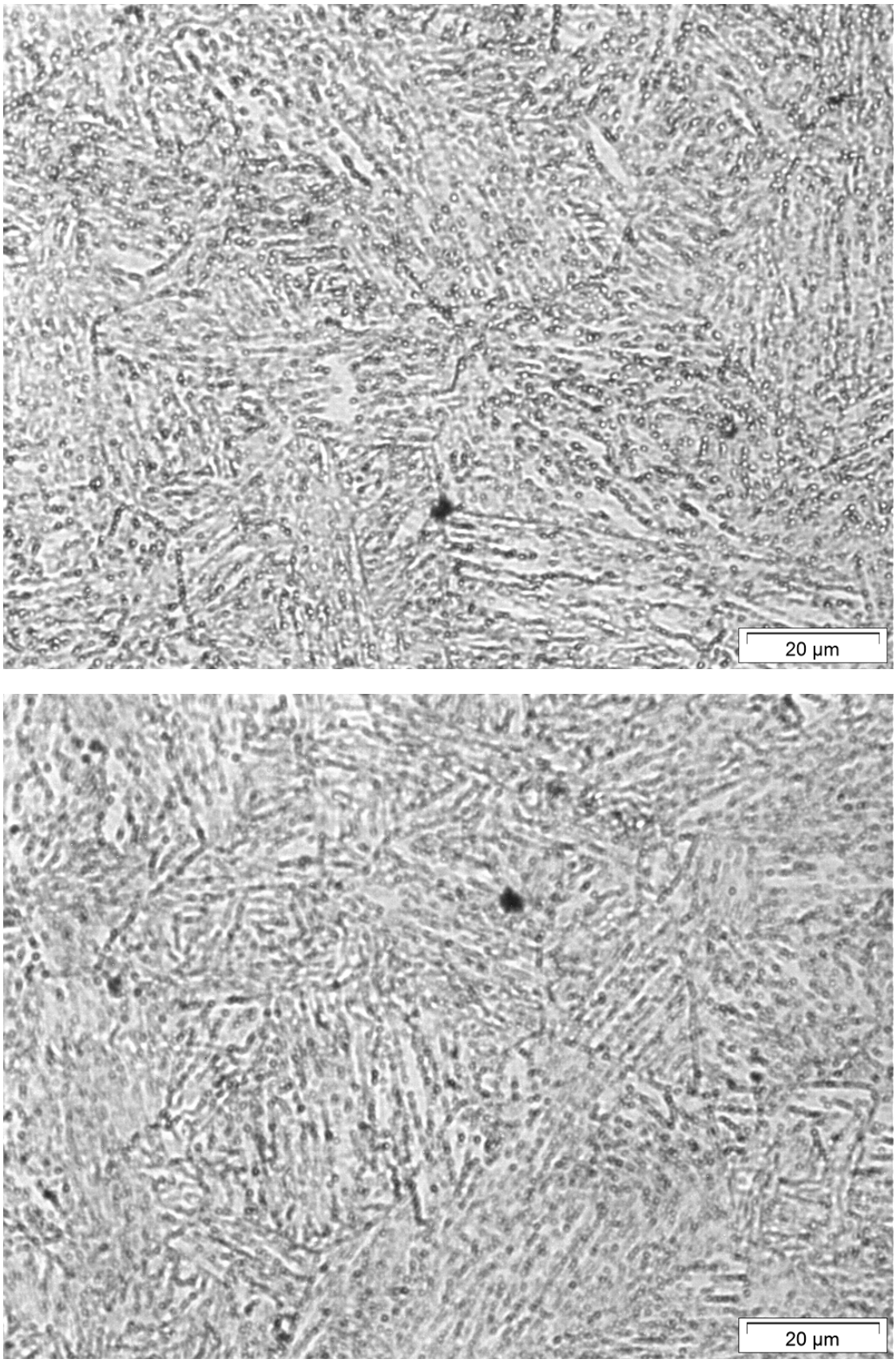

… X20CrMoV 12-1 tempered 2h after normalization; optical microscope; Aqua regia etching 40s; samples treated at 780°C; 800°C;…

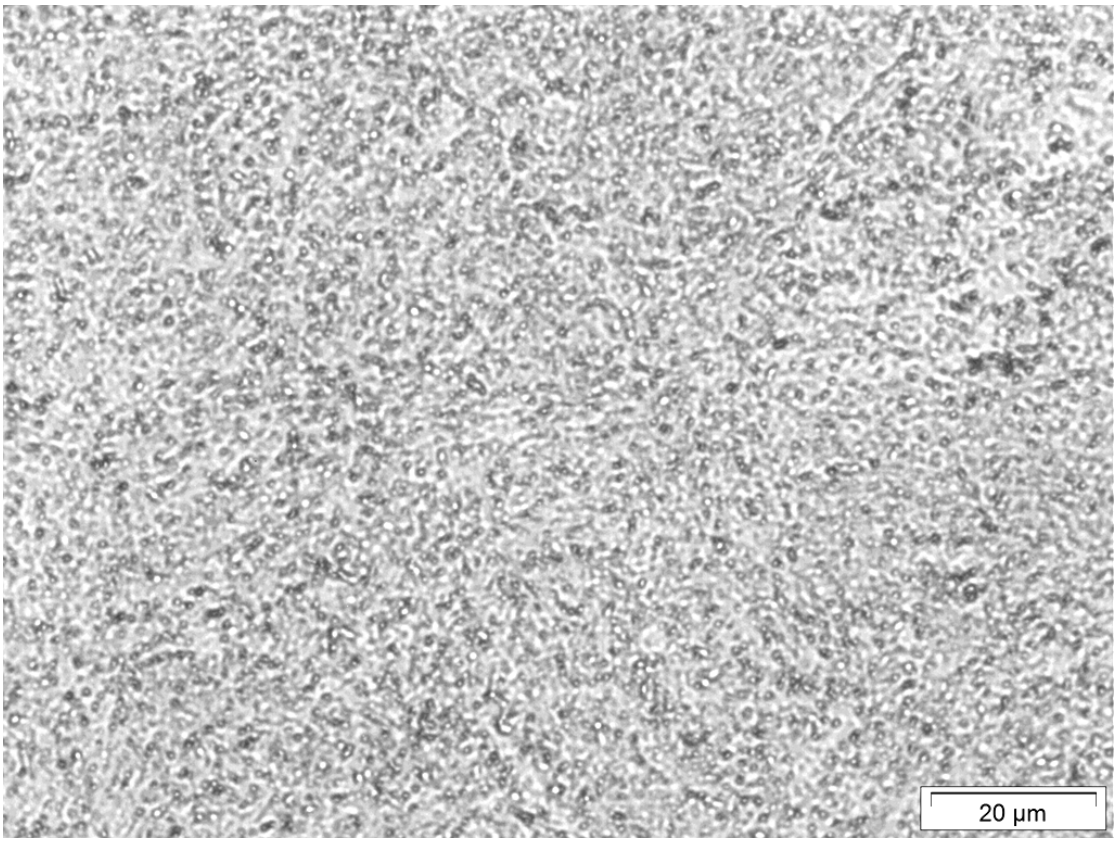

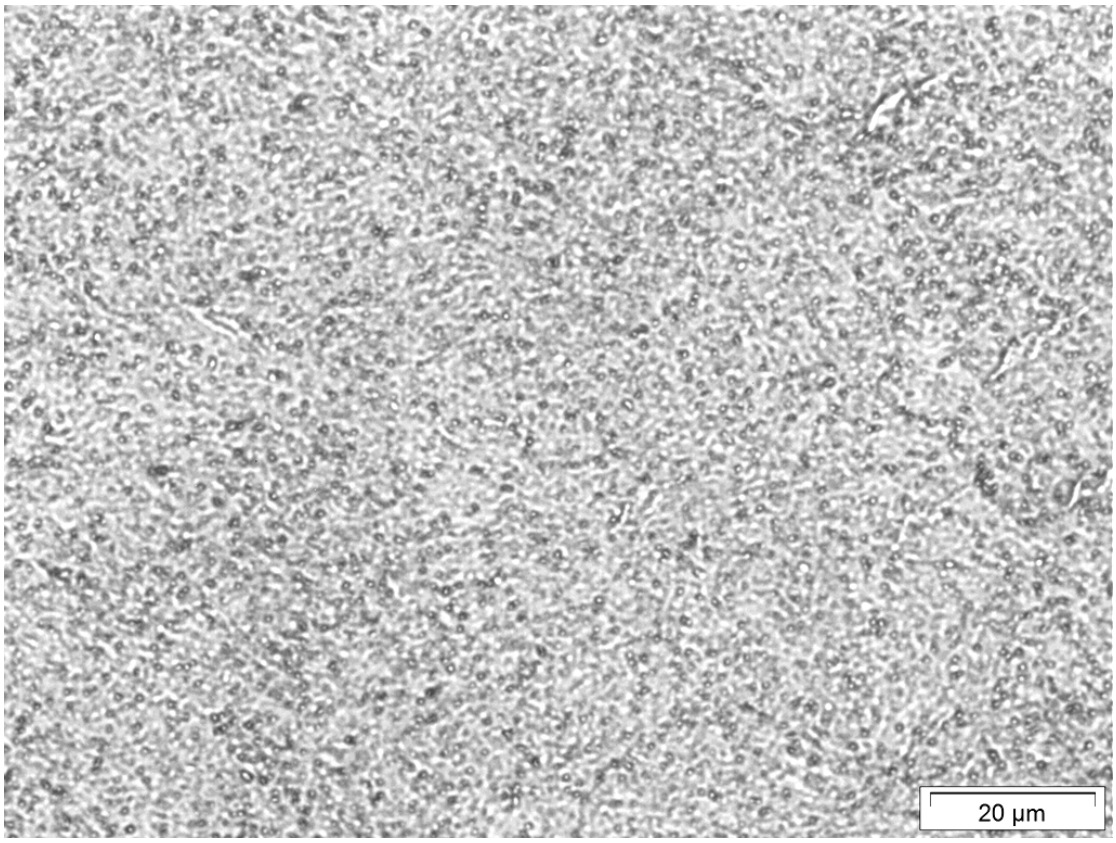

… X20CrMoV 12-1 tempered 2h after normalization; optical microscope; Aqua regia etching 40s; samples treated at 820°C; 840°C;…

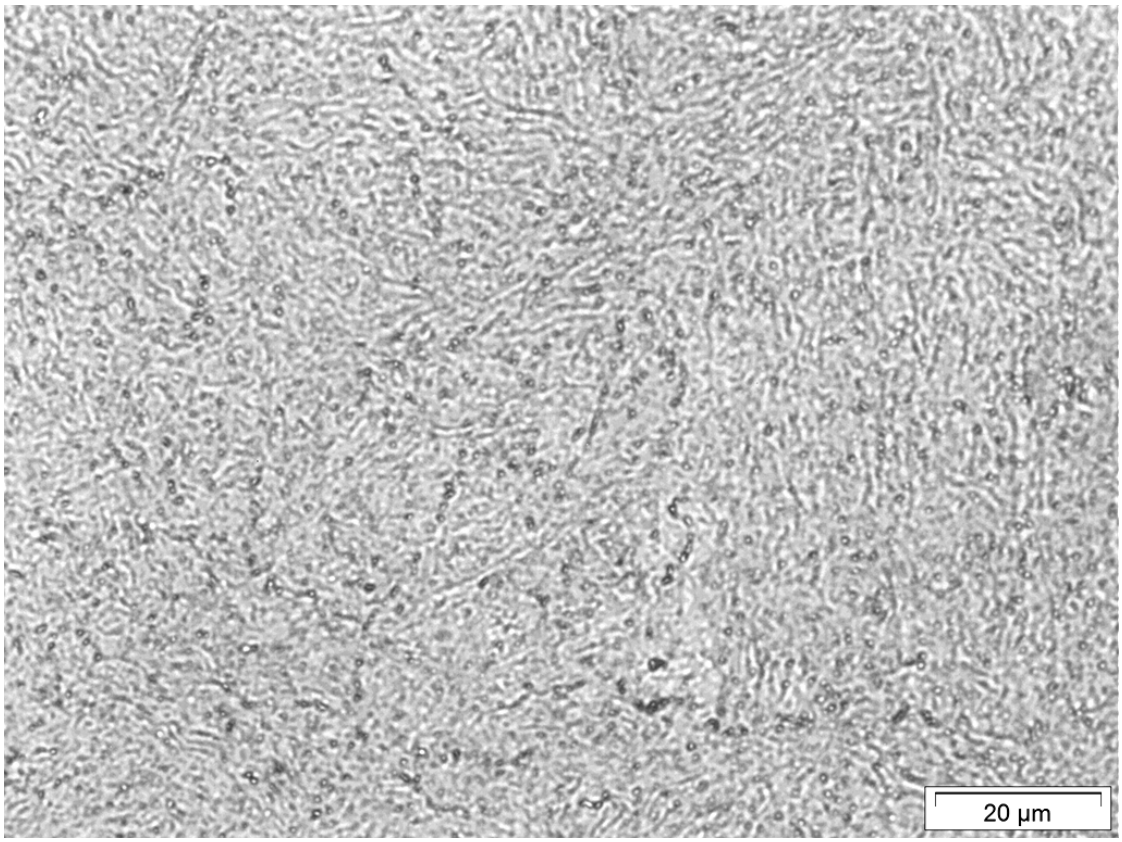

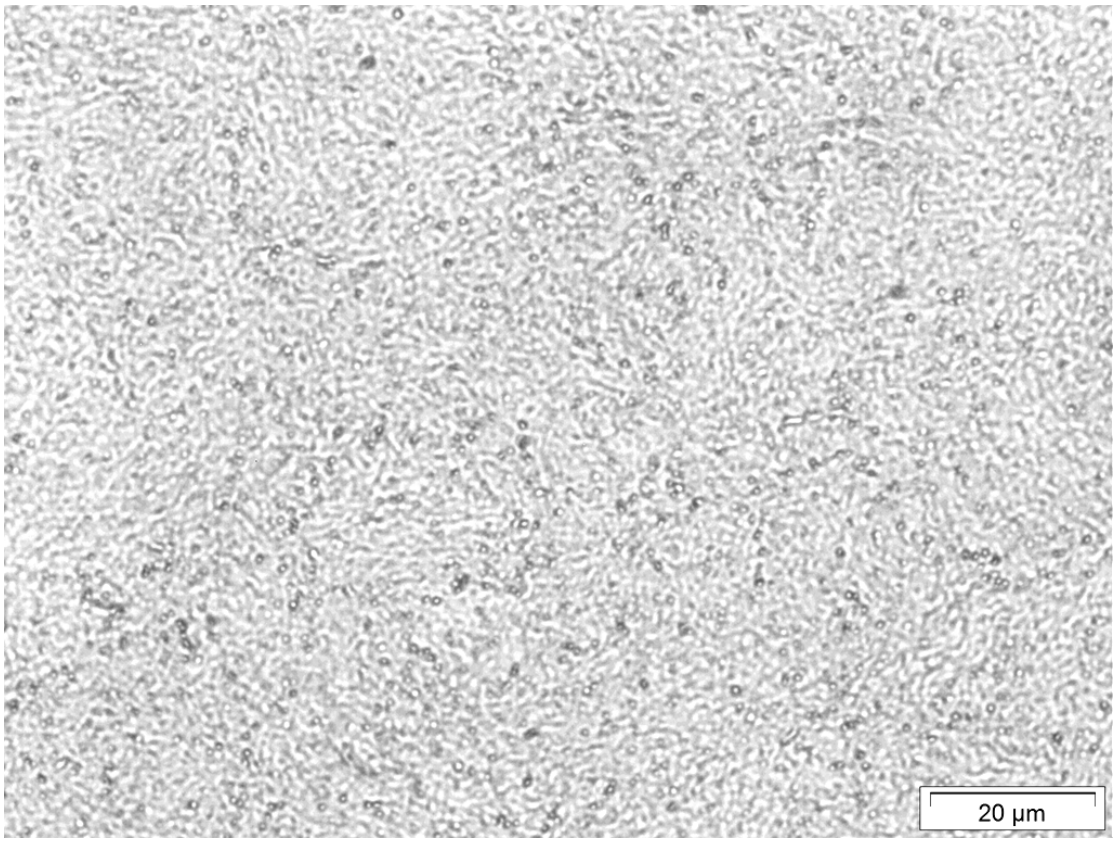

… X20CrMoV 12-1 tempered 2h after normalization; optical microscope; Aqua regia etching 40s; samples treated at 860°C; 900°C;…

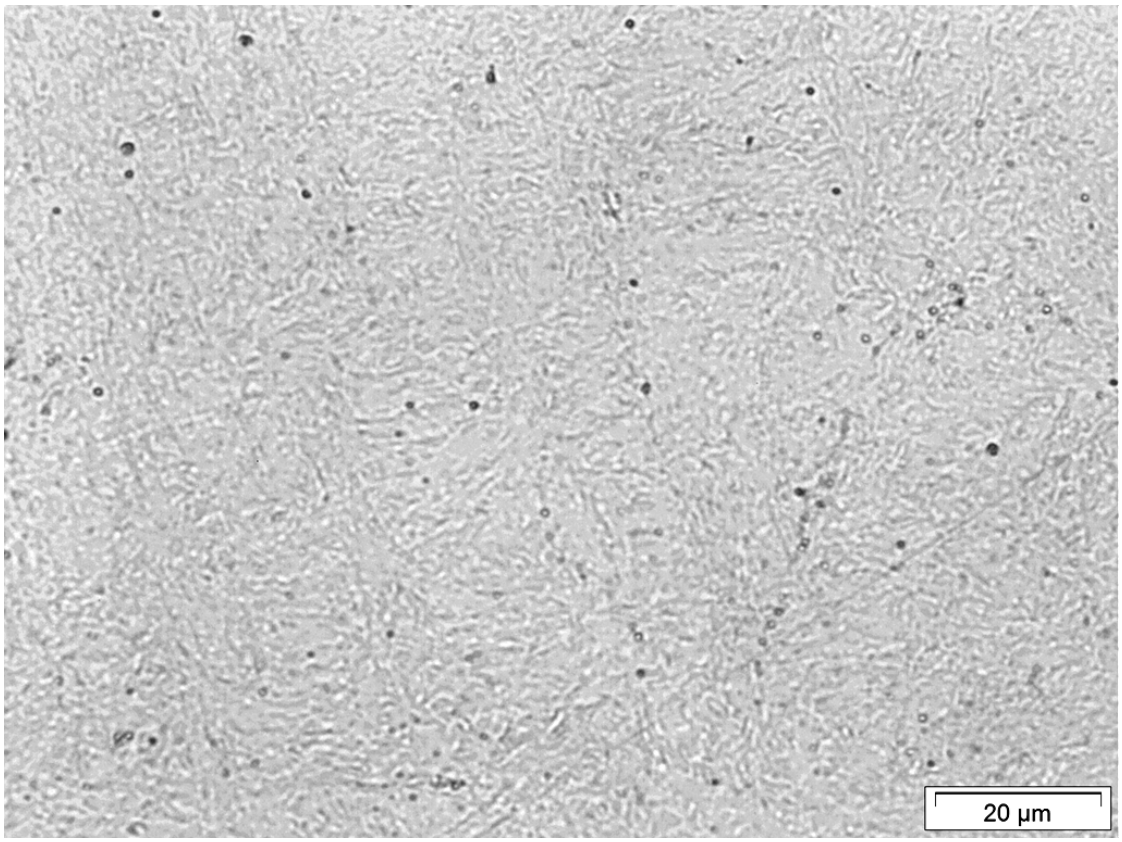

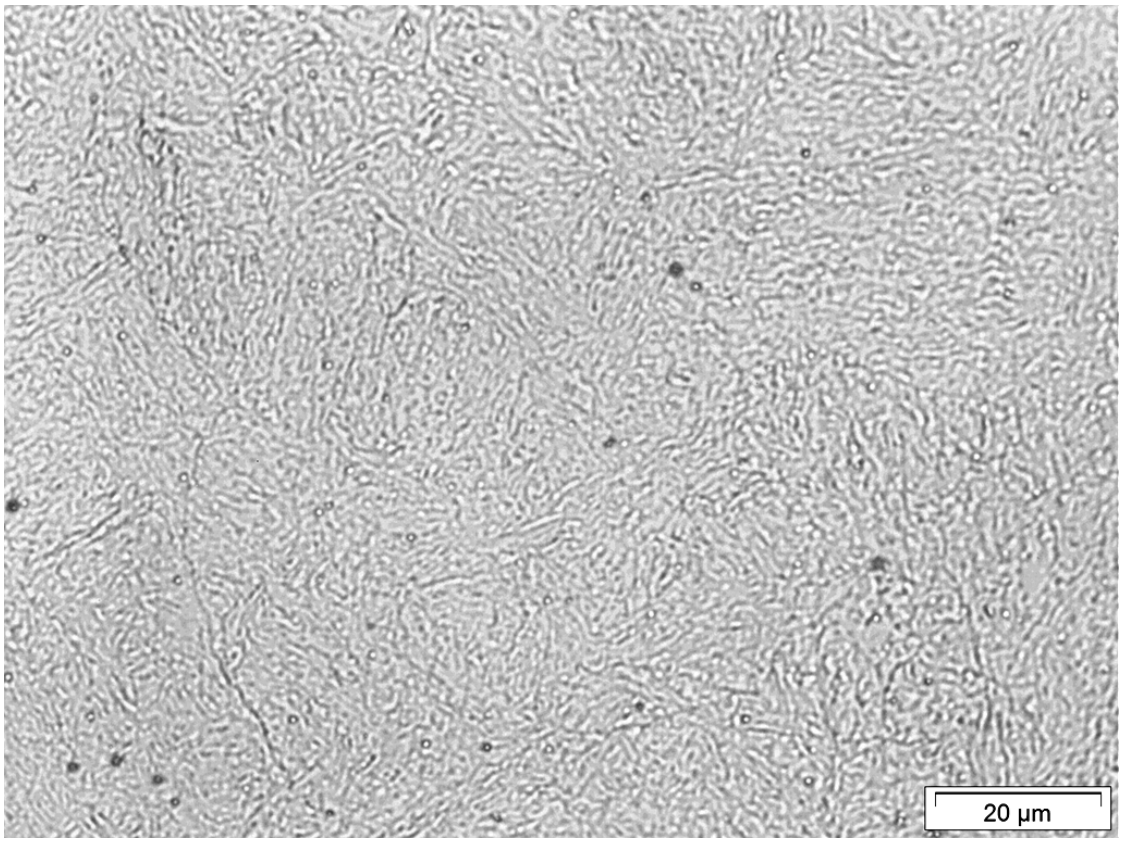

...continue: X20CrMoV 12-1 tempered 2h after normalization; optical microscope; Aqua regia etching 40s; samples treated at 940°C; and material as normalized.

6.4. DILATOMETRY

6.4.1. Intercritical treatments analysis

6.4.1.1. Experimental method

The fraction of austenite formed during the tempering treatment, both below and above the critical temperatures, was determined through a comparison of linear expansion coefficients.

Three thermal cycles are needed. First the steel was austenitized; the linear expansion coefficient of the austenite is then measured during the subsequent cooling process.

Afterwards, an isothermal anneal (tempering) was performed, both below and above the critical temperatures; the linear expansion coefficient of the resulting steel is measured during the following cooling process before the temperature reaches M_s.

The steel is then cooled to room temperature (more generally a temperature below M_f). Finally, the linear expansion coefficient of the fully martensitic steel was measured during the subsequent heating.[21]

The fraction of austenite formed was determined assuming a linear correspondence between the fraction of a phase and the linear expansion coefficient of the steel as shown in Equation 8:

$$\alpha = \alpha_\alpha X_\alpha + \alpha_\gamma X_\gamma = \alpha_\alpha (1 - X_\gamma) + \alpha_\gamma X_\gamma \rightarrow X_\gamma = \frac{\alpha - \alpha_\alpha}{\alpha_\gamma - \alpha_\alpha}$$

Equation 8. Austenite content after tempering. α represents the linear expansion coefficient of the steel after tempering, α_α the linear expansion coefficient of pure martensite, α_γ the linear expansion coefficient of pure austenite.

[21] The thermal cycles in details had been:

1. Start heating to 1050°C at 1 °C/s;
2. Austenitization at 1050°C for 15 minutes to dissolve delta ferrite and homogenize the structure;
3. Cooling to room temperature at 1 °C/s (comparable with the one obtained in air cooling);
4. Heating as fast as possible (90°C/s) to different temperature at: 700°C, 740°C, 780°C, 820°C, 860°C, 900°C;
5. Tempering/austenitizing 2h at the different temperatures;
6. Cooling to room temperature at 1 °C/s;
7. Heating to 700°C at 1 °C/s;
8. Final cooling.

As the linear expansion coefficients are dependent on temperature, the temperature interval for their determination was chosen where the three different values can be measured:

$$M_s < T < T_{tempering}$$

Equation 9. Temperature interval for the determination of the fraction of austenite formed.

The interval chosen was from 500°C to 675°C.

The linear expansion coefficient of martensite resulted to be different for the different samples. The one measured for the sample treated at the lower temperature had been considered for the whole analysis since effects due to phenomena occurring in samples heated at higher temperature, like precipitations, are avoided. The sensitivity of the analysis to phenomena occurring during tempering is shown in Figure 47.

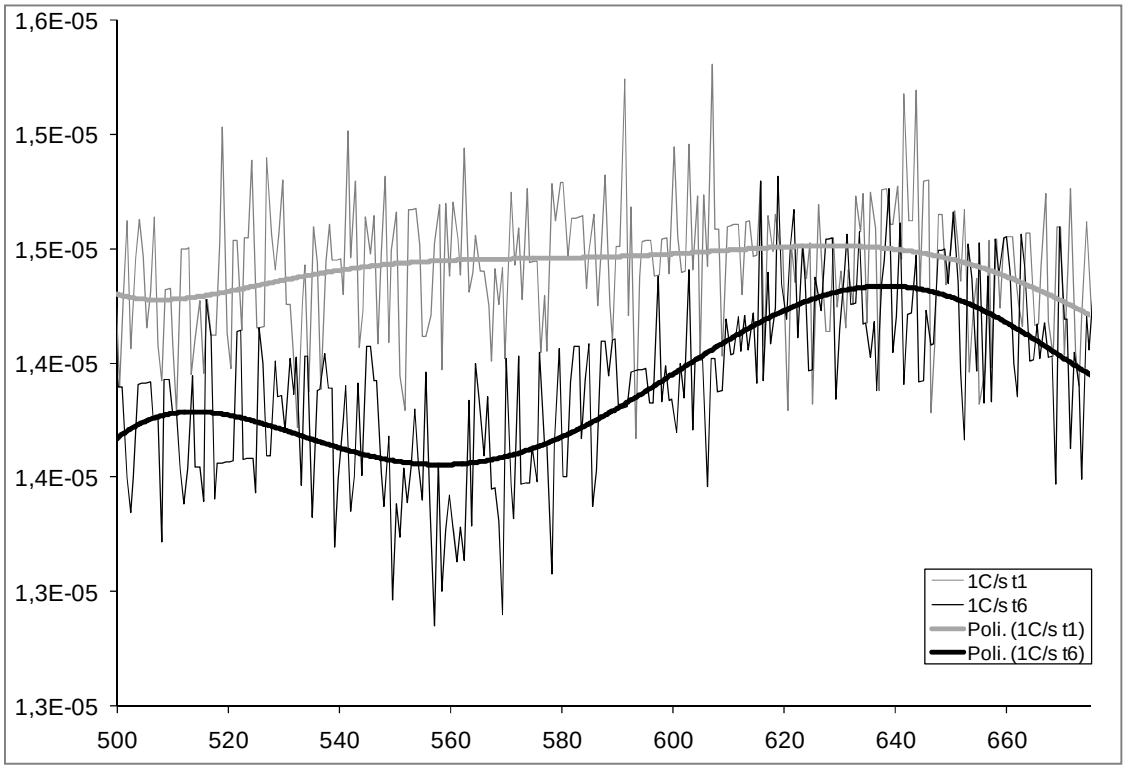

Figure 47. Alloy 2504, samples austenitized 15 minutes and then tempered at different temperatures for 2 hours. Their linear expansion coefficients during a subsequent heating differs in the interval of interest.

6.4.1.2. *Experimental results*

The analysis was performed on as rolled 2504. The M_s temperature for the different samples after normalization is revealed to be almost constant (Figure 48). As this temperature is strongly dependent on the elements content, the composition of the different samples can be assumed constant as well.

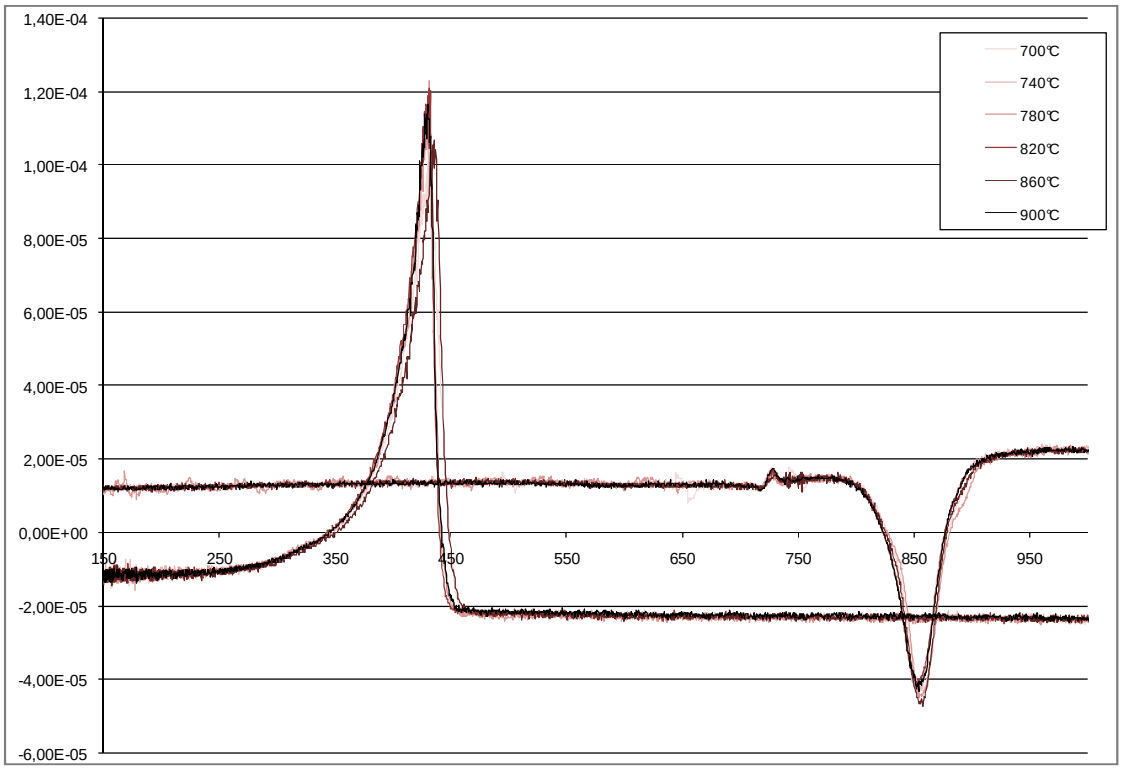

Figure 48. Alloy 2504, as rolled. Linear expansion coefficient as a function of temperature for the different samples, as reported by the dilatometer; austenitization cycle.

The annealing temperature intervals have been chosen between 700°C and 900°C. One test every 40°C had been done. The obtained results are reported in Table 5. The calculated fraction of fresh martensite after cooling is graphically shown in Figure 49.[22]

[22] All the utilized data are reported graphically in Appendix C.

Table 5. Alloy 2504. Results of the analysis performed. α refers to the linear expansion coefficients.

Temperature [℃]	α martensite	α austenite	α tempered steel	f. transformed
700	1,44E-05	2,25E-05	1,43E-05	-0,7%
740	1,44E-05	2,25E-05	1,48E-05	5,1%
780	1,44E-05	2,29E-05	1,75E-05	36,2%
820	1,42E-05	2,23E-05	2,05E-05	76,5%
860	1,41E-05	2,26E-05	2,23E-05	97,2%
900	1,39E-05	2,21E-05	2,20E-05	98,6%

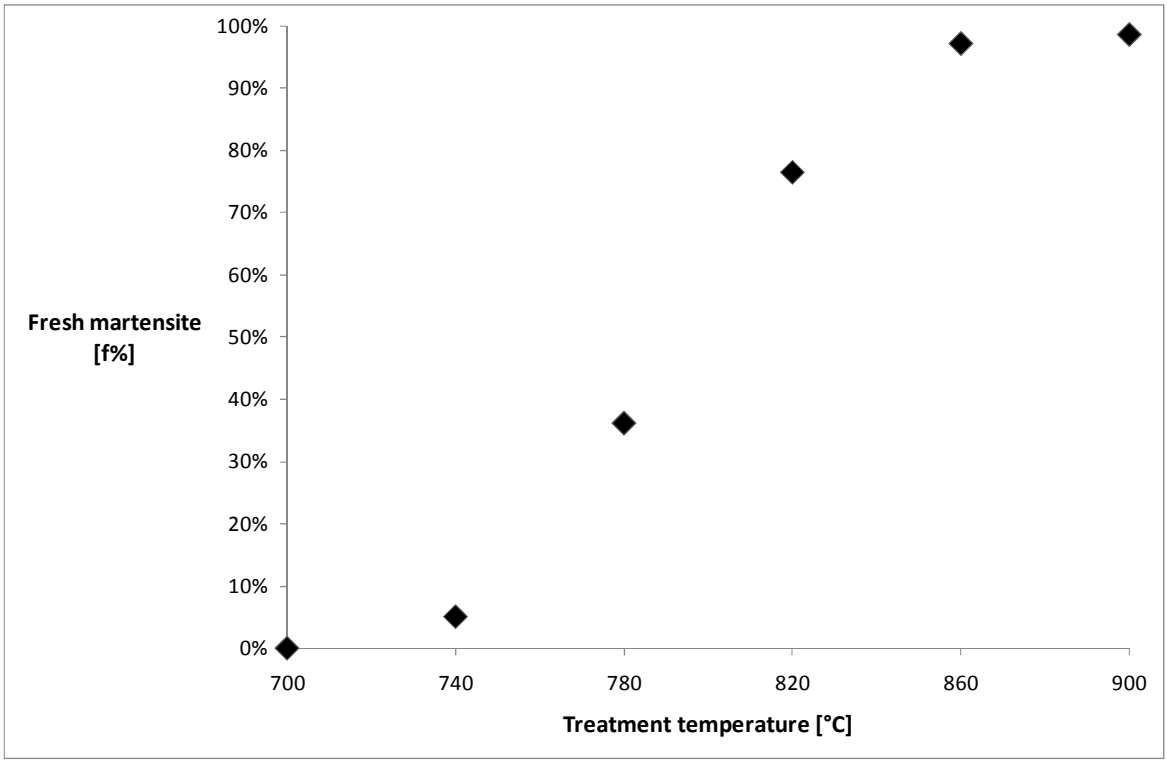

Figure 49. Measured fraction of fresh martensite for 2504 steel after tempering.

6.4.2. Isochronal dilatometry for the determination of the activation energy "E" for the transformation

6.4.2.1. Experimental method

The activation energy had been determined on the basis of the analysis presented by Mittemeijer (9).[23]

[23] The thermal cycles in details had been:

1. Start heating to 1050°C at 1° C/s;
2. Normalization at 1050°C for 15 minutes to dissolve delta ferrite and homogenize the structure;

The fraction of austenite formed was determined from:

$$X_\gamma = \frac{l - l_\alpha}{l_\gamma - l_\alpha}$$

Equation 10. Fraction of austenite formed as a function of temperature. l represent the measured length of the sample, l_α the hypothetic length of the sample if no transformation occur, l_γ the hypothetic length of a completely transformed sample.

As visible, a linear correspondence between fraction transformed and relative length change was considered. This assumption is justified for isothermal transformations (48) while, when a temperature cycle is applied, thermal expansion has to be taken into account. This was done through Equation 11:

$$l_\alpha = l_{start} + \alpha_\alpha(T - T_{start})$$
$$l_\gamma = l_{end} + \alpha_\gamma(T - T_{end})$$

Equation 11. Length of the sample due to the different contribution of austenite and martensite.

Where the starting and the ending points for the transformation are determined as indicated in 6.1.4.1.

The linear expansion coefficients of the phases, in the transformation interval, were inferred from its mean value before the transformation occurs, and after it is finished. As other phenomena occur at temperatures just below A_1, here a narrow interval of 15°C was considered; on the other hand, an interval of 30°C was considered above A_3 for the determination of the linear expansion coefficient "α_γ".

Afterwards, the fraction transformed was plotted as a function of temperature for the different heating rates. The temperatures corresponding to an equal fraction transformed for the different heating rates were determined graphically as shown in Figure 50. The analysis had been performed on the whole interval every 10%.

3. Cooling to 20°C: → 1°C/s;
4. Heating to 1050°C at 5 °C/min, 10 °C/min; 20°C/min;
5. Cooling to 20°C: → 1°C/s.

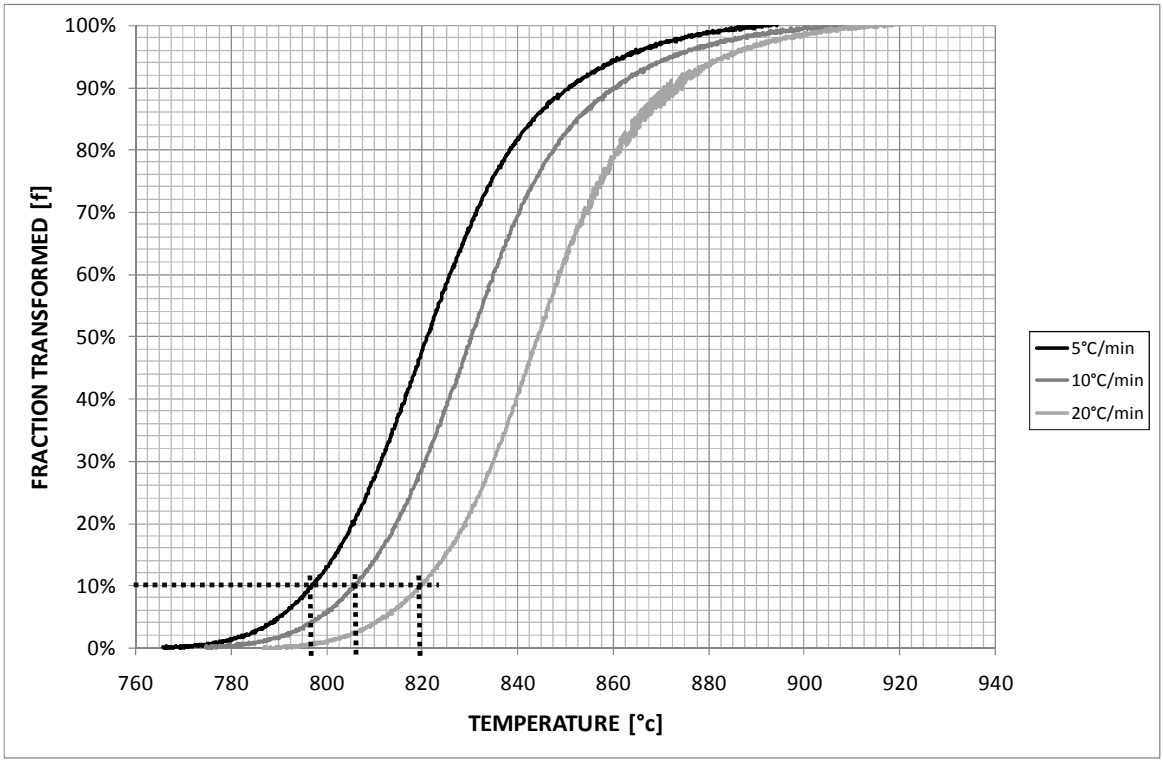

Figure 50. Alloy 2504 as rolled. Fraction transformed as a function of temperature for different heating rates.

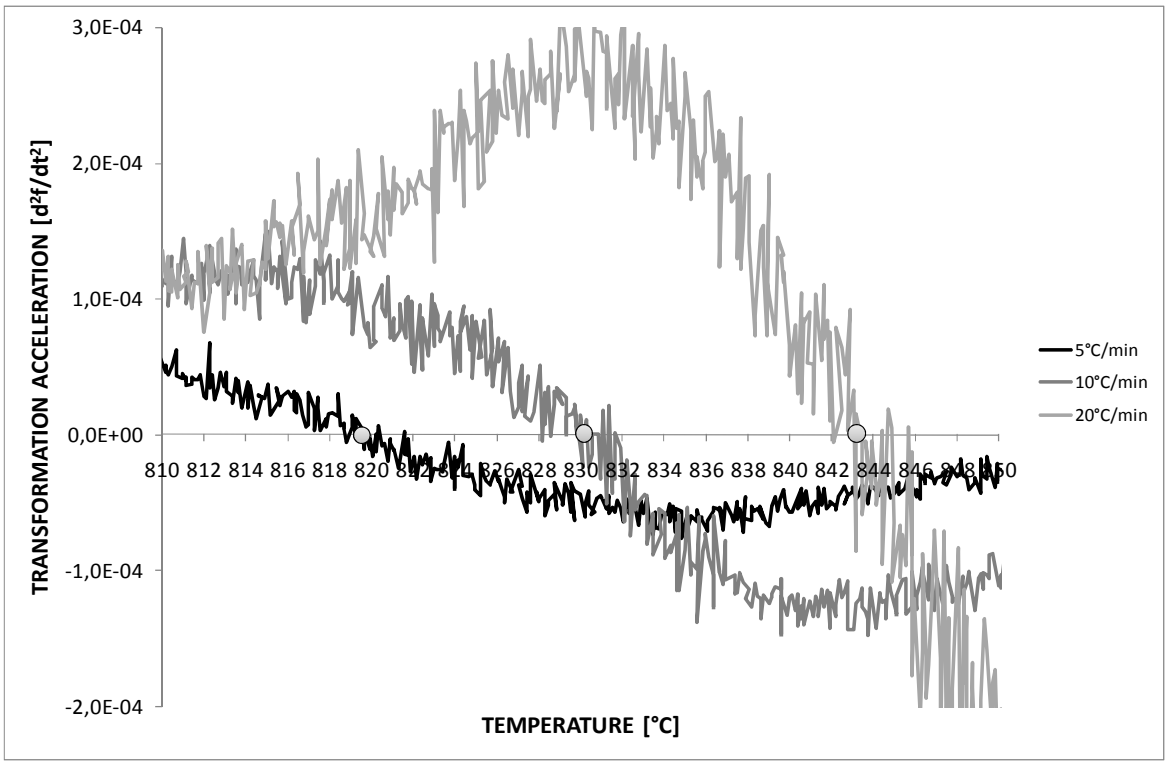

Figure 51. Acceleration of the transformation as a function of temperature for different heating rates. Zoom of the intercept with the X axis.

Finally, since the fraction transformed where the transformation rate reaches its maximum value is, in good approximation, independent from the heating rate, the acceleration of the transformation was plotted, applying a smoothening effect, and the temperatures determined (Figure 51).

The activation energy was determined plotting $\ln(T^2/\theta)$ versus 1/T and the slope of the curve multiplied by the universal gas constant R.

However, the analysis performed gave inconsistent results. This is discussed further in section 7.2.

6.4.2.2. Experimental results

The analysis was performed on as rolled 2504. The M_s temperatures for the different samples after normalization are almost equal for the samples heated afterwards at 5°C/min and 10°C/min, while it is a few degrees higher for the sample heated afterwards at 20°C/min (Figure 52). As this temperature is strongly dependent on the elements content, the composition of the different samples can be assumed as equal in a good approximation. Table 6 reports the results obtained applying the above reported method.[24]

Table 6. Results of the kinetic analysis. E 5→10 is the activation energy measured between the curves resulting from an heating rate of 5°C/min and 10°C/min. E 10→20 is the activation energy measured between the curves resulting from an heating rate of 10°C/min and 20°C/min. E is expressed in kJ/mol.

	5°C/min	10°C/min	20°C/min	E 5→10	E 10→20
T start	766	775	787		
10%	797	806	820	722	468
20%	805	815	829	658	475
30%	811	820	835	741	447
40%	816	826	840	672	485
$\frac{d^2f}{dt^2}=0$	820	830	843	677	527
50%	821	830	844	755	489
60%	826	835	849	762	493
70%	831	841	854	691	538
80%	838	848	860	699	591
90%	850	860	872	715	604
T finish	895	908	919		

[24] All utilized data are reported graphically in Appendix D.

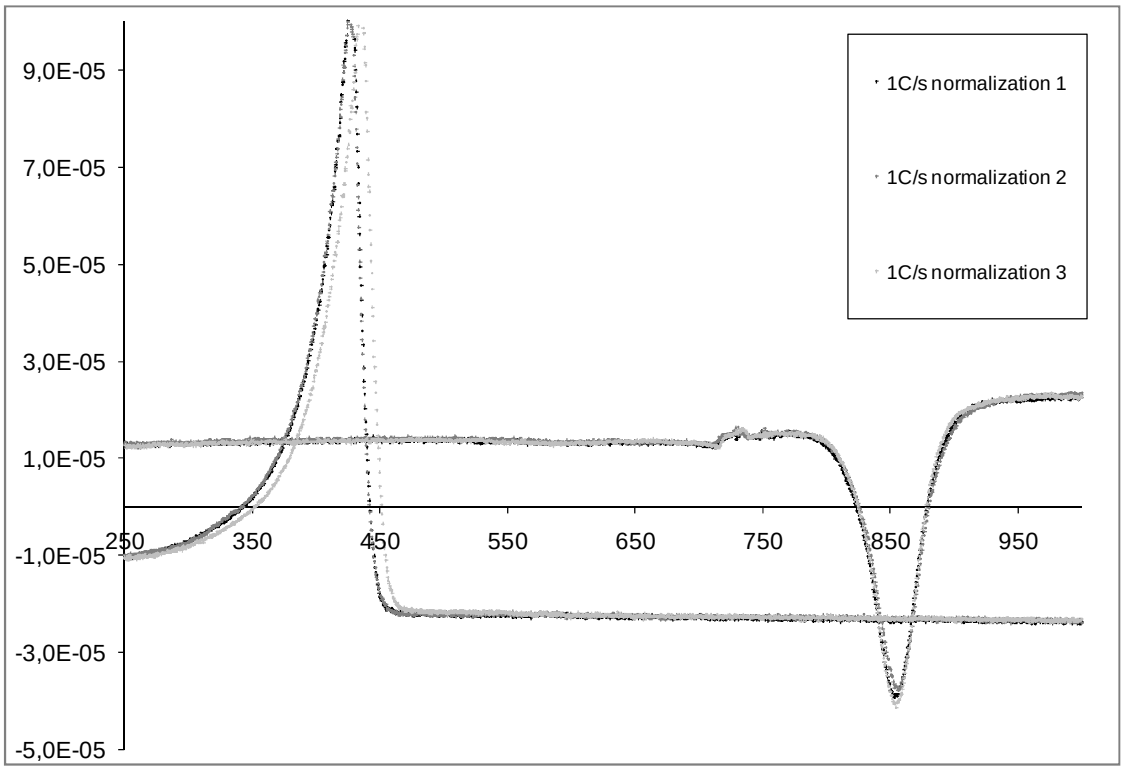

Figure 52. Alloy 2504 as rolled. Linear expansion coefficient as a function of temperature for the different samples, as reported by the dilatometer; austenitization cycle. Normalization 1 refers to the sample afterwards treated at 5°C/min; 2 to the sample treated at 10°C/min; 3 to the sample treated at 20°C/min.

6.4.3. The JMAK equation

The analysis was performed developing the approach presented by Mittemeijer. As reported in 3.5.2, Equation 6, the JMAK equation for non-isothermal transformation can be expressed as follow:

$$f = 1 - \exp\left[-\left(\int k_{(T)}dt\right)^{n}\right] = 1 - \exp\left[-\left(\frac{T^2}{\emptyset}\frac{R}{E}k_{(T)}\right)^{n}\right]$$

However, in order to obtain the "n" parameter (the order of the transformation), few more mathematical passages need to be performed:

$$-ln(1-f) = \left(\frac{T^2}{\emptyset}\frac{R}{E}k_{(T)}\right)^{n}$$

$$ln\left[ln\left(\frac{1}{1-f}\right)\right] = \mathrm{n} * \ln\left(\frac{T^2}{\emptyset}\frac{R}{E}k_{(T)}\right) = n\left[\left(2ln(T) - \frac{E}{RT}\right) + ln\left(\frac{Rk_0}{\emptyset E}\right)\right]$$
$$= n\left[2ln(T) - \frac{E}{RT}\right] + n\left[ln\left(\frac{Rk_0}{\emptyset E}\right)\right]$$

Equation 12. Development of the approach presented by Mittemeijer for the JMAK equation.

This means that "n" represents the slope of the curve obtained plotting $ln\left[ln\left(\frac{1}{1-f}\right)\right]$ as a function of $\left[2ln(T) - \frac{E}{RT}\right]$ for a fixed heating rate.

Equally, "n" represent the slope of the curve obtained plotting $ln\left[ln\left(\frac{1}{1-f}\right)\right]$ as a function of $ln\left(\frac{1}{\emptyset}\right)$ for a fixed temperature.

The kinetic parameter k_0, on the other hand, can be easily evaluated considering a fraction transformed $f = 1 - e^{-1} \approx 0{,}63$. When that is the case:

$$n\left[2ln(T) - \frac{E}{RT}\right] + n\left[ln\left(\frac{Rk_0}{\emptyset E}\right)\right] = 0$$

$$\rightarrow k_0 = \frac{\emptyset E}{RT^2}exp\left(\frac{E}{RT}\right)$$

Equation 13. Equation to be used for the evaluation of k_0,; in order to perform the analysis a fraction transformed of $f = 1 - e^{-1} \approx 0,63$ have to be considered

In performing the analysis an isokinetic reaction was supposed.

The analysis is reported in chapter 7 since a discussion about activation energy for the transformation is first needed.

7. DISCUSSION

7.1. TEMPERING AND INTERCRITICAL TREATMENTS

7.1.1. Extra low carbon alloys

First of all, hardness measurements can be analyzed coupled with the observed microstructure. Hardness measurements on extra low C steels, suggest that the new phase developed after tempering is fresh martensite resulting from the austenite formed during the treatment. Actually, the correlation is not easily visible: hardness measurement indicates a clear increase in hardness only above 770°C while the new structure appears at lower temperatures (740°C in 2504); that is relates to the fact that the initial martensite is becoming softer increasing the temperature while the fraction of harder fresh martensite is increasing: consequently, the hardening effect is shifted to higher temperature (30).

Dilatometric tests on alloy 2504 confirmed the presence of fresh martensite, adding quantitative results. In agreement with optical microscopy, samples treated at 740°C are expected to contain a small fraction of fresh martensite at room temperature; this quantity increases with temperature and is almost equal to 100% for treatment temperature of 860°C.

7.1.2. X20CrMoV 12-1

Analyzing the hardness of X20CrMoV 12-1 a clear increase is visible only above 800°C. Optical microscopy however is not able to confirm the presence of fresh martensite. This is consistent with the fact that, in such a kind of steel, distinguishing fresh and tempered martensite is normally considered not possible (19). The end of the transformation is not determinable either: above 860°C the structure changes and appears to be similar to that observed for normalized material (Figure 44); however a clear distinction between an intercritical treatment and a treatment done above A_3 cannot be observed.

Hardness measurements, moreover, indicates that hardening goes on till the end of the interval considered (940°C), but are not able to indicate the nature of the process responsible for hardening. First of all, hardening can be appointed to an increasing formation of fresh martensite increasing the treatment temperature; nevertheless, dissolution of carbrides can explain the hardnening effect as well: due to higher solubility of carbon in the austenitic phase, carbides could be dissolved into the matrix; consequentelly, dissolved carbon can contribute to strenghtening.

Optical microscopy shows the progressive dissolution of carbides increasing the treatment temperature; however, in order to appoint the hardening effect to carbon it is necessary to establish A_3.

Thermodinamical calculations can be used to add information: using MatCalc software the equilibrium fraction of phases as a function of temperature for the considered X20CrMoV 12-1 material. The result of the analysis is shown in Figure 53: it shows that austenite is expected to appear just around 780°C, and be almost completelly developed at 850°C; carbides, on the other hand, can be completelly dissolved only at higher temperatures (above 950°C).

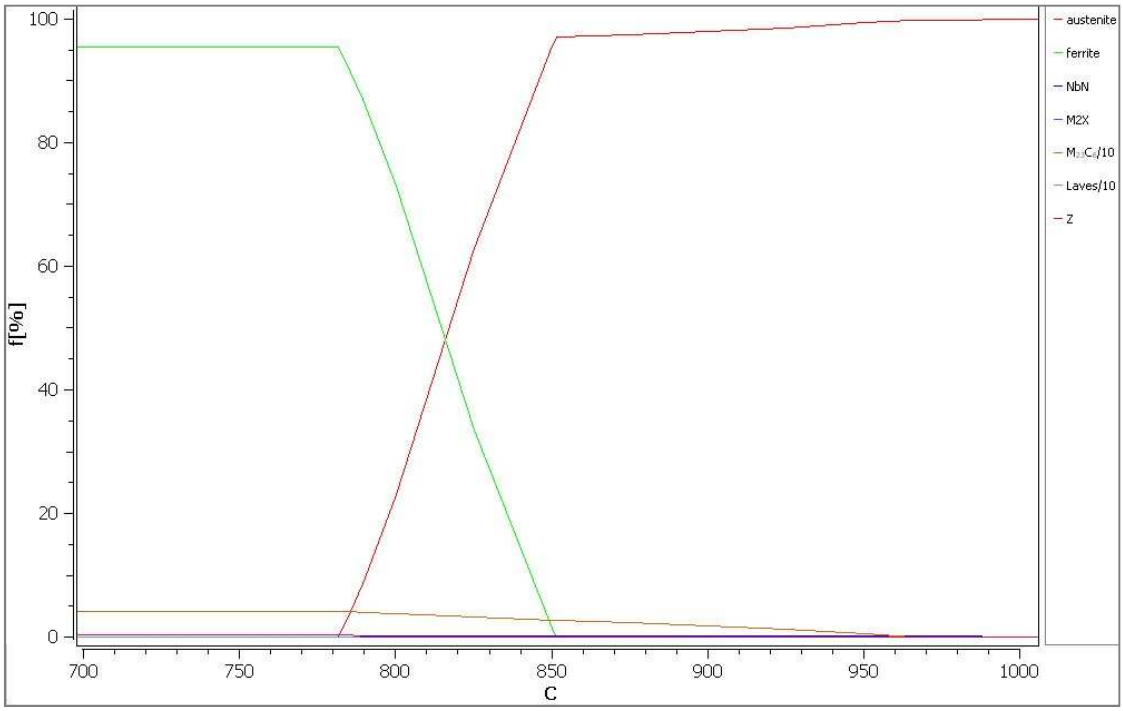

Figure 53. MatCalc. calculation for the reported composition (Table 3) of X20CrMoV 12-1; carbide dissolution (brown line) is complete only at 950°C. "f" indicates the equilibrium phase fraction.

Moreover, data can be found in literature: "*The X20CrMoV 12-1 steel has been in service since the early 1960s*" (50) and its critical temperature was determined by thermal analyses.

In (50), Ac_3 is reported to be 851°C,[25] reinforcing the result expressed by the reported numerical approach and the hypothesis done about the hardening role of C.

7.2. KINETIC ANALYSIS

[25] Actually, a precise value for A_3 cannot be assessed by literature review since composition differences are important in its definition.

7.2.1. Activation energy

As already mentioned in 6.4.2, the results obtained show some inconsistencies. As a matter of fact, the activation energy measured between 5°C/min and 10°C/min is expected to be equal to the one measured considering the data at 10°C/min and 20°C/min. This is not the case (Table 6).

The data received had then been analyzed in order to look for possible causes of inconsistency. Two inconsistencies were found in the data too. First of all, an anomalous behavior is visible for the sample treated at 5°C/min during transformation phenomena occurring below A_1 (Figure 54). They appear at higher temperature for lower heating rate. This is not consistent with what could be expected from kinetic considerations.

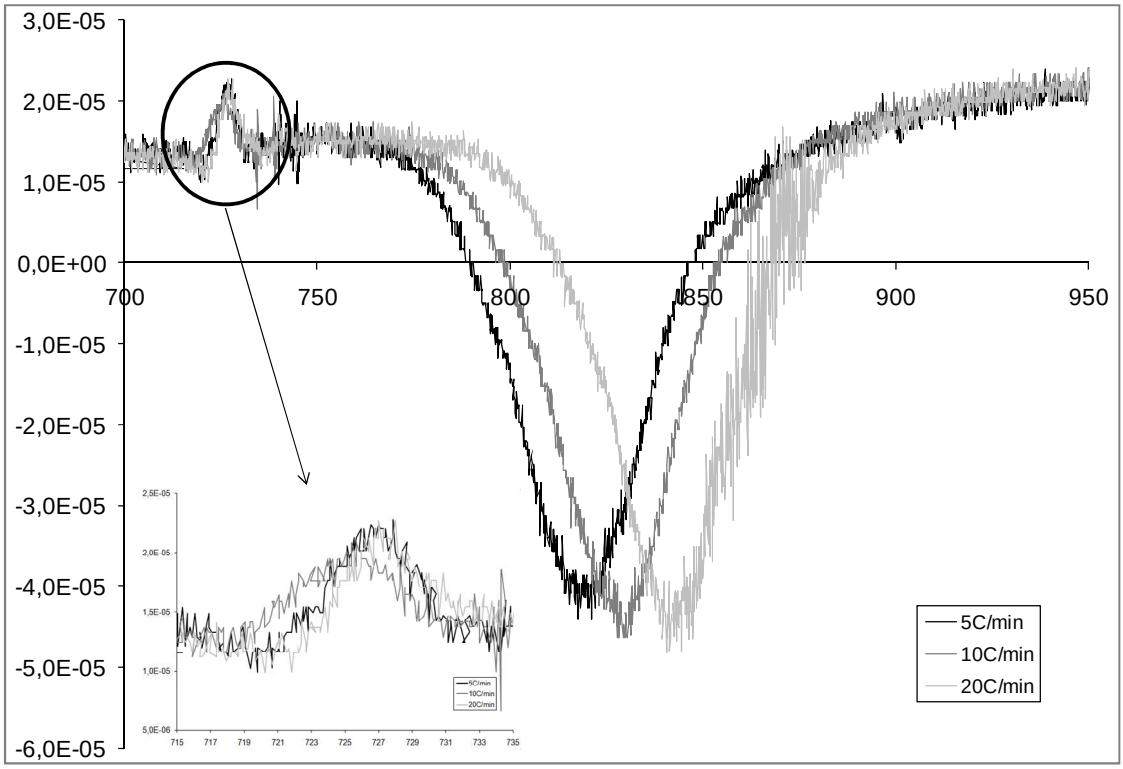

Figure 54. Alloy 2504 after normalization. First anomalous behavior for the transformation temperature.

The second anomalous behavior appears during the subsequent cooling. Comparing this data with the one obtained after normalization, M_s is shifted to higher temperatures. This effect is particularly pronounced for the sample heated at 5°C/min and is still clearly visible for the one heated at 10°C/min (Figure 55). As the composition of the austenitic matrix is not expected to change during the treatment, this behavior appears not consistent.

Both the anomalies seem to indicate a shift of the reference temperature during heating in the direction of a lower temperature.

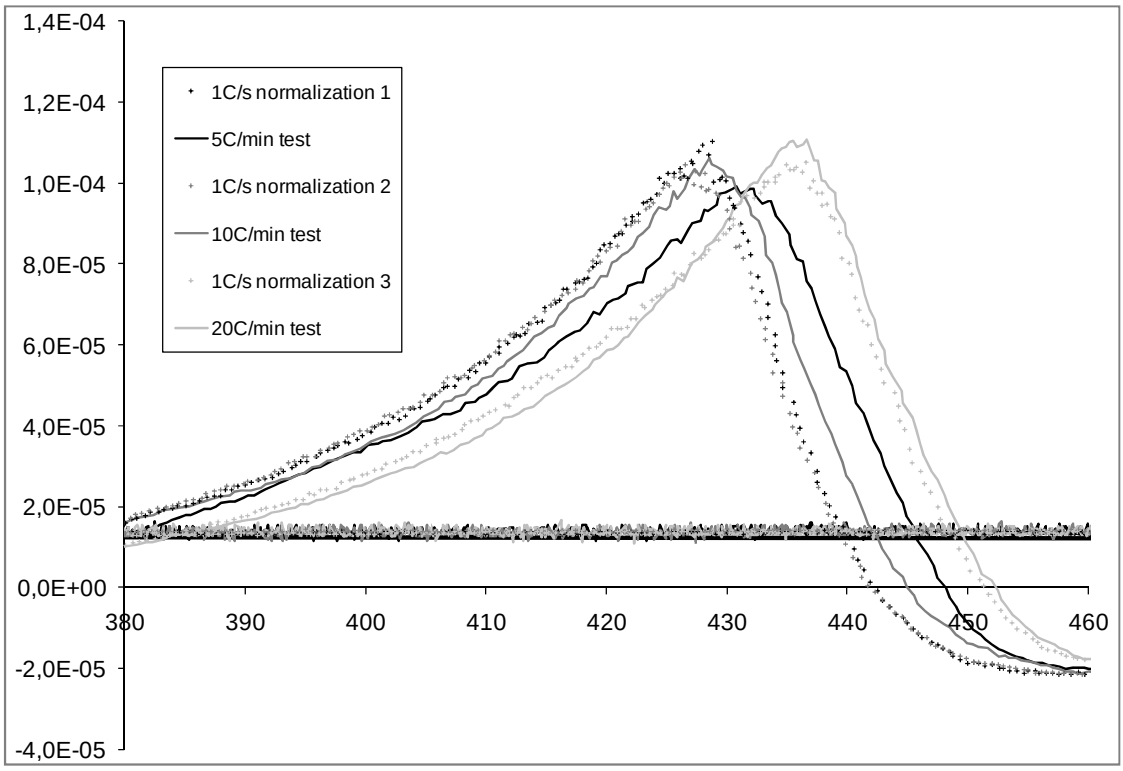

Figure 55. Alloy 2504 after normalization and heating to 1050°C. Second anomalous behavior (Ms shifting).

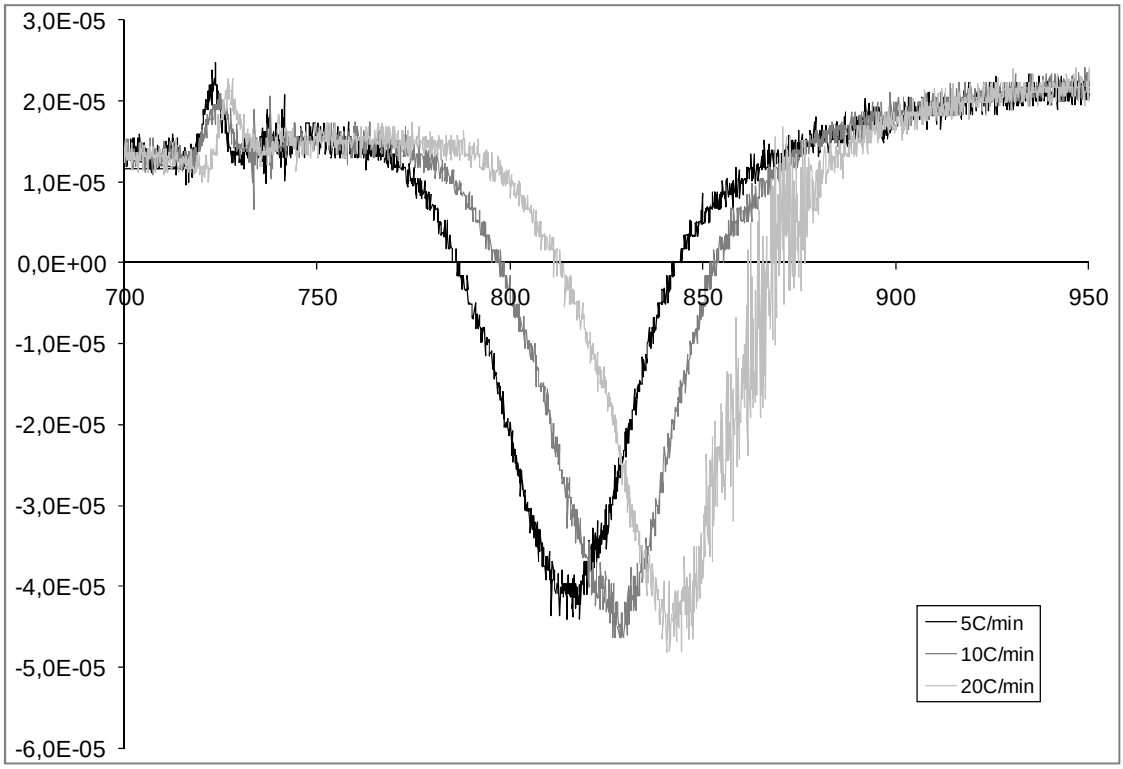

Figure 56. Alloy 2504, as rolled. Vanishing of the first anomalous behavior; the second is vanishing due to the method itself.

On the basis of that observation, data were shifted using M_s temperature[26] after normalization as a reference. Data obtained from the 5°C/min cycle was shifted 5°C; a shift of 1.5°C was applied to data obtained at 10°C/min. Both the anomalous behavior observed vanished (Figure 56).

All the results of the new analysis are shown in Table 7. The inconsistency is no more present: the plot of $\ln(T^2/\theta)$ versus 1/T results in a straight line since the activation energy measured between 5°C/min and 10°C/min are similar to the one measured considering the data at 10°C/min and 20°C/min (Table 7, Figure 75).[27]

Table 7. Results of the kinetic analysis. E 5→10 is the activation energy measured between the curves resulting from an heating rate of 5°C/min and 10°C/min. E 10→20 is the activation energy measured between the curves resulting from an heating rate of 10°C/min and 20°C/min. E is expressed in kJ/mol.

	5°C/min	10°C/min	20°C/min	E 5→10	E 10→20
T start	762	774	787		
10%	792	805	820	491	435
20%	800	814	829	462	442
30%	806	819	835	504	418
40%	811	825	840	472	451
$\frac{d^2f}{dt^2}=0$	815	829	843	475	488
50%	816	829	844	514	455
60%	821	834	849	519	459
70%	826	840	854	485	498
80%	833	847	860	492	544
90%	845	859	872	502	556
T finish	890	907	919		

The activation energy was determined considering the temperature where the transformation rate is maximum: an activation energy of 481.5 kJ/mol had been measured. A similar value (480 kJ/mol) is obtained considering the mean value for E in the interval $0.2 < f < 0.8$.

This value is quite high for diffusion phenomena, indicating a mixed process of both nucleation and diffusion processes during the whole transformation process.

[26] Actually M_s cannot be assessed with the required precision. To translate the presented physical concept in an implementable solution, the peak of the γ→α' transformation was used as reference.
[27] All the utilized data are reported graphically in Appendix E.

7.2.2. Transformation mechanism and JMAK analysis

The kinetic parameter "n" and "k_0" were determined assuming an isokinetic reaction with activation energy of 481.5 kJ/mol.[28] The obtained results for the Avrami exponent "n" are resumed in Table 9 and Table 10 while results for the kinetic parameter k_0 are shown in Table 8.

The kinetic parameter k_0 appears to be not influenced by the heating rate. The same is true for the Avrami exponent "n" (Table 9). However "n" is decreasing during the transformation process, indicating a dependence on the fraction transformed.

Measured data for "n" as a function of "f" are plotted in Figure 57.

Table 8. Obtained value for the kinetic parameter "k_0" [s^{-1}]; $\overline{k_0}$ represent the average for the obtained values.

"k_0"$_{5°C/min}$	"k_0"$_{10°C/min}$	"k_0"$_{20°C/min}$	$\overline{k_0}$
$3{,}4 \cdot 10^{20}$	$3{,}9 \cdot 10^{20}$	$3{,}8 \cdot 10^{20}$	$3{,}7 \cdot 10^{20}$

Table 9. Obtained value for the Avrami exponent "n" as a function of the fraction transformed "f"; $\overline{n}$ represent the average for the obtained values.

"f"	"n"$_{5°C/min}$	"n"$_{10°C/min}$	"n"$_{20°C/min}$	$\overline{n}$
0,1-->0,2	1,8	1,6	1,7	1,7
0,2-->0,3	1,5	1,9	1,6	1,6
0,3-->0,4	1,4	1,2	1,5	1,4
0,4-->0,5	1,2	1,5	1,6	1,4
0,5-->0,6	1,1	1,1	1,2	1,1
0,6-->0,7	1,1	0,9	1,1	1,1
0,7-->0,8	0,8	0,9	1,0	0,9
0,8-->0,9	0,6	0,6	0,6	0,6

Table 10. Obtained value for the Avrami exponent "n" at different temperature "T". "f" represent the fraction transformed [%] for different heating rates at the considered temperatures. "n" represent the resulting slope of the curve.

T [°C]	"f" 5°C/min	"f" 10°C/min	"f" 20°C/min	"n" 5→10	"n" 10→20
800	1	6	18	2.6	1.7
810	4	15	34	2.0	1.4
820	10	30	56	1.8	1.2
830	22	52	74	1.6	0.9
840	40	71	85	1.3	0.6
850	63	84	92	0.9	0.5
860	79	91	96	0.6	0.4

[28] The result of the analysis is graphically shown in Appendix E.

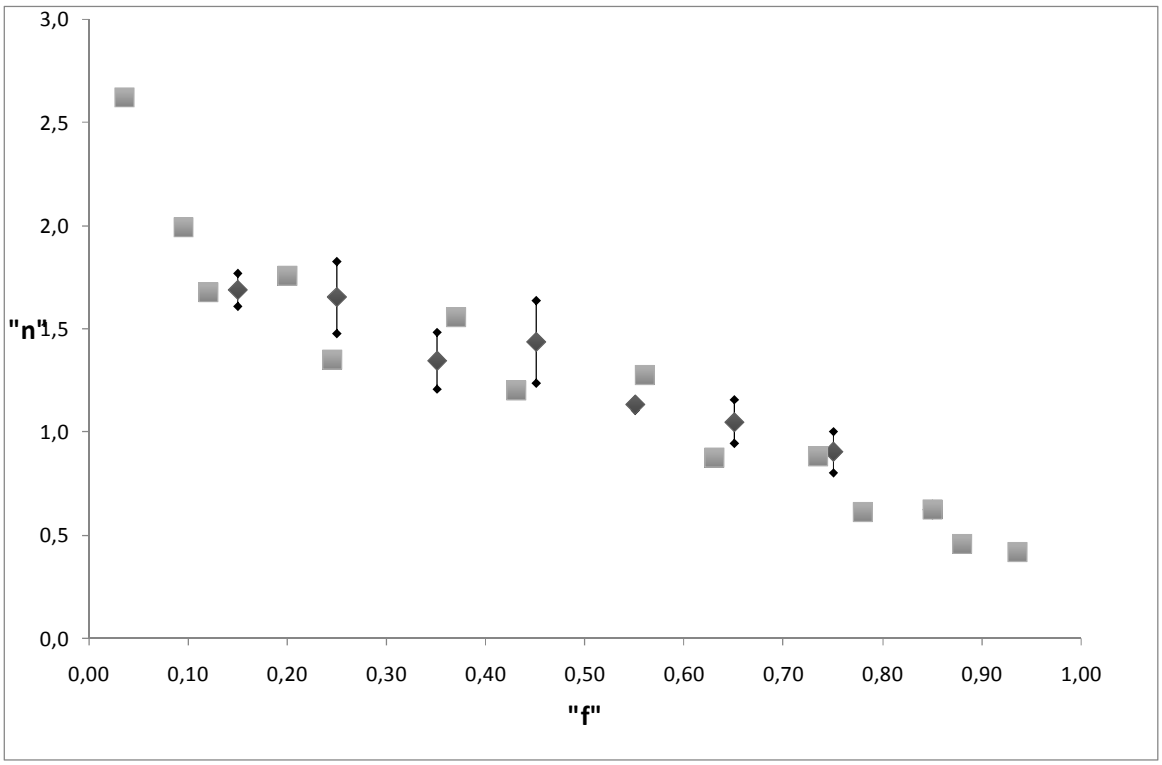

Figure 57. Kinetic parameter "n" as a function of the fraction transformed "f". The fraction transformed "f" is the average value of the considered in performing the analysis. The dark grey serie showing error bars reports the result of the first plotting operation; the average value for "n" ± the standard deviation connected to the three different heating rates is presented.

This dependence can be connected to a decreasing in the nucleation rate during the process, or to impingements phenomena.

Impingement naturally occurs for this transformation, while the high value measured for the activation energy during the whole transformation indicates that nucleation continues to play an active role in the process. Moreover, the low value for "n", means that diffusion is controlling the transformation.

As the exponential law summarized in Avrami's equation is valid for diffusion controlled growth only in the early stages of transformation (38), only the initial value of "n" is relevant to understand the nature of the process.

Cristian (38) indicates a value of 1.5 for "n" in condition of "*all shapes growing from small dimension with zero nucleation rate*"; this means, when the nucleation sites were already present in the steel at the beginning of transformation, and that the transformation continue only due to growing of the preexisting areas. A higher value for "n" is instead symptomatic of a certain degree of nucleation happening during the transformation process.

The last is actually measured confirming the observation done in the previous paragraph about the calculated value for the activation energy as given from two different contribution.

As already mentioned, afterwards “n” decreases with increasing “f”. A deeper analysis of the reasons can be set. First of all, diffusion conditions can evolve: the hypothesis of composition constancy for equilibrium phases required for the analysis reported in (38) is probably not respected but could be considered valid in good approximation[29] since no dependence for “n” from temperature is shown; furthermore, soft impingement can occur.

Moreover, assuming that the growing phase has a 3D shape is absolutely not possible considering the interlath position observed by optical microscopy: during the evolution of the process a 2D growing process (lamellae) followed by 1D thickening process (due to impingements when lamellae edges overlap) is realistic.

Coupling the analysis with optical microscopy (and the information obtained on the transformation after isothermal tempering) we can go further and attempt a description of the earlier stages of the process. At the beginning of the transformation all nucleation sites are available: grain boundaries nucleation is preferred and a 3 dimensional growth is taking place (Figure 43); n assumes the value 2.5. Very soon these nucleation sites are saturated while nucleation is going on in interlath position: here, growth of plate is preferred; as a result n is predicted in the interval 1->2.

Afterwards impingements phenomena have to be taken into account and the validity of any interpretation is doubtful.

In conclusion, the decrease in the order of transformation can be explained as a result of the illustrated phenomena but their precise role cannot be expressed.

[29] To be precise, its influence on the transformation is not relevant.

8. CONCLUSIONS

Optical microscopy is able to clearly indicate the overcoming of the critical temperatures A_1 and A_3 in an extra low carbon steel; that possibility is lost increasing the C content: the presence of fresh martensite is easily visible in alloy 2422, 2504, 2536, whereas it is impossible to distinguish fresh and tempered martensite analyzing an X20CrMoV 12-1. Moreover, temperatures are indicated only between intervals.

Hardness measurements show a shifting of hardening at temperature higher than A_1. As a result it becomes difficult to use this technique in order to set up tempering: the upper temperature limit to avoid the formation of brittle fresh martensite is not easily determinable. Moreover hardening can be dependent on phenomena like carbide dissolution or secondary precipitation.

Furthermore both optical microscopy and hardness measurements are not able to yield any indication about M_s and M_f.

Dilatomertry is able to overcome these limits adding further information. As a matter of fact A_1 and A_3 can be determined with a precision down to a decade of degrees with a slow continuous heating process. M_s and M_f can be determined as well during a cooling cycle. Moreover a quantitative analysis of the fraction transformed can be performed both in a direct way, during a heating cycle, and in an indirect way, analyzing the linear expansion coefficient of the steel. Through this method, the critical temperatures can be determined only into intervals.

Finally, coupling the three different techniques it was possible to deeply investigate the $\alpha \rightarrow \gamma$ transformation in the extra low C experimental alloy 2504.

A_1 had been determined to be between 730°C and 740°C. Above this temperature, austenite starts to develop on grain boundaries, while inter-lath nucleation and growing becomes dominant at temperature higher than 750°C. The transformation process goes on till the critical temperature A_3 is overcome at treatment temperature between 860°C and 880°C. Moreover isochronal dilatometry gave us information about the kinetics of the process: the activation energy for the transformation had been directly measured from experimental data and it appears to be almost constant during the transformation process and equal to 480 kJ/mol.

Finally, analyzing the kinetics of the transformation, the complementary role played by nucleation and diffusion processes during the whole transformation had been clarified.

9. CONTINUATION OF THE WORK

9.1. INTRODUCTION

The work performed on alloy 2422, 2504, 2536 had shown that, coupling hardness measurements and optical microscopy techniques, the critical temperatures of an extra low C steel can be determined.

The same kind of work had then been repeated on new experimental steels being developed by CSM starting from the X20CrMoV 12-1 steel. Steels 2558-2559 had been prepared as reported in 6.1.1. with a carbon content of 0.025% and 0.05% respectively. Due to the fact that these alloys are still part of the research program by CSM and DONG Energy, in relation to CRESTA project, their composition can't be fully revealed.

The interest on these alloys is connected to their particularly low A_1: the α'→γ transformation appears to start below 700°C. Moreover, dilatometry on the material as rolled indicates the overlapping of two different processes in the range 650-750°C (Figure 58).

Table 11. Critical temperature [°C] estimated by dilatometric curve for the experimental alloys as rolled. The value is the average one resulting from the 3 different tests performed, approximate to the nearest decades.

Steel	A_c1	A_c3	M_s	M_f
2558	640	900	380	110
2559	650	900	340	<100

In order to confirm the nature of the different phases observed by optical microscopy, intercritical treatment had been included in the interval chosen. As a matter of fact, the presence of two different processes in the interval between 650-700°C makes it necessary to distinguish between the formation of γ phase, that is growing in the whole interval, and another process independent on the α'→γ transformation (probably precipitation).

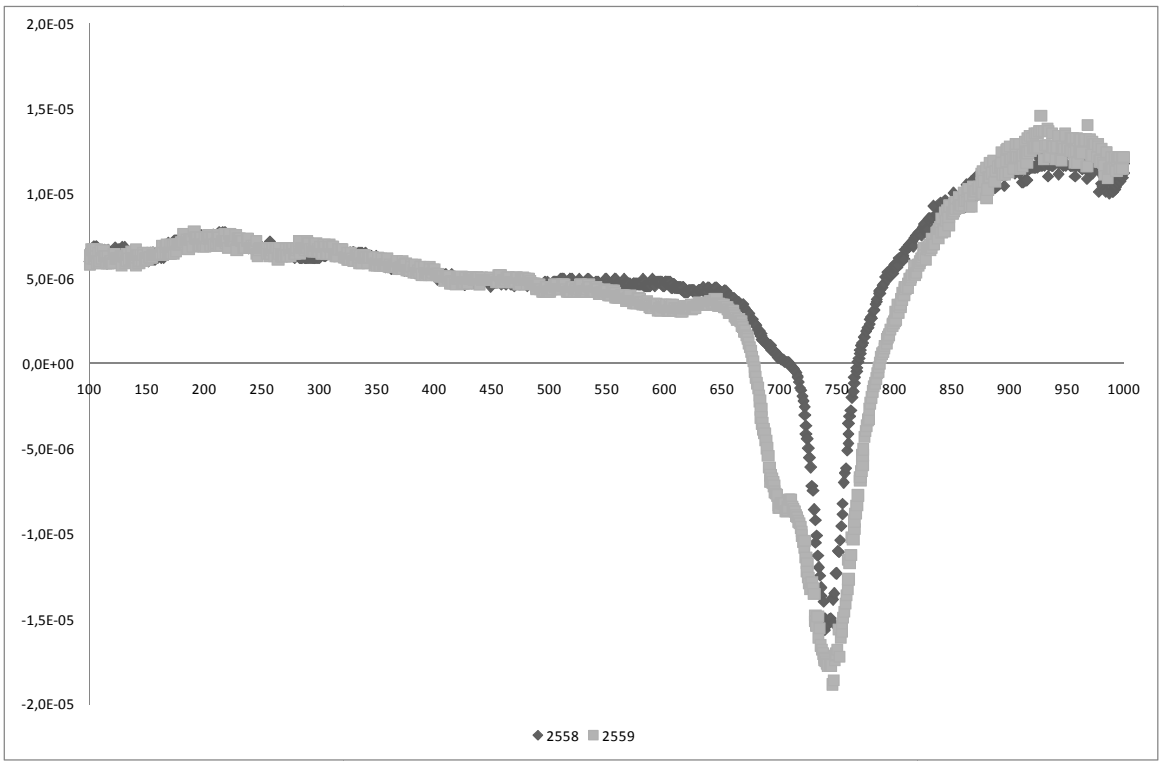

Figure 58. Alloys 2558, 2559; determination of the critical temperature: particular regarding heating cycle. Linear expansion coefficient alfa as a function of temperature T.

9.2. EXPERIMENTAL RESULTS

Like already observed in the other experimental alloys, the as rolled material consists of fresh martensite with a small amount of δ-ferrite. The presence of δ-ferrite is easily distinguishable in the direction of rolling (white phase in Figure 59).

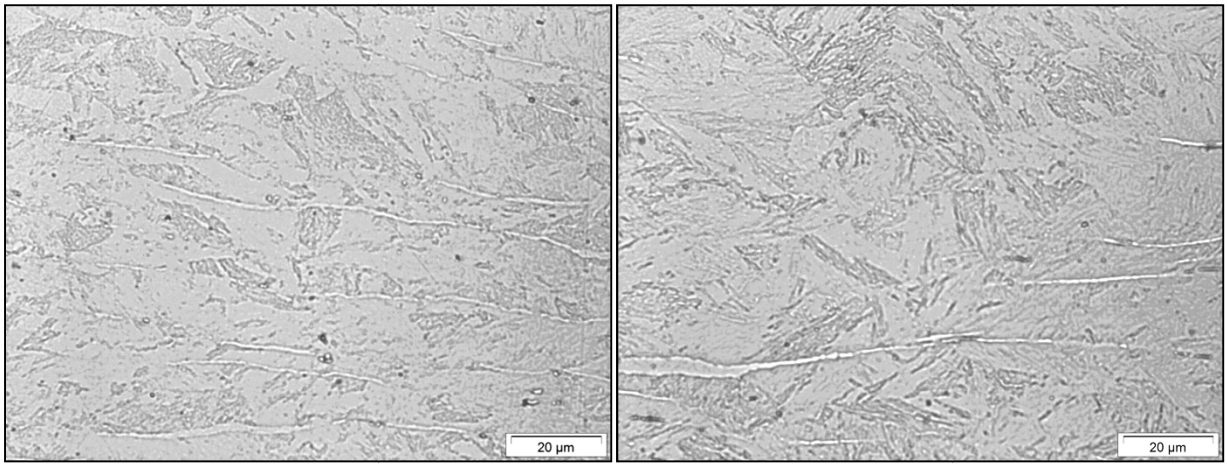

Figure 59. Material as rolled; optical microscope 500X; Villella's etching 10s; alloys 2558 (left), 2559 (right).

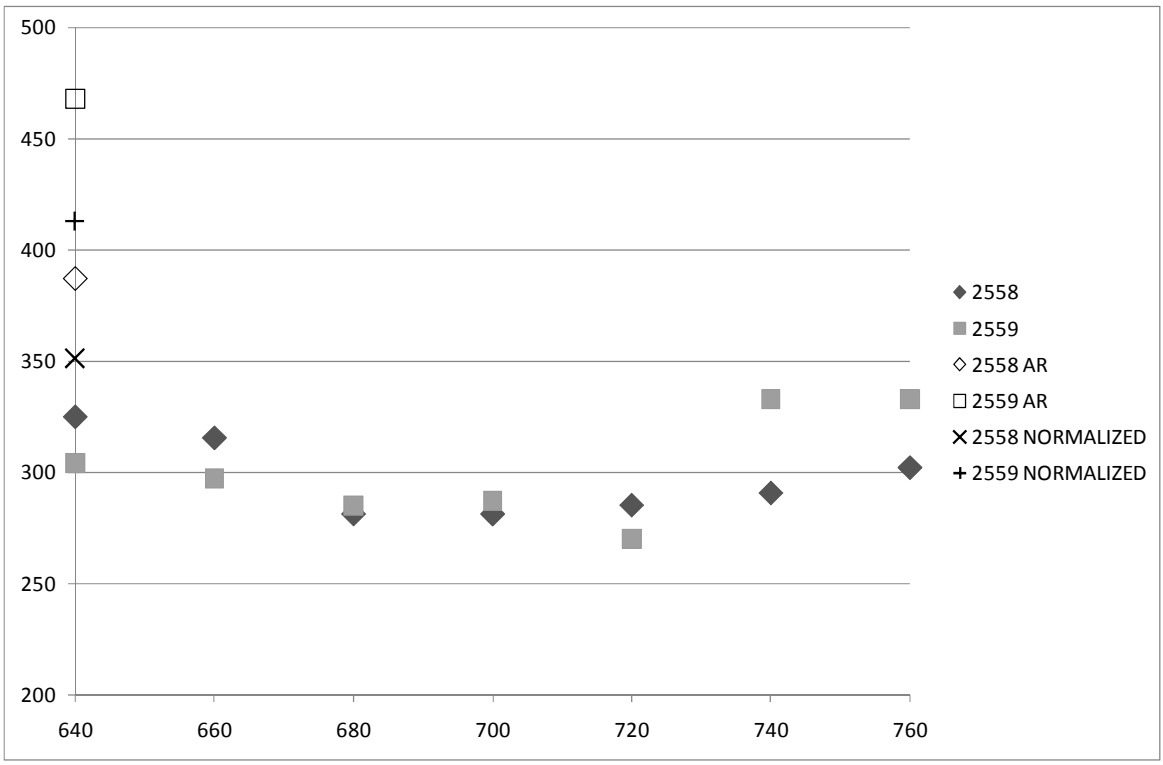

Figure 60. Hardness resulting from the tempering process as a function of the tempering temperature. AR means as rolled.

Figure 61 shows the presence of δ-ferrite in alloy 2559 even after normalization, whereas it seems to be completely dissolved in normalized 2558 material. Clearly, δ-ferrite will remain un-dissolved even after the tempering process of 2559.

After tempering, fresh martensite is distinguishable indicating an interval for A_1: fresh martensite starts to be visible in inter-lath position in both the samples treated at 680°C, which indicates that 660°C<A_1<680°C.[30] The process goes on at higher temperatures: optical microscopy of samples treated at 740°C indicates that the two phases are uniformly distributed in the sample and almost balanced as indicated by dilatometry (Figure 58).

Hardness measurements are consistent with the analysis performed. However, this analysis is unable to indicate the nature of the second process happening in the material. As a result, hardness measurements becomes not relevant for the determination of A_1.

[30] Details of the images taken on samples treated at 680°C are visible in Appendix F.

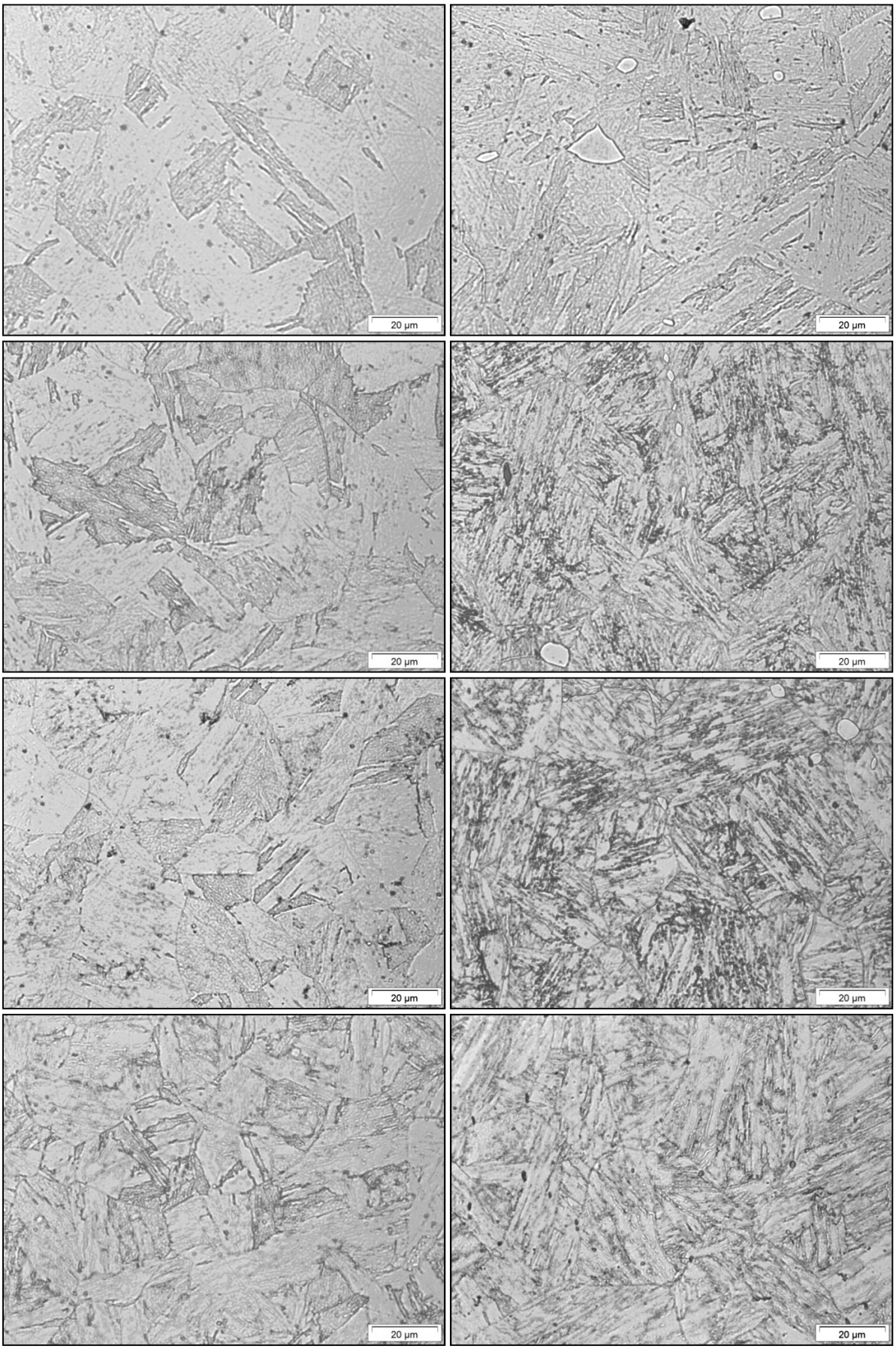

Figure 61. Material normalized at 1050°C, 1,5h; optical microscope 500X; Villella's etching 10s; 2558 (left), 2559 (right); from the top: as normalized; tempered 2h at: 640°C, 660°C, 680°C,…

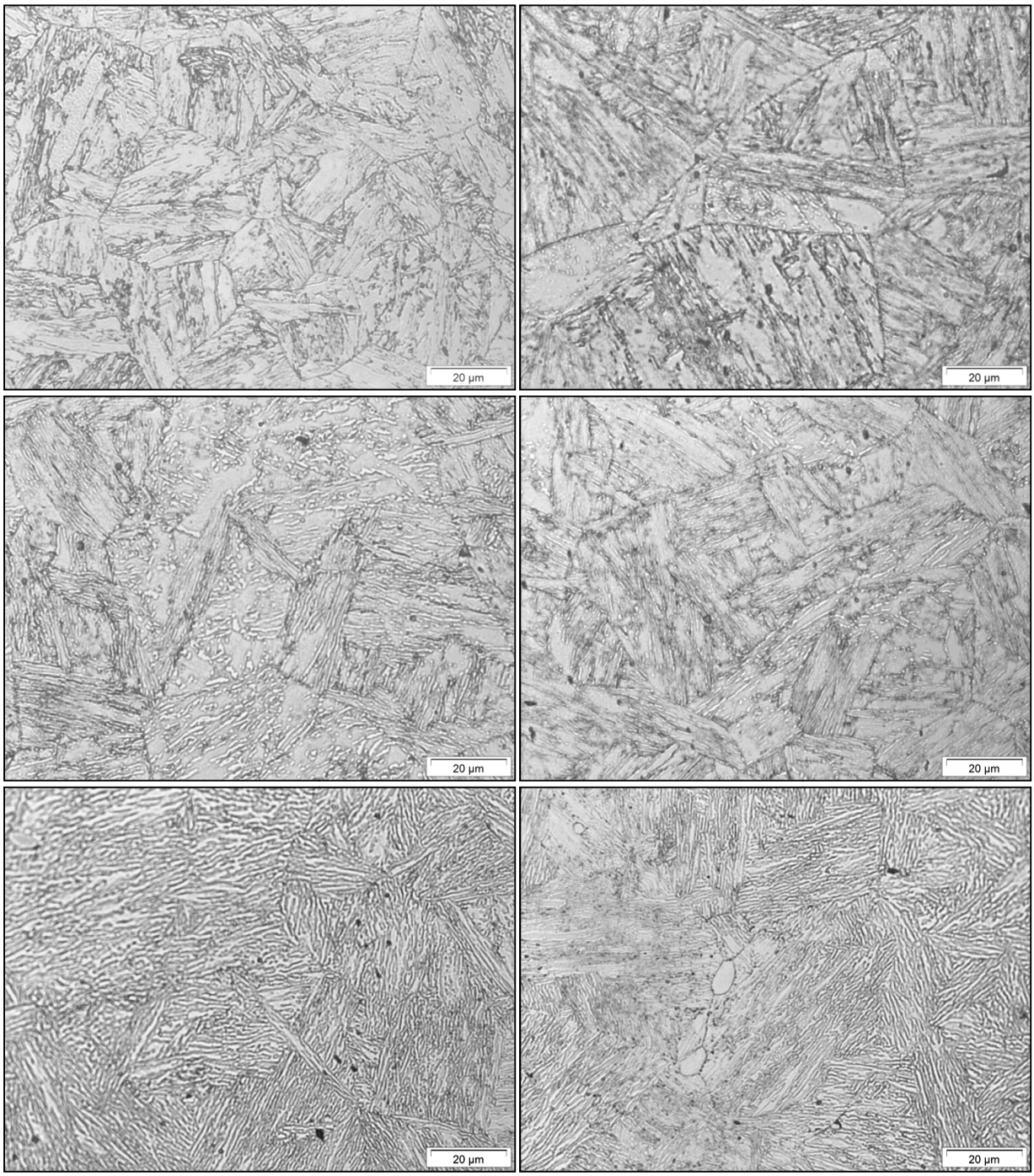

… 2558 (left), 2559 (right); from the top: as normalized: tempered 2h at: 700°C, 720°C, 740°C.

ACKNOWLEDGEMENTS

Acknowledgements are expressed to all the people that collaborated with me to develop this work: Prof. Somers for his help in all stages of the collaboration, from the fundaments to the final part; Dott. Danielsen for his constant presence; Dott. Hald for his support especially in relation to references; Leonardo and “CSM” for their availability and their accurate experimental work.

Professor Nicodemi, Mapelli and Firrao that supported my project from inception to graduation.

Moreover, I have to thank my friends and classmates since we work together like a team helping each other and sharing a lot of time to reach graduation. I want to thank even Jacopo, Andrea and all the guys of Skolestraede for the good time spent in Denmark during the period this project was developed.

Finally, a special thanks is for my parents that have supported me in all these years as student, giving me the opportunity to reach my goals and to develop all my interest.

REFERENCES

1. **Briggs, J.Z. e Parker, T.D.** *The super 12% Cr steels.* New York : Climax Molybdenum company, 1977.

2. **Cipolla, L. e Danielsen, H.K.** *Formation of Z-Phase in12% CrVNbN model steel.* Rome, Copenhagen : CSM, DTU, 2009.

3. **Korcakova, Leona.** *Microstructure evolution in high strength steel for power plant application: microscopy and modelling.* Copenhagen : DTU, August 2002.

4. **Alberry, P.J. e Gooch, D.J.** 12CrMoV - A status review. *Welding and metal fabrication.* november 1985, p. 332-335.

5. **Burgel, R.** *Handbuch Hochtemperatur-Werkstofftechnik.* Germany : Vieweg, 2006.

6. **Pickering, F.B.** *Microstructural Development and Stability in High Chromium Ferritic Power Plant Steels.* Cambridge : A.Strang et al, 1996.

7. **Honeycombe, R. W. K.** *Steels Microstructure and Properties.* London : Edward Arnold Ltd, 1981.

8. **Lenel, U.R.** TTT curves for the formation of austenite. *Scripta metallurgica.* Vol 17. 1983, p. 471-474.

9. **Mittemeijer.** Review Analysis of the kinetics of phase transformation. *Journal of material science.* n° 27 1992, p. 3977-3987.

10. **Liu, Y., Sommer, F. e Mittemeijer, E.J.** Abnormal austenite-ferrite transformation kinetics of ultra-low-nitrogen Fe-N alloys. *Metallurgical and materials transactions A.* Vol. 39A October 2008, p. 2306-2318.

11. —. Isothermal austenite-ferrite transformatio of Fe-0,04at.% C alloy: dilatometric measurements and kinetics analysis. *Acta Materialia.* n° 56 2008, p. 3833-3842.

12. **Tokunaga, T., Hasegawa, K. e Masuyama, F.** Phase transformation behaviour of grade 91 ferritic steel. *Materials science and Engineering A.* 2008.

13. **Krauss, G.** *Steel Heat Treatments and Processing Principles.* Materials Park,Ohio,. : ASM, 1989.

14. **Klotz, Ulrich E., Solenthaler, Christian e Uggowitzer, Peter J.** Martensitic–austenitic 9–12% Cr steels—Alloy design, microstructural stability and mechanical properties. *Materials Science and Engineering A.* 2008, 476.

15. **Thelning, K. -E.** *Steel and its heat treatments.* London : Butterworths, 1984.

16. **D.R. Barraclough, D.J. Gooch.** Effect of inadeguate heat treatment on creep strenght of 12Cr-Mo-V steel. *Materials science and technology.* november 1985, p. 961-965 VOL 1.

17. **E, Otero, et al.** elationship between microstructure and high temperature corrosion behaviur of X20CrMoV 12-1 stainess steel. *Material at high temperature.* 1995, Vol. 13, 2.

18. **Semiatin, S.L., Stutz, D.E. e Harry, I.L.** *Induction Heat treatment of steels.* Metals Park,Ohio,. : ASM, 1986.

19. **Samuels, L.E.** *Optical Microscopy of carbon steels.* Metals Park,Ohio 1980,. : ASM, 1980.

20. **ASM.** *Metals handbook 8: Atlas of microstructure of industrial alloys.* Metals Park,Ohio,. : ASM, 1972.

21. **Danielsen, Hilmar KJartansson.** *Z-phase in 9-12%Cr steels.* Lyngby : DTU, February 2007.

22. **Shen, Yin Zhon, et al.** TEM investigations of MN nitride phases in 9% chromium ferritic/martensitic steel with normalization conditions for nuclear reactors. *Journal of Nuclear Materials.* 2009, 384, p. 48-55.

23. **Servant, C. e Cizeron, G.** Investigation into the structural evolutions of a low alloy steel during tempering.

24. **Gavriljuk, V.G. e Berns, H.** Precipitates in tempered stainless martensitic steels alloyed with nitrogen, carbon or both. *Materials science forum.* Vols. 318-320 1999, p. 71-80.

25. **Wiedermann, J., Zalecki, W. e Malec, M.** The influence of nitrogen on the structure and properties of Fe-10Cr-N and Fe-10Cr-1MO-N steels after tempering in the temperature range of 650-750°C. *Journal of Materials Processing Technolgy.* n° 133 2003, p. 225-229.

26. **Jung, Minsu, Lee, Seok-Jae e Lee, Young-Kook.** Microstructural and dilatational changes during tempering and tempering kinetics in medium-carbon steel. *Metallurgical and material transactions A.* Vol. 40 March 2009.

27. **Morra, P.V., Bottger, A.J. e Mittemeijer, E.J.** Decomposition of iron-based martensite. *Journal of thermal analysis and calorimetry.* Vol. 64 2001, p. 905-914.

28. **J, Wiedermann, W, Zalecki e M, Malec.** The influence of ntrogen on the structure and properties of Fe-10Cr-N and Fe-10Cr-1Mo-N seels after tempering in the temperature range 650-750°C. *Journal of materials processing technology.* 2003, Vol. 133, p. 225-229.

29. **Rickett, R.L., et al.** Isothermal trasformation, hardening and tempering of 12% Chromium steel. 1951, *American Society for Metals*, p. 138-169.

30. **C. Loier, C. Leymonie.** Structural transformations and mechanical properties of a 12Cr-Ni-Mo-V steel. 1984-1985, *Materials science and engineering*, 68, p. 165-174.

31. **Kalwa, G.** *steel grade x20CrMoV 12-1 the state of development and application.* s.l. : Mannesmann Industries.

32. **D. Ragone**. *Thermodynamics of Materials*. John Wiley and Sons, on 1995

33. **Yang, H.S. and Bhadeshia, H.K.D.H**. Uncertainties in dilatometric determination of martensite start temperature. *Institute of Materials, Mineral and Mining, published by Maney, 2007.*

34. **Liu, Y., et al.** Isothermal austenite-ferrite transformation of Fe-0.04at.% C alloy: Dilatometric measurment and kinetic analysis. *Acta Materialia.* 56, 2008, p. 3833-3842.

35. **Oliveira, F.L.G., Andrade, M.S. e Cota, A.B.** Kinetics of austenite formation during continuous heating in a low carbon steel. *Materials characterization.* 58, 2007, p. 256-261.

36. **Caballero, F.G., Capdevilla, C. e Garcia de Andres, C.** Kinetics and dilatometric behaviour of non isothermal ferrite-austenite transformation. 2000.

37. **Garcia de Andres, C., et al.** Application of the dilatometric analysis to the study of solid-state transformations in steels. *Materials characterization.* 48, 2002, p. 101-111.

38. **Christian, J.W.** *The theory of transformations in metals and alloys. An advanced book in physical metallurgy. 2 ed 1*: Oxford. Pergamon press, 1975.

39. **Kutz, Mayer.** *Handbook of materials selection.* s.l. : John Wiley and Sons, 2002.

40. **ASM.** *Bearing steels: the rating of non metallic inclusion.* Philadelphia : s.n., 1975.

41. **Bergh, S. e Lindberg, O.** *Jernkontorets Annaler.* Stockolm : s.n., 1965.

42. **Rost, F. e Oldfield, R.** *Photography with a microscope.* s.l. : Cambridge university press, 2000.

43. **MacCrowe, W.C.** *Polarized light microscopy.* Ann Arbor, Mich. : s.n., 1978.

44. **Richardson, J. H.** *Hardbook for the light microscope - A user's guide.* Park Ridge, N.J. : Noyes, 1991.

45. **Petzow, Gunter.** *Metallographic Etching.* s.l. : ASM international, 1999.

46. **PACE Technologies.** Metallographic Etchants. *PACE Technologies - 3601 E. 34th St. - Tucson, AZ 85713 USA.* [Online] 2009. [Reported: 12 May 2009.] http://www.metallographic.com/Etchants/Etchants.htm.

47. **Max Plank Institute.** Dilatometry. [Online] [Reported: 13 May 2009.] http://www.mf.mpg.de/de/abteilungen/mittemeijer/english/resources/dilatometry.html

48. **Takahashi, M., Bhadeshia H.K.D.H.** The interpretation of dilatometric data for transformation in steels: *Journal of materials science letters.* 8, 1989, p. 477-478.

49. **Bhadeshia, H. K. D. H.** *Dilatometry.* s.l. : University of Cambridge, Materials science and metallurgy.

50. **Electric Power Research Institute; D., Gandy.** X20 CrMoV12-1 Steel Handbook, September 2006

[Online] 2009. [Reported: 2 Oct 2009.] http://mydocs.epri.com/docs/public/000000000001012740.pdf

51. **H.K.D.H. Bhadeshia and colleagues**. Modelling of kinetic and dilatometric behavior of non-isothermal pearlite-to-austenite transformation in an eutectoid steel. [Online] 2009. [Reported] http://www.msm.cam.ac.uk/phase-trans/abstracts/eutectoid.pdf

APPENDIXES

Appendix A - *JMAK equation in non-isothermal conditions*

Starting from Equation 4, an expression valid for non-isothermal conditions can be derived (51):

$$f = 1 - \exp\left(-k_{(T)}t^4\right) \rightarrow d\left(\ln\frac{1}{1-f}\right) = \frac{df}{1-f} = 4k_{(T)}t^3dt$$

Changing variables, $t = \frac{\Delta T}{\emptyset} \rightarrow dt = \frac{dT}{\emptyset}$, and substituting:

$$\frac{df}{1-f} = 4k_{(T)}\frac{\Delta T^3}{\theta^4}dT$$

And finally, integrating:

$$f = 1 - \exp\left(\int_{Ac1}^{T}\frac{4\pi}{3\emptyset^4}\dot{N}G^3\Delta T^3\,dT\right)$$

Equation 14. The JMAK equation for constant nucleation and growing rates in non-isothermal conditions as presented by Bhadeshia and colleagues (50). In the referenced study, the integral had been evaluated numerically.

In order to extend the approach presented by Bhadeshia and colleagues to a general formulation, consideration reported by Mittemeijer in (9) have to be inserted. As reported in section 3.5 Equation 5, the general formulation for the JMAK equation in non-isothermal condition is the following:

$$f = 1 - \exp\left[-\left(\int k_{(T)}dt\right)^{\mathrm{n}}\right]$$

Furthermore, as just reported, "$k_{(T)}$" is related to growing and nucleation rates. These can be expressed as thermal activated processes (obtaining the formulation given by Mittemeijer in (9)) but, in more general terms, they are a more complex function of T.

Let's for example consider $k_{(T)} = k_0 p_{(T)}^x \exp\left(-\frac{\mathrm{E}}{\mathrm{RT}}\right)$ with $p_{(T)}^x$ polynomial function of temperature of grade x.[31] The equation for the fraction transformed becomes much more complicated:

$$f = 1 - \exp\left[\left(-\int k_0 p_{(T)}^x \exp\left(-\frac{\mathrm{E}}{\mathrm{RT}}\right)\ \mathrm{dt}\right)^{\mathrm{n}}\right] = 1 - \exp\left[\left(-\frac{k_0}{\emptyset}\int p_{(T)}^x \exp\left(-\frac{\mathrm{E}}{\mathrm{RT}}\right)\ \mathrm{dT}\right)^{\mathrm{n}}\right]$$

Equation 15. The JMAK equation; mathematical result of the implementation performed.

The last approach is surely more complete than the one utilized in this study, but the obtained result is much difficult to be handled: a generic solution to the integral cannot be expressed. As a consequence, numerical approaches have to be considered.

[31] Expression for nucleation and growing processes which leads to this expression are reported for example in (32).

Appendix B - *Optical microscopy*

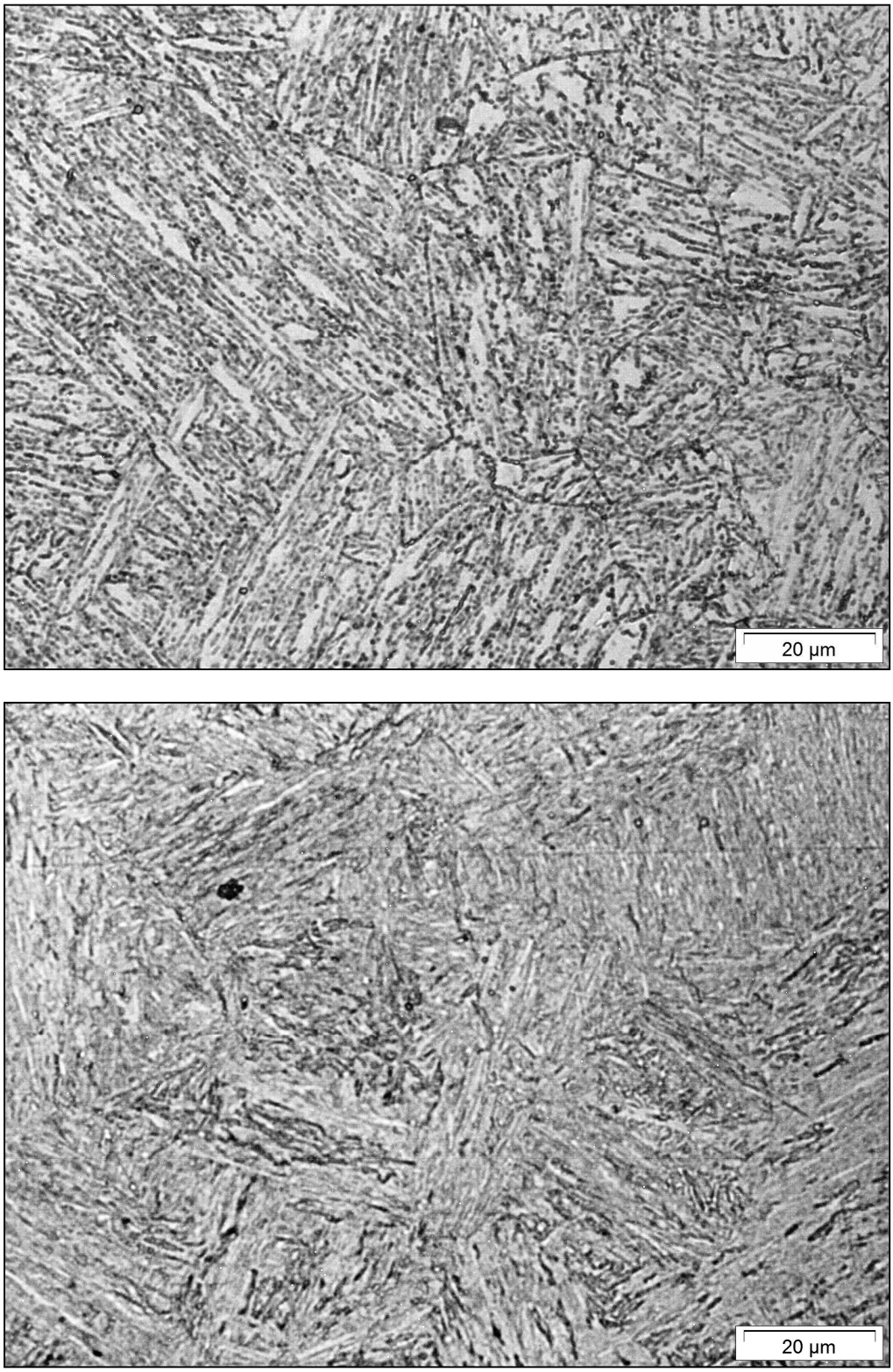

Figure 62. X20CrMoV 12-1 tempered 2h after normalization; optical microscope; Villella's etching 10s; from the top: 840°C, 880°C.

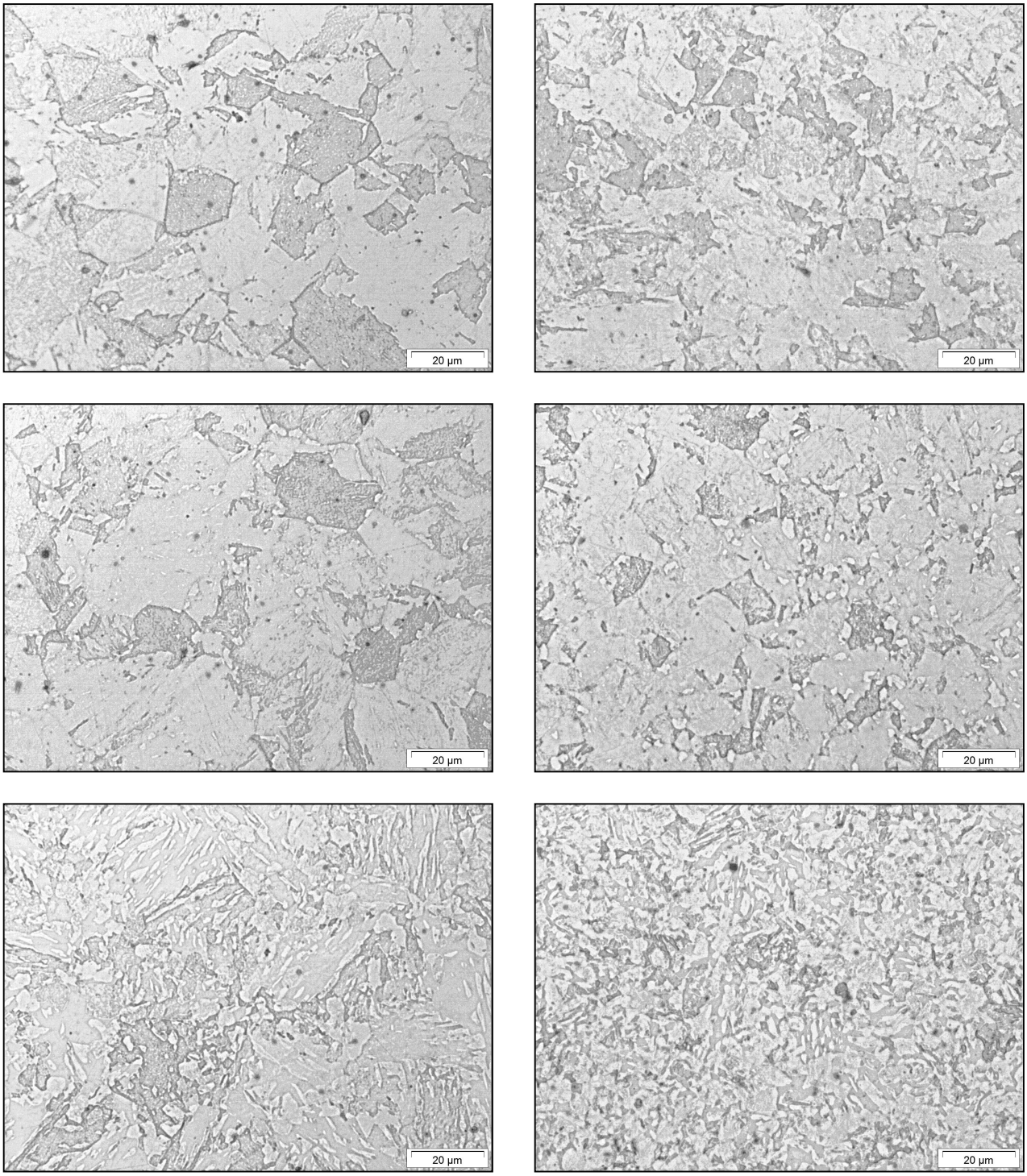

Figura 63. Alloy 2422 (left), 2536 (right) tempered for 2h after normalization; optical microscope; Villella's etching 10s; from the top: samples treated at 700°C (left), 750°C (right), 800°C.

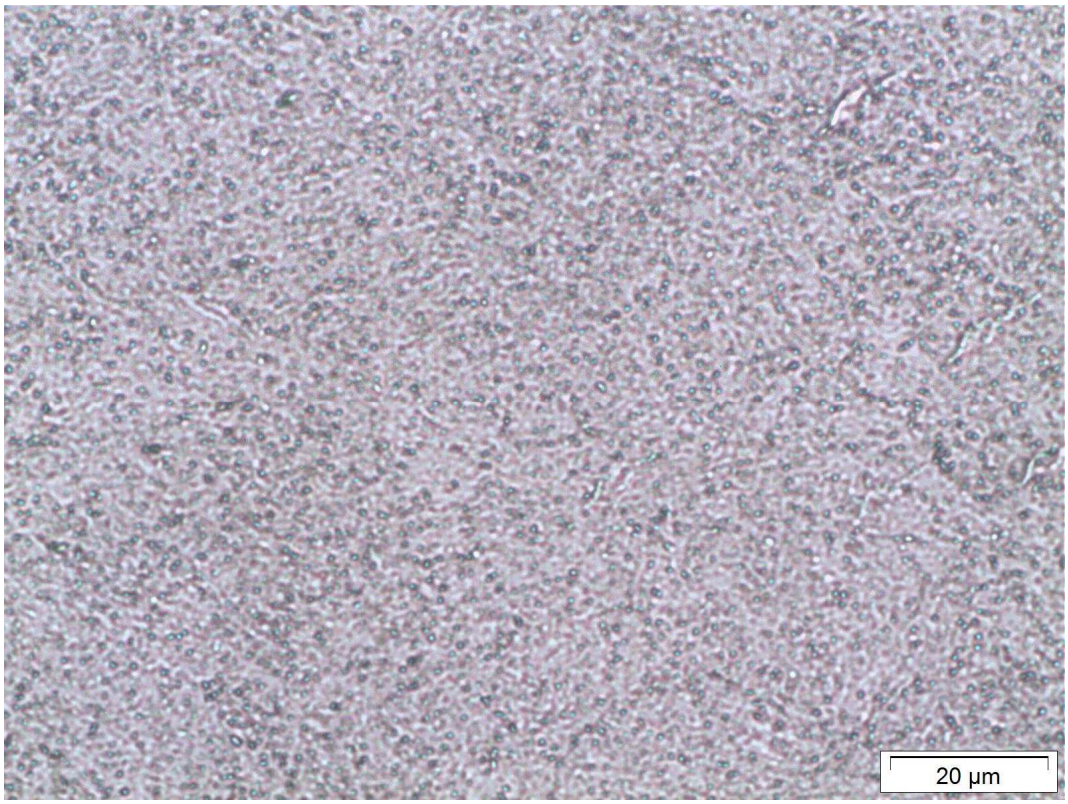

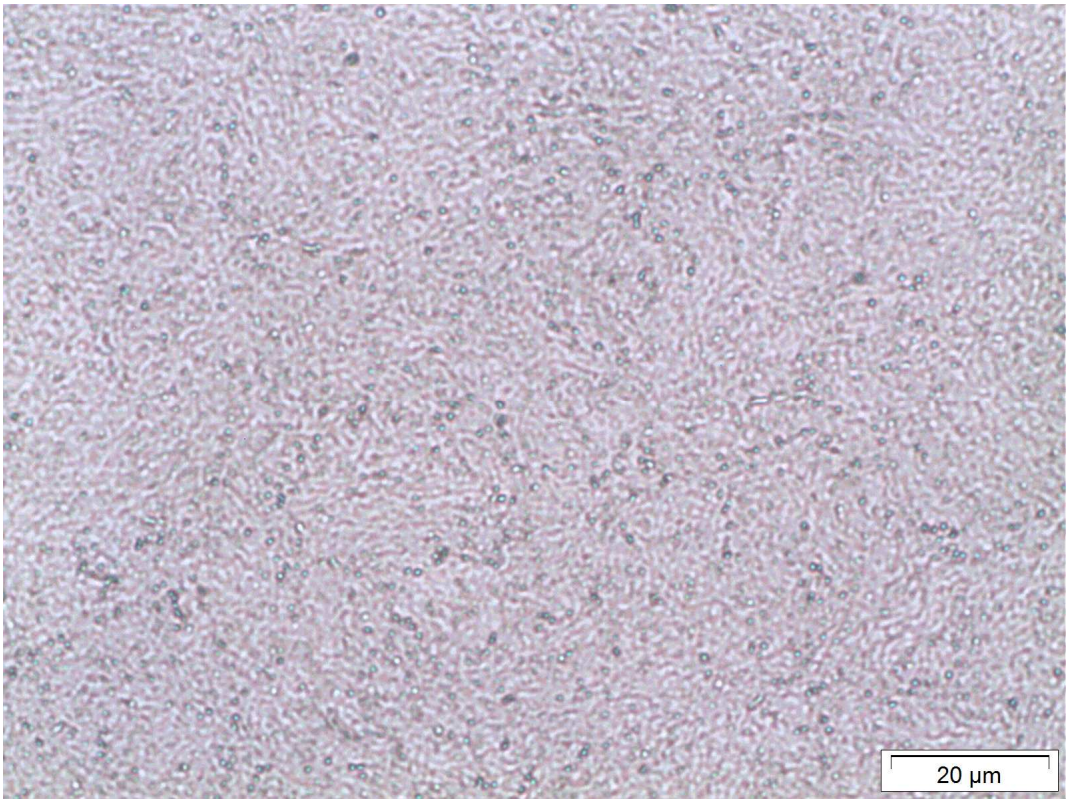

Figure 64. X20CrMoV 12-1 tempered 2h after normalization; optical microscope; Aqua regia etching 40s; sample treated at 840°C; 900°C; colored pictures.

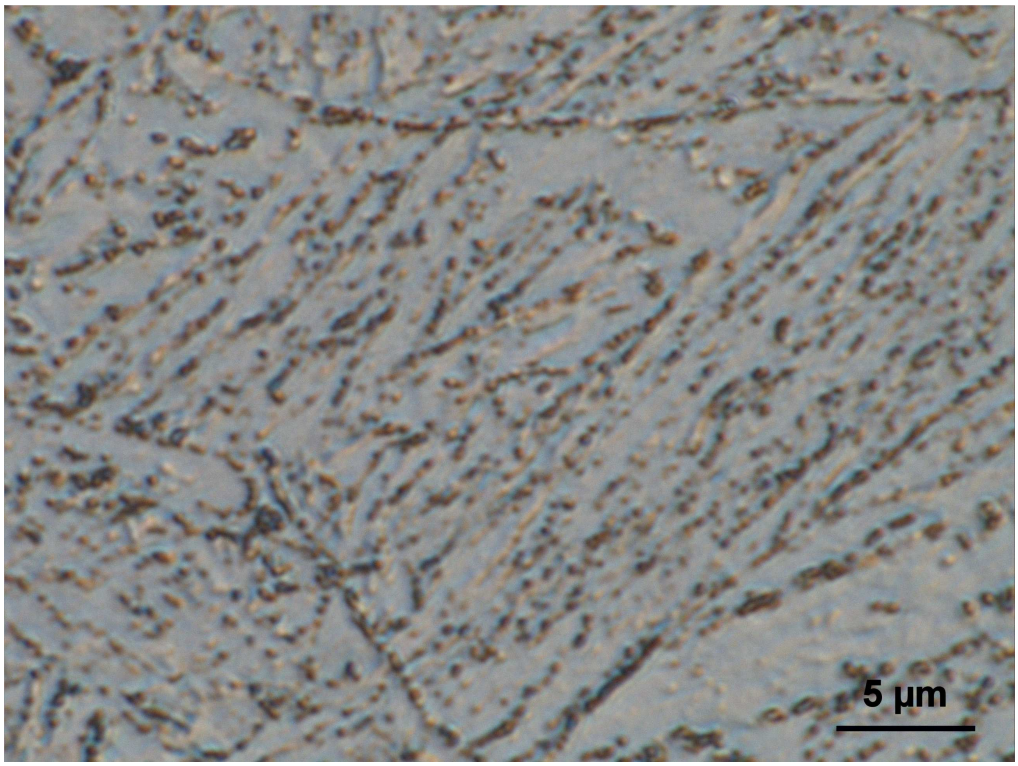

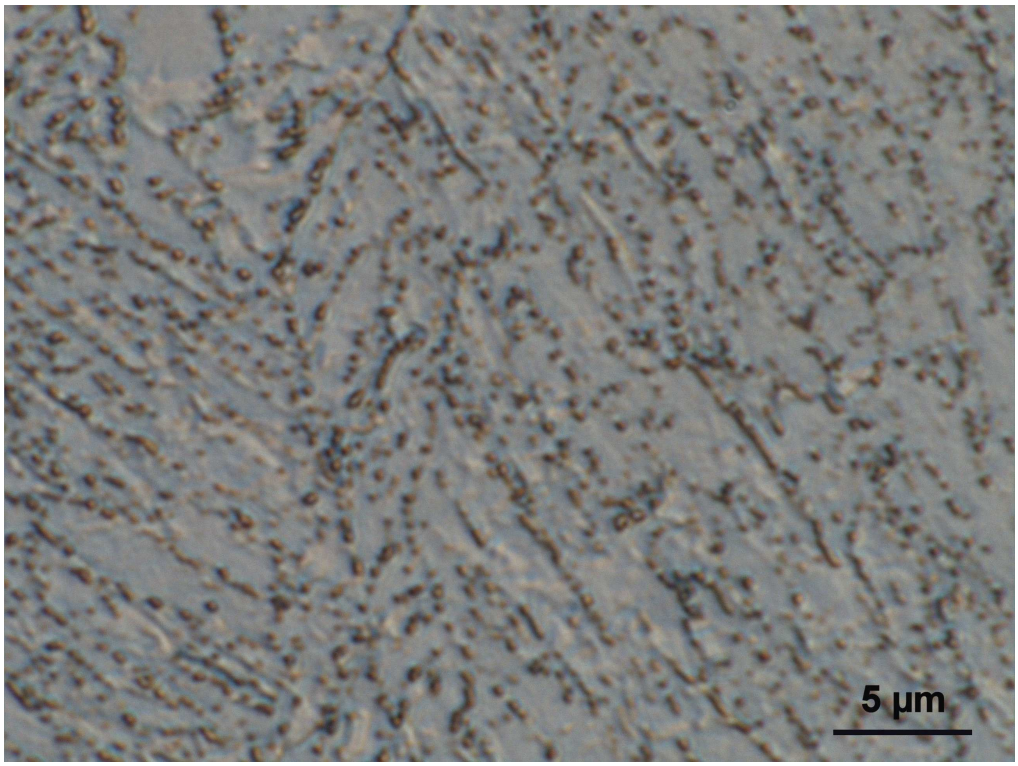

Figure 65. X20CrMoV 12-1 tempered 2h after normalization; optical microscope: oil with refraction index 1.51 was used as media; Aqua regia etching 40s; colored pictures. Sample treated at 780°C; 800°C;…[32]

[32] To be notice that the improved resolution is able to suggest the overcoming of A_3. This observation can be used to set a deeper analysis.

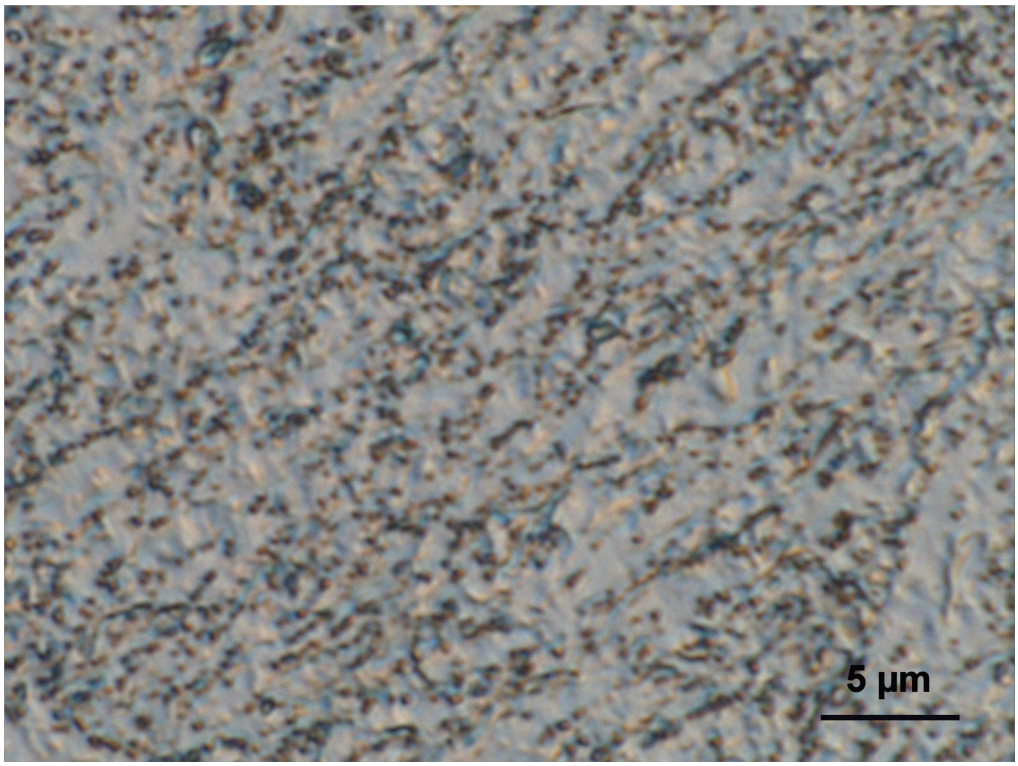

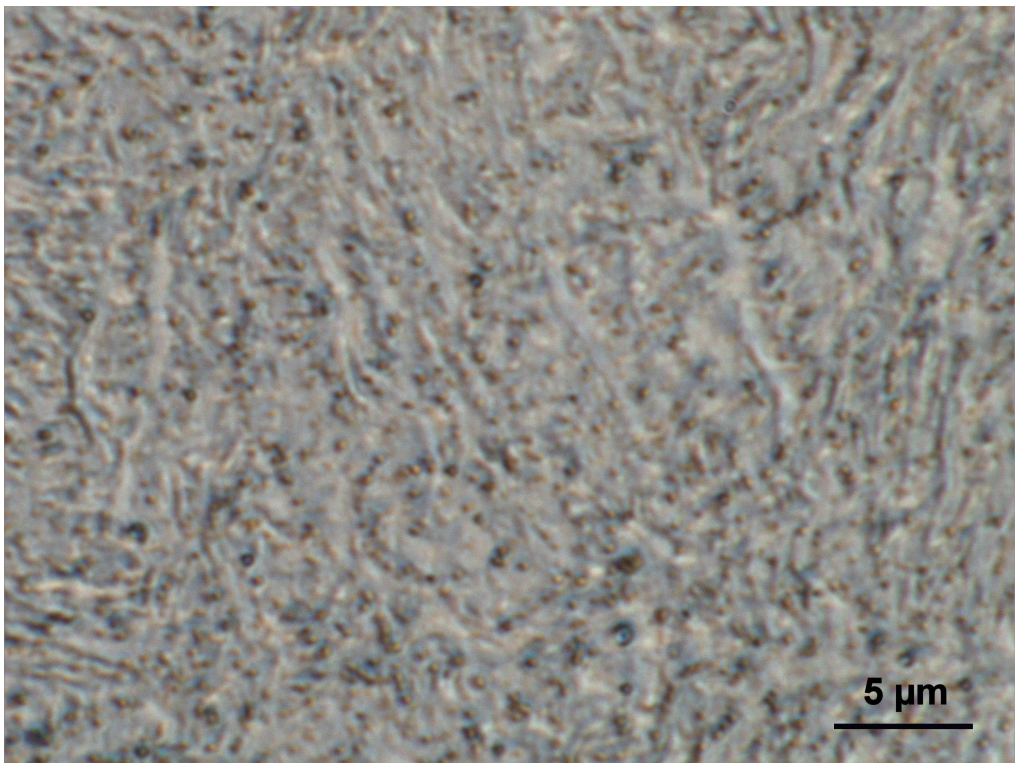

… X20CrMoV 12-1 tempered 2h after normalization; optical microscope: oil with refraction index 1.51 was used as media; Aqua regia etching 40s; sample treated at 840°C; 900°C; colored pictures.

Appendix C – *Dilatometry: intercritical treatment analysis*

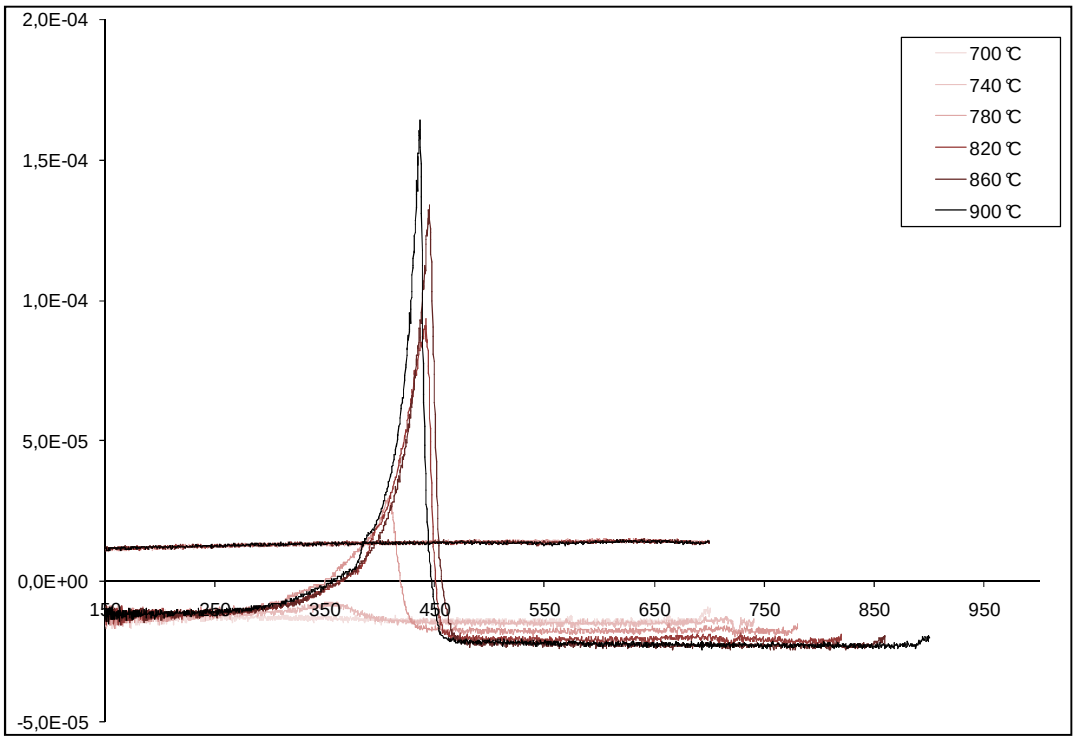

Figure 66. Alloy 2504, tempered steel: linear expansion coefficient during cooling at 1°C/s.

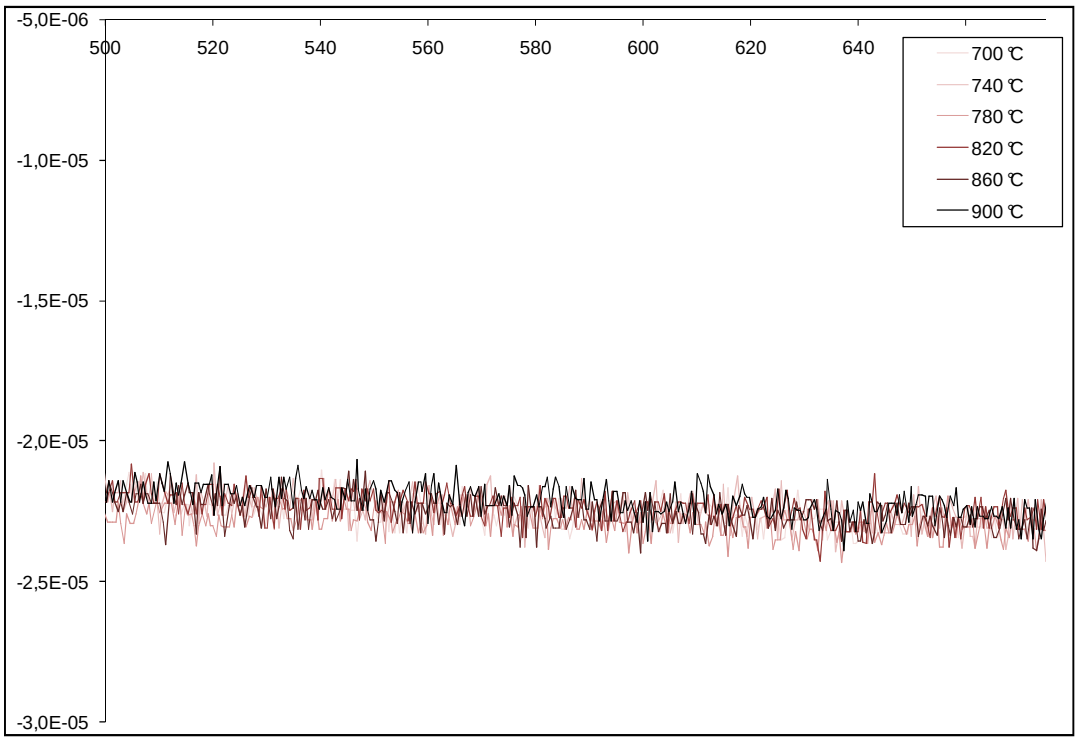

Figure 67. Alloy 2504, linear expansion coefficient of austenite.

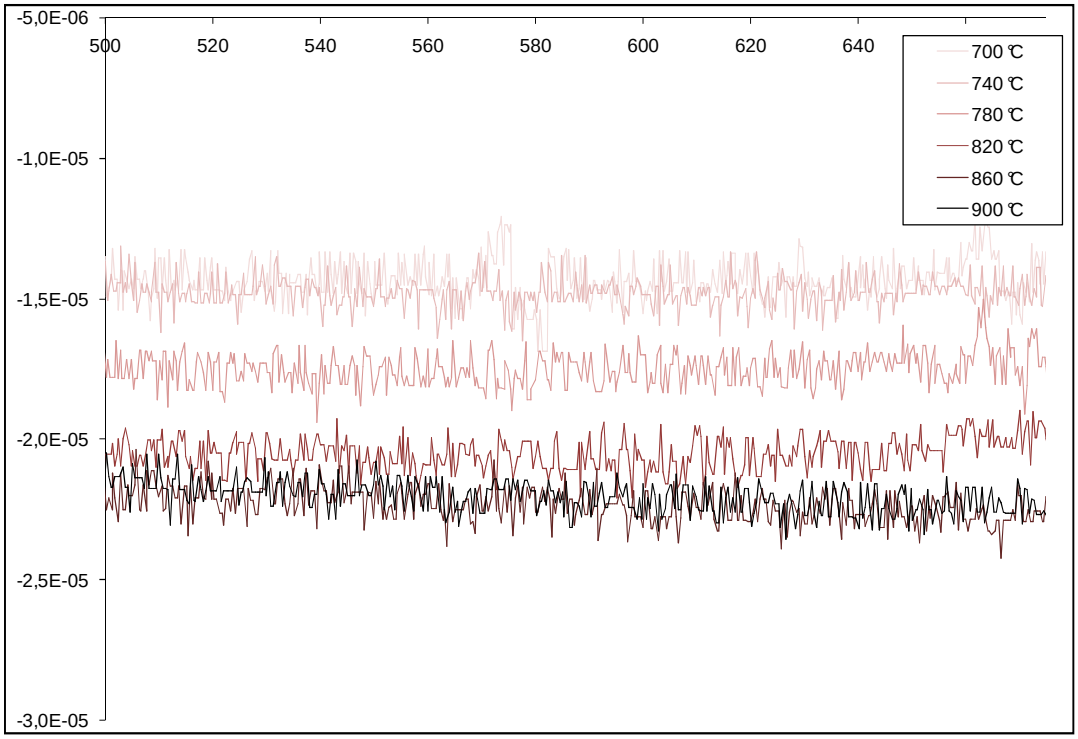

Figure 68. Alloy 2504, linear expansion coefficient of tempered steel.

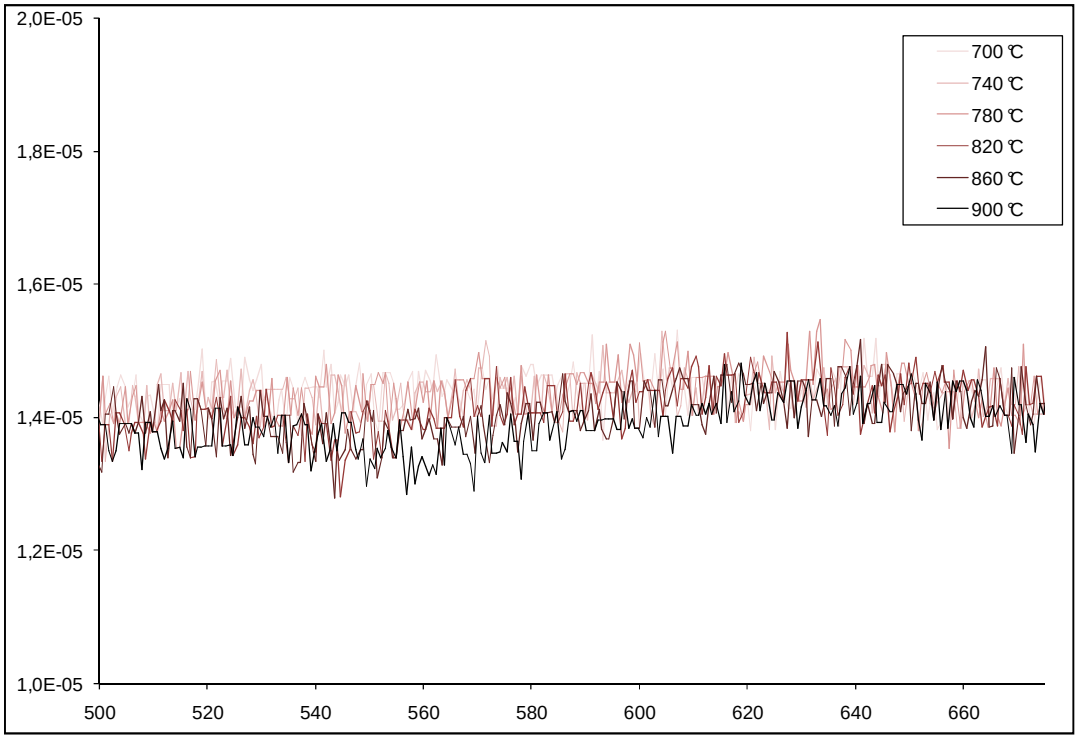

Figure 69. Alloy 2504, linear expansion coefficient of martensite.

Appendix D – *Kinetic analysis: data as received*

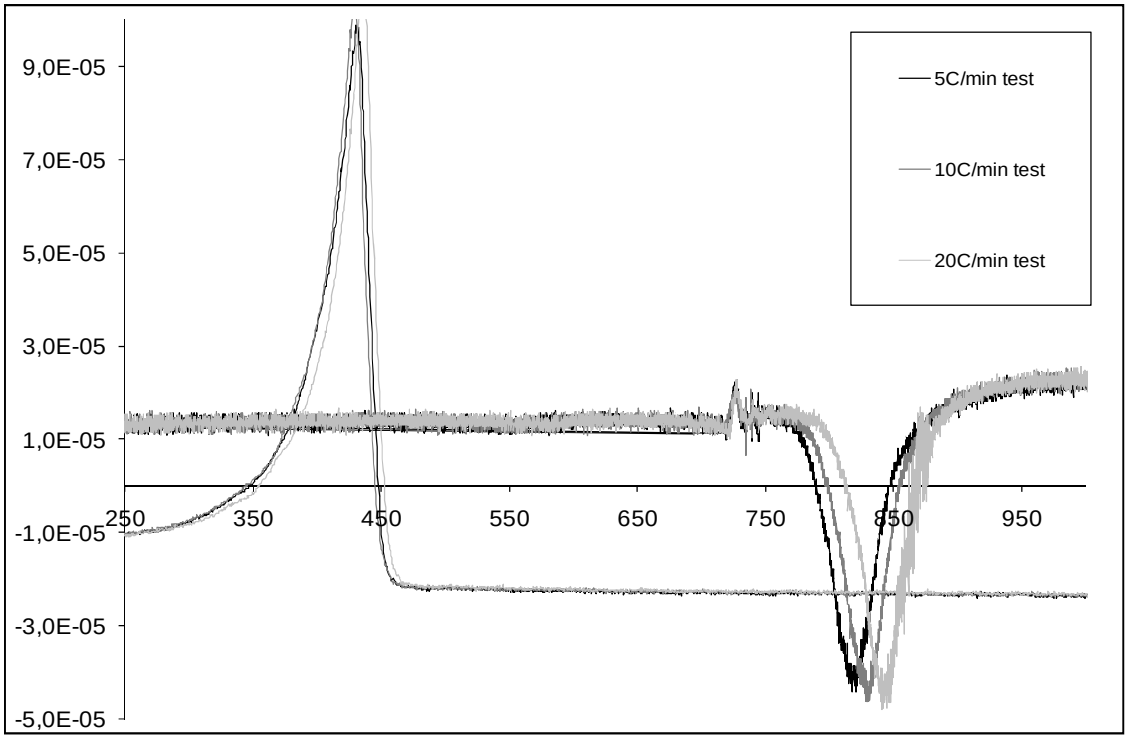

Figura 70. Alloy 2504, as rolled. Linear expansion coefficient as a function of temperature at different heating rates.

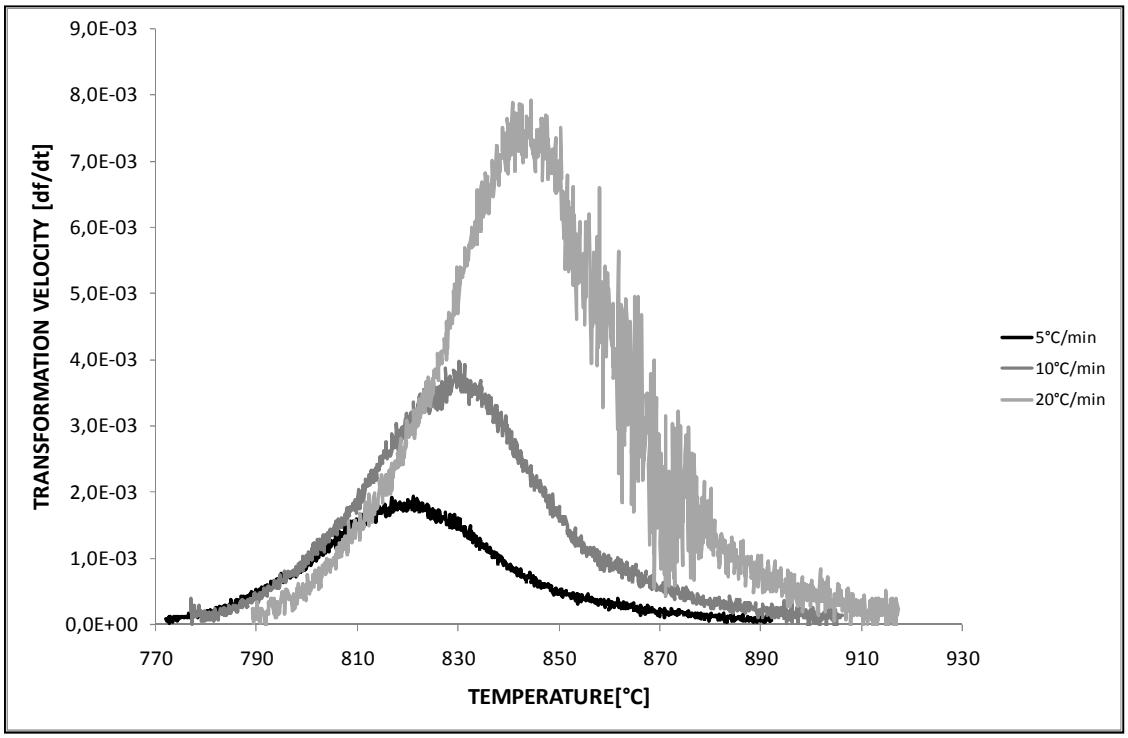

Figure 71. Alloy 2504, α→γ transformation rate as a function of temperature.

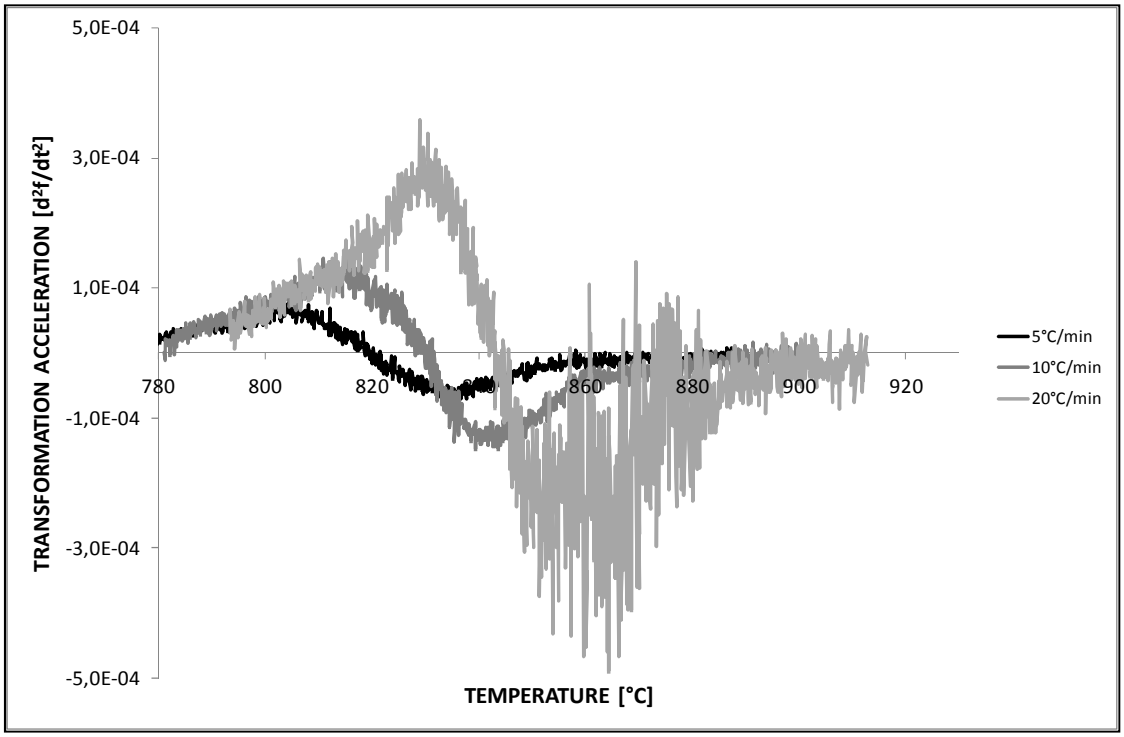

Figure 72. Alloy 2504, acceleration of the α→γ transformation as a function of temperature.

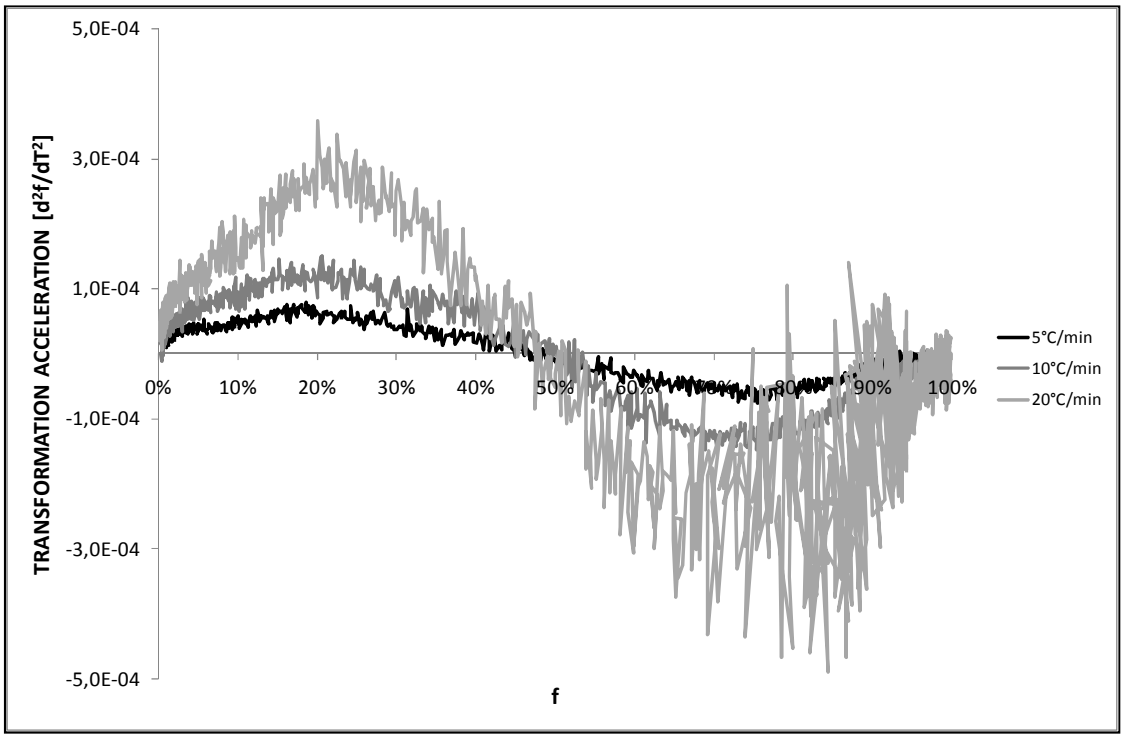

Figure 73. Alloy 2504, acceleration of the α→γ transformation as a function of the fraction transformed.

Appendix E – *Kinetic analysis: data after temperature shifting*

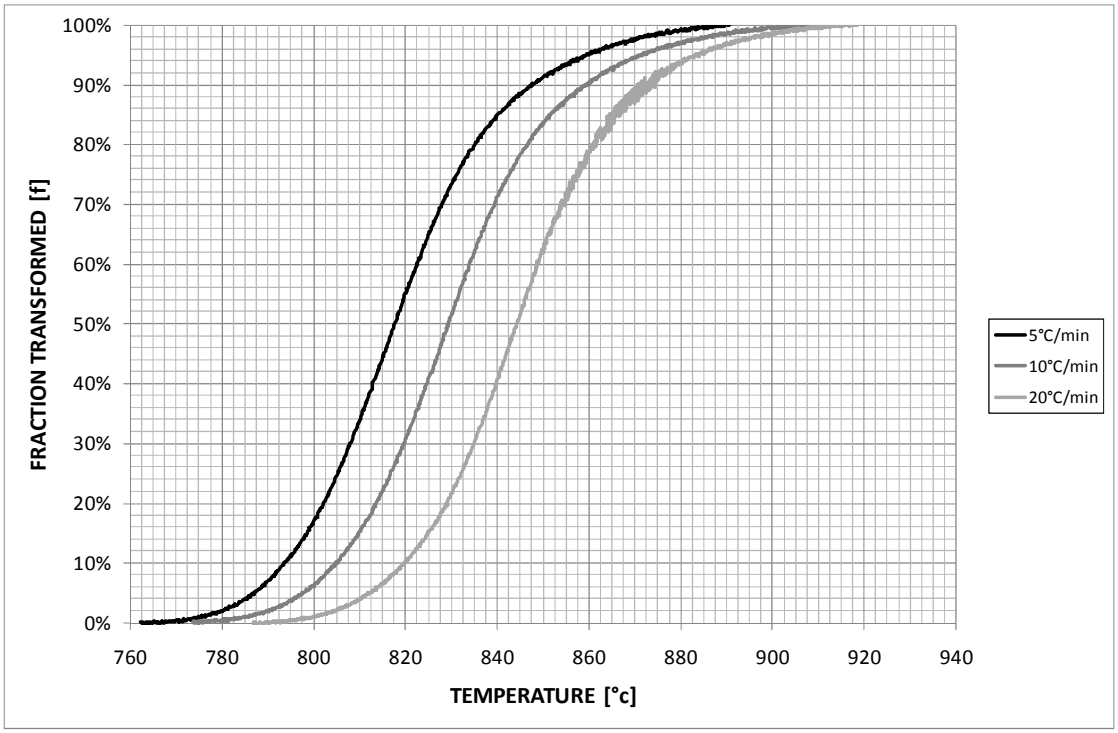

Figure 74. Fraction transformed as a function of temperature resulting after the curve shifting.

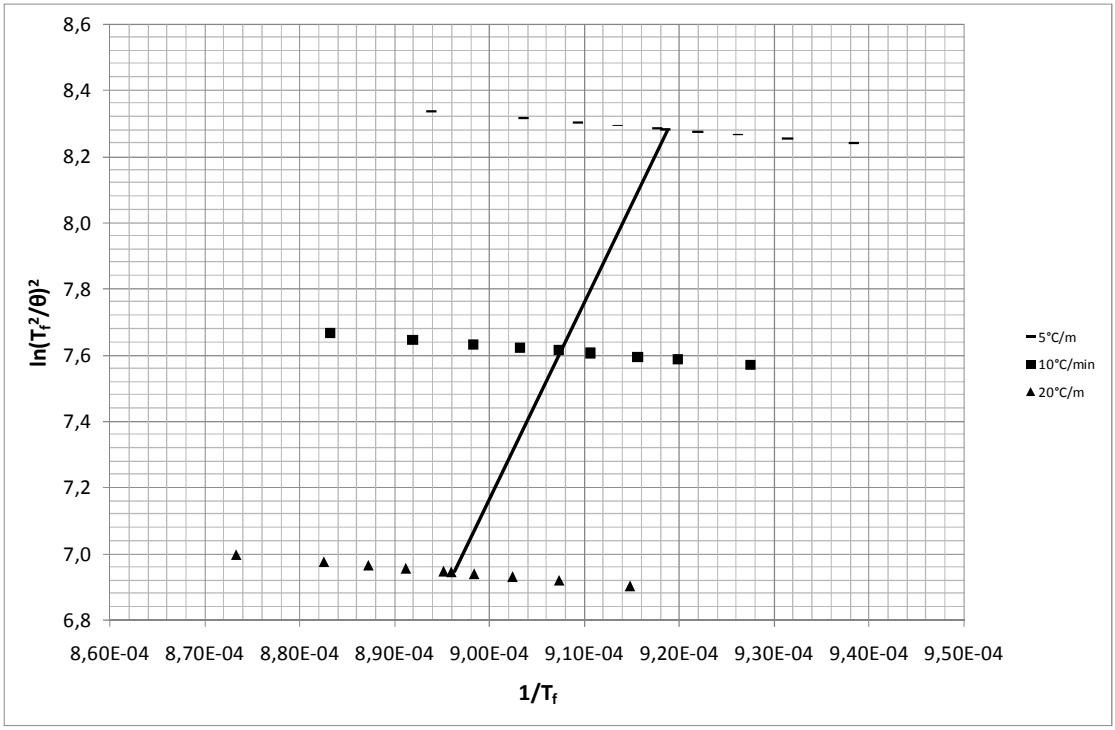

Figure 75. Plotting of $\ln(T_f^2/\theta)^2$ versus 1/T: the activation energy E is calculated from the slope of the resulting straight line.

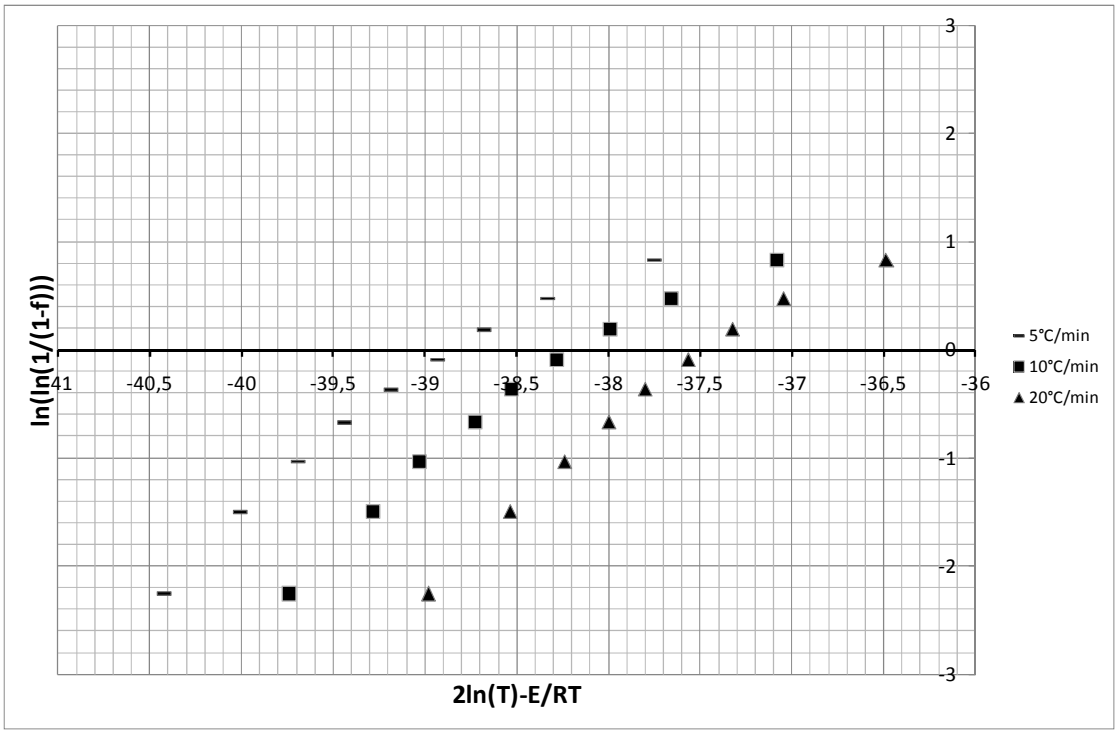

Figure 76. Plotting of ln(ln(1/(1-f))) as a function of 2ln(Tf)-E/RT: the Avrami exponent "n" for the transformation is calculated from the slope of the curve; an activation energy for the transformation of 481,5 kJ/mol was assumed.

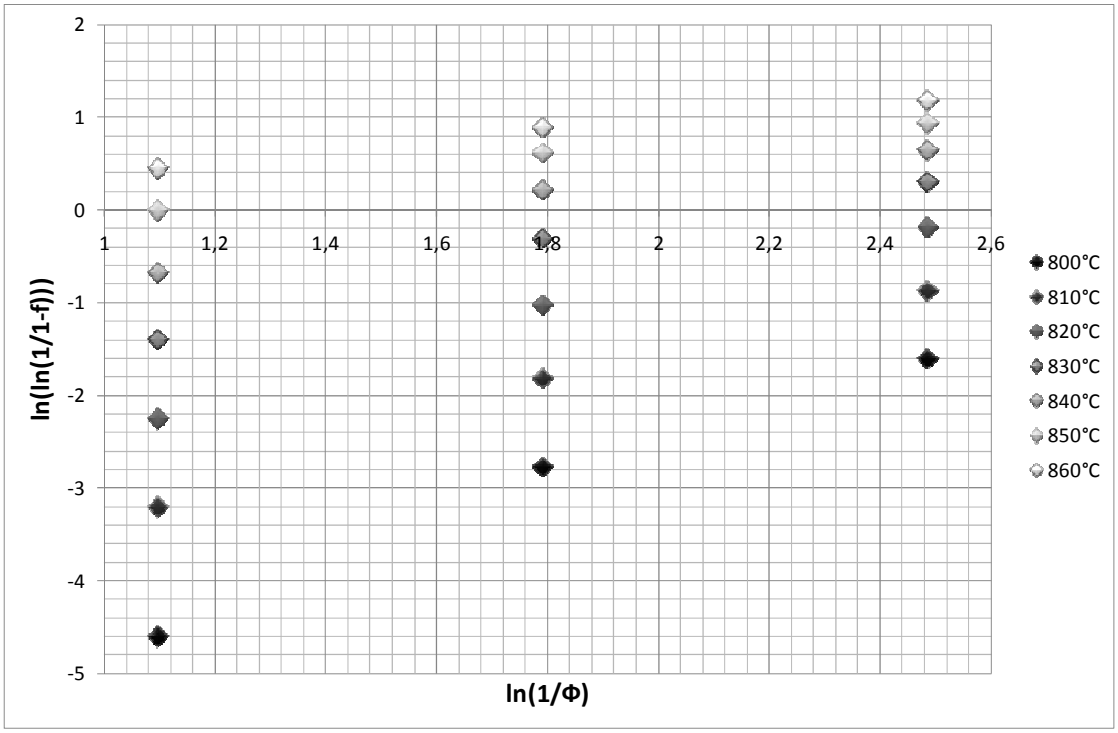

Figure 77. Plotting of ln(ln(1/(1-x))) as a function of ln(1/ϕ); the Avrami exponent "n" for the transformation is calculated from the slope of the curve; an activation energy for the transformation of 481,5 kJ/mol was assumed.

Dependence of temperature

The dependence of temperature is excluded from Figure 76 since no differences are shown when transformation temperatures are shifted due to different heating rates. The apparent dependence for "n" from a function of temperature shown during the processes is explained considering the connection with the fraction transformed.

This connection can be expressed as follow: let's consider $y = ln\left[ln\left(\frac{1}{1-f}\right)\right]$, $x = 2ln(T) - \frac{E}{RT}$ and the dependence of "n" from x as a generic function $\gamma_{(T,f)}$. It results in:

$$\frac{dy}{dx} = n \rightarrow \frac{dn}{dx} = \gamma_{(T,f)} = \frac{dn}{dy} \cdot n \rightarrow n \cdot dn = \gamma_{(T,f)} \cdot dy = \gamma_{(T,f)} \cdot \frac{-f}{1-f} \cdot ln\left(\frac{1}{1-f}\right) df$$

Finally, $n = \sqrt{2 \int \gamma_{(T,f)} \cdot \frac{-f}{1-f} \cdot ln\left(\frac{1}{1-f}\right) df} = \sqrt{2\left(\emptyset_{(T,f)} + C\right)}$ and, if no dependence from temperature is assumed:

$$n_{(f)} = \sqrt{2\left(F_{(f)} + C\right)}$$

Appendix F – *Continuation of the work*

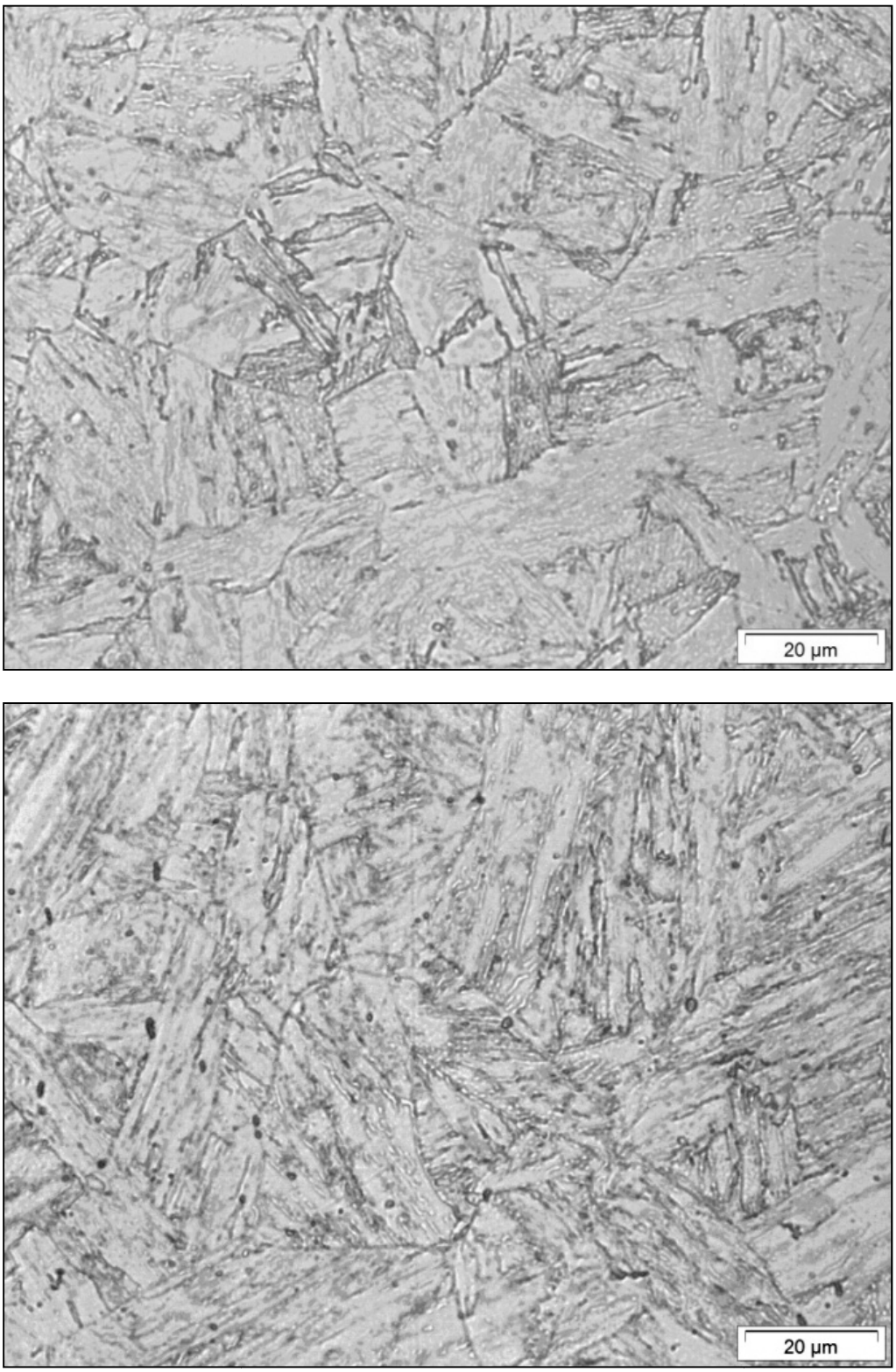

Figure 78. Alloy 2558 (top), 2559 (down) tempered 2h at 680°C after normalization; optical microscope; Villella's etching 10s.